Karlova Univerzita

Přírodovědecká fakulta

Studijní program: Biologie

Studijní obor: Imunologie

Bc. Michaela Vondráčková

Nádorový supresor NDRG1 a jeho ovlivnění chelátory železa

Tumor suppressor NDRG1 and its regulation by iron chelators

Diplomová práce

Školitel: Mgr. Jaroslav Truksa, Ph.D.

Konzultant: MSc. Cristian Sandoval-Acuña, Ph.D.

Praha 2021

Prohlášení

Prohlašuji, že jsem závěrečnou práci zpracovala samostatně a že jsem uvedla všechny použité informační zdroje a literaturu. Tato práce ani její podstatná část nebyla předložena k získání jiného nebo stejného akademického titulu.

V Praze,

Podpis…..……..

Bc. Michaela Vondráčková

Acknowledgements

I would like to express my gratitude to my supervisor Mgr. Jaroslav Truksa Ph.D. for giving me the opportunity to work in his laboratory and for his patient guidance and valuable advice during the preparation of this thesis. My thanks go also to my consultant MSc. Cristian Sandoval-Acuña, PhD. for his experimental help, great patience and valuable insights. I would also like to thank to all my colleagues from the Laboratory of tumour resistance IBT CAS for great working atmosphere. And last but not least, my family and friends also deserve huge thanks for their support and patience throughout all those years.

Abstrakt

Železo je esenciálním stopovým prvkem nezbytným pro mnoho životně důležitých procesů v buňce, včetně syntézy DNA a progrese buněčného cyklu. Kromě toho je zásadní pro buněčné dýchání v mitochondriích. Vzhledem ke zvýšené rychlosti proliferace nádorových buněk jsou rakovinné buňky více závislé na železe a odebrání tohoto prvku pomocí chelátorů u nich vede k inhibici ribonukleotid reduktázy, zastavení buněčného cyklu a apoptotické buněčné smrti. V nedávné době byl vedle těchto účinků navržen alternativní mechanismus zahrnující zvýšenou expresi N-myc downstream regulated gene 1 (*NDRG1*) a jeho inhibiční působení na proteiny c-MET, EGFR či NF-κB, které mohou v určitém kontextu působit jako onkogeny.

NDRG1 je nádorový supresor, jehož exprese je snížena u mnoha typů nádorových buněk a tato nižší exprese koreluje s progresí nádoru, nižším stupněm diferencovanosti a vyšším metastatickým potenciálem. Ukazuje se, že expresi NDRG1 lze regulovat přítomností železa v buňce, tedy, že pokles intracelulárního železa vede ke zvýšení NDRG1 na úrovni mRNA i proteinu a to HIF-1 dependentním mechanismem, který je závislý na inhibici buněčných enzymů prolylhydroxyláz.

V nedávné době jsme představili koncept chelátorů cílených do mitochondrií, které fungují jako protirakovinné látky a v této práci jsme se zaměřili na zhodnocení efektu mitochondriálně cíleného deferoxaminu (mitoDFO) a deferasiroxu (mitoDFX) na indukci NDRG1 v MCF7 buňkách rakoviny prsu a tento účinek jsme porovnali s nemaligními fibroblasty MRC5. Naše výsledky ukazují, že indukce NDRG1 nekoreluje s cytostatickou a cytotoxickou aktivitou daného chelátoru. Dále jsme zhodnotili efekt testovaných chelátorů na vybrané signálních dráhy (EGFR, NF-kB a c-MET), které jsou ovlivněny NDRG1, a zjistili jsme, že hladina jaderného proteinu p-NFκB Ser^{536} byla snížena v MCF7 buňkách, zatímco v MRC5 fibroblastech došlo k poklesu EGFR a c-MET. Ve snaze lépe porozumět roli NDRG1 v nádorových buňkách jsme zkonstruovali MCF7 *NDRG1* knockout klony a ukázali, že delece genu *NDRG1* změnila fenotyp MCF7 buněk, nicméně nezměnila odpověď na působení testovaných chelátorů. Nakonec jsme zjistili, že mitochondriálně cílené chelátory zvýšily procento pozitivních buněk na kalretikulin, což by mohlo ukazovat na možnost navození immunogenní buněčné smrti. V souhrnu můžeme říci, že indukce NDRG1 po působení chelátorů na buňky MCF7 není klíčovým mechanismem, který by ovlivňoval účinnost těchto chelátorů a spíše může reflektovat jejich schopnost vytvářet „pseudohypoxii“ pomocí nedostatku železa.

Klíčová slova: NDRG1, MCF7, MRC5, železo, chelátory železa, signální dráhy, knockout

Abstract

Iron is an essential trace element required for many processes within a cell, including DNA synthesis and cell cycle progression. Moreover, it is critical for cellular respiration in mitochondria. Due to their proliferative nature, cancer cells are dependent on iron, and depleting this element *via* iron chelators results in the inhibition of ribonucleotide reductase, leading to cell cycle arrest and apoptosis of cancer cells. Recently, an alternative mechanism for the effect of iron chelators have been proposed, including induction of N-myc downstream regulated gene 1 (*NDRG1*) expression and its inhibitory effect on c-MET, EGFR, and NF-κB pathways, which can act as oncogenes in a certain context.

NDRG1 is a tumour suppressor gene, which is downregulated in many cancers and its downregulation correlates with cancer progression, poor differentiation, and higher metastatic potential. It has been shown that NDRG1 expression can be regulated by intracellular iron – a decrease in intracellular iron leads to upregulation of NDRG1 at mRNA and protein level *via* the HIF-1-dependent mechanism by inhibiting prolyl hydroxylases.

Recently, we have conceived the concept of mitochondrially targeted chelators as an effective anti-cancer agent and in this work, we focused on the evaluation of mitochondrially targeted deferoxamine (mitoDFO) and deferasirox (mitoDFX) on NDRG1 induction in MCF7 breast cancer cells and compared this effect with non-malignant MRC5 fibroblasts. Our results show that induction of NDRG1 does not correlate with the cytostatic and cytotoxic potency of the chelators. In addition, we evaluated the role of tested iron chelators on selected signalling pathways (EGFR, NF-kB, and c-MET) that are affected by NDRG1, and we found that the level of nuclear p-NFκB Ser^{536} was reduced in MCF7 cell line, while EGFR and c-MET were downregulated only in MRC5 cells. To better understand the role of NDRG1 in tumour cells, we constructed MCF7 *NDRG1* knockout clones and showed that the deletion of the *NDRG1* gene changed the phenotype of MCF7 cells. However, it did not affect the response to the tested chelators. Finally, we have shown that mitochondrially targeted iron chelators might induce immunogenic cell death as evidenced by an increase in calreticulin-positive cells after exposure to these chelators. Overall, it seems that NDRG1 induction is not the critical mechanism that would dictate the efficacy of iron chelators, but it rather reflects their ability to induce “pseudohypoxia” by iron deprivation.

Keywords: NDRG1, MCF7, MRC5, iron, iron chelators, signalling pathways, knockout

Contents

List of abbreviations

AKT	Protein kinase B
APS	Ammonium persulfate
BCA	Bicinchoninic acid
BSA	Bovine serum albumine
cDNA	Complementary DNA
c-MET	Mesenchymal epithelial transition factor
c-Src	Cellular Src kinase
DAMP	Damage-associated molecular pattern
DCF	Dichlorofluorescein
DCF-DA	Dichlorofluorescin diacetate
DFO	Deferoxamine
DFX	Deferasirox
DMEM	Dulbecco's modified eagle medium
DMSO	Dimethylsulfoxide
Dp44mT	Di-2-pyridylketone-4,4-dimethyl-3-hiosemicarbazone
DpC	Di-2-pyridylketone 4,4-dimethyl-3-thiosemicarbazone
EDTA	Ethylenediaminetetraacetic acid
EdU	5-ethynyl-2′-deoxyuridine
EGF	Epidermal growth factor
EGFR	Epidermal growth factor receptor
EMT	Epithelial-to-mesenchymal transition
ER	Endoplasmic reticulum
ERK	Extracellular signal-regulated kinase
ESR	Oestrogen receptor
FBS	Fetal bovine serum
FDA	Food and Drug Administration
FPN	Ferroportin
GAB1	GRB2-associated-binding protein 1
gDNA	Genomic DNA
GSK3	Glycogen synthase kinase 3
HBSS	Hank's balanced salt solution
HDL	High-density lipoprotein

HER2	Human epidermal growth factor receptor 2
HER3	Human epidermal growth factor receptor 3
HGF	Hepatocyte growth factor
HIF	Hypoxia inducible transcription factor
HMGB1	High mobility group box 1
HRE	Hypoxia responsive elements
HSP	Heat shock proteins
HTH	Helix-turn-helix
ICD	Immunogenic cell death
IKK	IκB kinase
IL	Interleukin
IκB	Inhibitor of κB
KO	Knockout
LDL	Low-density lipoprotein
MAPK	Mitogen-activated protein kinase
mitoDFO	Mitochondrially targeted DFO
mitoDFX	Mitochondrially targeted DFx
MMP	Matrix metalloproteinase
mTOR	Mechanistic target of rapamycin
NDRG	N-myc downstrem regulated
NDRG1	N-myc downstream regulated gene 1
NF-κB	Nuclear factor kappa-light-chain-enhancer of activated B cell
PaCa	Pancreatic cancer cells
PBS	Phosphate buffer saline
PCR	Polymerase chain reaction
PERK	Protein kinase R-like endoplasmic reticulum kinase
PI	Propidium iodide
PI3K	Phosphoinositide 3-kinase
pMLC2	Phosphorylated myosin light chain 2
PPAS	Phosphopantetheine attachment site
qPCR	Quantitative PCR
Rac1	Ras-related C3 botulinum toxin substrate 1
RBC	Red blood cell

RIPA	Radioimmunoprecipitation assay
ROCK1	Rho associated coiled-coil-containing protein kinase 1
ROS	Reactive oxygen species
RTK	Receptor tyrosine kinase
SDS	Sodium dodecylsulphate
SDS-PAGE	Sodium dodecylsulphate - polyacrylamide gel electrophoresis
SGK1	Serum- and glucocorticoid-induced kinase 1
SMAD	Mothers against decapentaplegic homolog
STAT	Signal transducers and activators of transcription
SUMO-2	Small ubiquitin-like modifier 2
TEMED	Tetramethyl ethylenediamine
TGF	Transforming growth factor
TMRM	Tetramethyl rhodamine methyl ester
TPP^+	Triphenylphosphonium ion
VEGF	Vascular endothelial growth factor
WNT	Wnt family member
WT	Wild type

1. Introduction

Cancer is one of the most common and serious chronic non-transmissible diseases with a high mortality rate. Since the time of Hippocrates, several theories of cancer origin have been proposed, but eventually have been replaced by the current molecular genetic concept. Our understanding of the mechanism of tumour initiation and its spreading may help us improve the ability to treat cancers, which nowadays includes surgery, chemotherapy, radiotherapy, and immunotherapy.

Cancers are thought to originate from a single cell that has experienced an initial mutation, but the progeny of this cell has to undergo a series of further changes to become cancerous. These changes are usually linked with the regulation of the cell cycle and can be divided into two main classes: *i*) activation of oncogenes and *ii*) the inactivation or loss of tumour suppressor genes. The activity of these genes can be caused by changes at the DNA level by chromosomal translocation, point mutation, and gene amplification or can be regulated by epigenetic modifications. Oncogenes arise from proto-oncogenes, whose products are involved in key biological processes and may function as growth factors, transducers of cellular signals, and nuclear transcription factors. Changes in regulation or activity of these genes may induce cell proliferation, survival, and inhibit apoptosis. In contrast, tumour suppressors play a major role in the normal growth and differentiation of the cell and block the development of cancer. Both copies of a tumour-suppressor gene must be in an inactive state before a cancer cell can proliferate or survive further. Lack or inactivation due to mutations of tumour-suppressor genes leads to cancer. So far, there is number of known tumour suppressors whose mutation can contribute to cancer development. The most known are the *RB1*, which was the first identified tumour suppressor gene, and the *TP53*, which is mutated in more than 50 percent of human tumours [1][2].

Oncogenes as well as tumour suppressors can be a promising target for cancer therapies. Most molecular targeted therapies are inhibitors of oncogenes, because inactivated tumour suppressor genes cannot be easily re-activated by drugs. Nevertheless, in cancers, tumour suppressor genes undergo alteration more frequently than oncogenes. One possible approach to target tumour suppressors is gene therapy, which includes transferring genetic material into a host cell through viral and non-viral vectors, and modulation of tumour cells. Another possible way is indirectly through target molecules that restore the activity of the tumour suppressor genes, which were repressed by the low

abundance of the protein, protein degradation, or inactivation [2-4]. One of the tumour suppressors is the N-myc downstream regulated gene 1 (*NDRG1*), which is usually not present in cancer cells, but its expression is increased after the application of certain drugs and its activity suppress tumour growth.

1.1. Iron chelating drugs for anticancer therapy

Iron is an essential element required for many processes within cells, including DNA synthesis and cell cycle progression. Moreover, it is critical for cellular respiration in mitochondria. The biological activity of iron lies in the ability to accept or donate electrons [5]. Nevertheless, its level in cells has to be tightly regulated to avoid its remarkably high reactivity that could induce severe damage due to reactive oxygen species (ROS) production *via* the Haber Weiss/Fenton reaction [6]. Haem iron served as a cofactor for haemoglobin and myoglobin is involved in many important physiological processes including oxygen binding, its transport and oxygen metabolism. Non-haem iron usually found in the form of the iron-sulphur clusters is the active centre of many important enzymes involved in DNA synthesis and cell cycle.

Some reports suggest that excess iron in the body may lead to an increased risk of cancer, which is partly due to free radicals produced by the Fenton reaction which further damages DNA and other biomolecules [7]. Iron also plays a crucial role in promoting cancer cell proliferation, because iron is a co-factor of ribonucleotide reductase and several subunits of DNA polymerases, the critical enzymes for DNA synthesis. Therefore, the high requirement of iron is prevalent in cancer cells. [5]. Many studies have provided new insights into cancer treatment by depleting iron [8-13].

Iron chelators are a class of drugs decreasing intracellular iron levels by binding iron with a high affinity. This class includes deferoxamine (DFO) and deferasirox (DFX), both United States Food and Drug Administration (FDA) approved drugs for iron overload, and the experimental iron chelator di-2-pyridylketone-4,4-dimethyl-3-hiosemicarbazone (Dp44mT) developed for cancer treatment by prof Richardson (Illustration 1) [14].

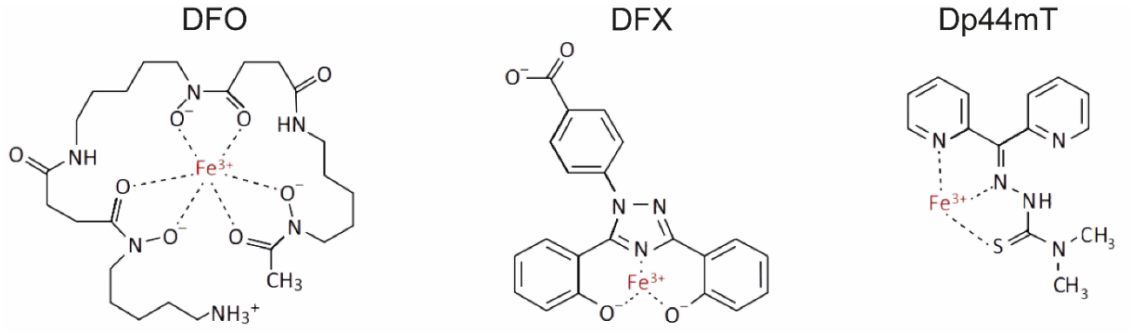

Illustration 1: Schematic picture of iron chelators and their binding activities. DFO forms six bonds with a central iron atom, rendering the $Fe3^{+}$ inert. Tridentate chelators, such as DFX and Dp44mT, only form three bonds with iron, allowing iron reduction and Fenton chemistry with subsequent ROS generation. Adapted from [15].

1.1.1. Deferoxamine

Deferoxamine belongs to the class of siderophores, i.e. naturally occurring chelators secreted by microorganisms. In the case of DFO, it is the bacteria *Streptomyces pilosus*. DFO binds ferric ions (Fe^{3+}) by means of its hydroxamic acid groups to form stable redox inactive complexes. It prevents cells from the production of ROS and thus decreases the oxidative stress in iron-overloaded cells [16, 17]. However, the high hydrophilicity of DFO molecule limits its efficiency and causes a poor oral bioavailability with a very short half-life in plasma (about 20 min). So, DFO must be administered subcutaneously or intravenously over 8-24 hours by slow infusion at least five times per week at a daily dosage of 20 to 60 mg/kg to achieve a negative iron balance [18].

Deferoxamine is the first drug approved by FDA for iron chelation. Currently, it is commercially available under the name Desferal® and is indicated for the treatment of acute iron intoxication and chronic iron overload due to blood transfusions [19]. Also, DFO was the first chelator to be clinically tested for cancer therapy. It was administrated to a six-week patient with neonatal acute leukaemia not responding to conventional chemotherapy and showed antiproliferative effects both *in vitro* and *in vivo* [8]. Although other *in vitro* studies and clinical trials have confirmed the significant anticancer effect of DFO, its toxic side effects besides harder administration led to a search for alternatives that are safer and easier to administer [20].

1.1.2. Deferasirox

Deferasirox is a member of the group of synthetic iron chelators. It is orally bioavailable and has a longer half-life than DFO, ranging from 8 to 16 h in plasma, which allows once-daily dosing at 10-40 mg/kg. At neutral pH, DFX is capable of binding either Fe^{2+} or Fe^{3+}

and, unlike DFO, it is highly lipophilic. The tridentate structure of the chelator molecule requires two chelator molecules to bind one iron atom. Tridentate molecules can form partially coordinated complexes with iron, which generate ROS that play an important role in their anti-cancer activity, while the hexadentate structure of DFO allows forming stable complexes at ratio 1:1, thus preventing the formation of ROS [21].

Deferasirox is available as Exjade® and Jadenu®, both developed by the international pharmacological company Novartis. It is approved for the treatment of transfusional iron overload in patients with beta thalassaemia and for the treatment of chronic iron overload requiring chelation therapy when deferoxamine therapy is contraindicated or inadequate. DFX has shown anticancer effect in several *in vitro* pre-clinical studies [22].

1.1.3. Thiosemicarbazones

Thiosemicarbazones, di-2-pyridylketone 4,4-dimethyl-3-thiosemicarbazone (Dp44mT) and di-2-pyridylketone-4-cyclohexyl-4-methyl-3-thiosemicarbazone (DpC), are a recently developed group of metal chelators with potent and selective activity against tumour cells *in vitro* and *in vivo* [23, 24]. This class of anticancer agents was shown to mediate antitumor activity by iron and copper chelation, and redox cycling of its complexes to generate ROS [25, 26]. In addition, Dp44mT can induce apoptosis. The molecular mechanism behind this effect lies in the efflux of holo-cytochrome c from the mitochondria, increased activity of caspase-3, 8 and 9 proteins and a decrease in the mitochondrial transmembrane potential after incubation with Dp44mT. Moreover, Dp44mT treatment results in decreased expression of the anti-apoptotic Bcl-2 protein, increased expression of the pro-apoptotic Bax protein and induced G1 cell cycle arrest [23, 27]. Dp44mT was also shown to induce DNA double-strand breaks, activate DNA damage and cell cycle checkpoints and selectively inhibit DNA topoisomerase IIα [28]. Unfortunately, *in vivo* studies revealed that Dp44mT is cardiotoxic and can induce cardiac fibrosis at high non-optimal doses [29]. DpC represents the second generation of the novel thiosemicarbazones developed to get a more potent, yet less toxic agent [30]. DpC was shown to be more effective and better tolerated *in vitro* and *in vivo* compared to Dp44mT. Also, DpC has demonstrated *in vivo* anti-tumour activity by both the intravenous and oral routes, which is a significant advantage, as Dp44mT is toxic when given orally [24, 30]. Both DpC and Dp44mT have been shown to increase the level of NDRG1 and the cyclin-

dependent kinase inhibitor, $p21^{CIP1/WAF1}$, and reduce cyclin D1 level [30]. Further studies describing their antitumor effect have shown that both agents can modulate key oncogenic receptor tyrosine kinases (RTKs) such as epidermal growth factor receptor (EGFR), human epidermal growth factor receptor 2 (HER2), human epidermal growth factor receptor 3 (HER3), and mesenchymal epithelial transition factor (c-MET), by mediating their degradation [31, 32]. DpC is currently under the first phase of clinical trials *NCT02688101*.

1.1.4. Novel mitochondrially targeted iron chelators

Recently, mitochondria have become a focus of research as a very promising target for anti-cancer drugs. This is because mitochondria are the site of vital metabolic processes such as the Krebs cycle, beta oxidation of fatty acids, and oxidative phosphorylation. In healthy cells, mitochondria are tightly controlled to maintain their cellular cycle. However, mitochondria of tumour cells are significantly dysregulated to fulfil the higher metabolic demand of these rapidly proliferating cells [33]. Mitochondrial targeting of anticancer drugs is based on the differences between mitochondria of cancer cells and mitochondria of normal cells. Mitochondria of cancer cells exhibit higher membrane potential and more basic environment in the mitochondrial matrix [34]. Membranes, in general, are impermeable for charged molecules and their transport is thus facilitated by membrane transporters that overcome the activation energy required for transport across the lipid membranes. Molecules with delocalized positive charge can lower this activation energy, which allows them to pass the membrane and enter the mitochondria [35]. Association of some molecules with the triphenylphosphonium ion (TPP^+), which is a widely used mitochondria-targeting vector, results in the fast and selective entry of positively charged molecules especially to the cancer mitochondria [36]. Modification of standard iron chelators with the TPP^+ group represents a promising strategy for cancer treatment by disrupting mitochondrial metabolism. Recently, our laboratory in cooperation with Service Technology Laboratory (Both IBT, CAS) and SmartBrain s.r.o. developed the mitochondrially targeted DFO (mitoDFO) (Illustration 2), which is modified by tagging deferoxamine with two TPP^+ groups, and has demonstrated anticancer properties *in vitro* and *in vivo*. Within mitochondria, mitoDFO reduces biogenesis of [Fe-S] clusters, haem synthesis and destabilizes the level of several iron-containing subunits of mitochondrial respiratory complexes. Furthermore, in syngeneic

and xenograft mice models, mitoDFO has shown anticancer activity by suppressing tumour growth and by inhibition of metastasis of cancer cells. Importantly, mitoDFO has not shown cytotoxic side effects and has not affected organismal iron metabolism in mice models [37]. Similarly, we continued our work and synthesised mitochondrially targeted deferasirox (mitoDFX), however, since it is under patent application and has not been published yet, the structure is not revealed in this thesis. Nevertheless, the effect of these new chelators on induction NDRG1 has not yet been studied and is thus one of the aims of this thesis.

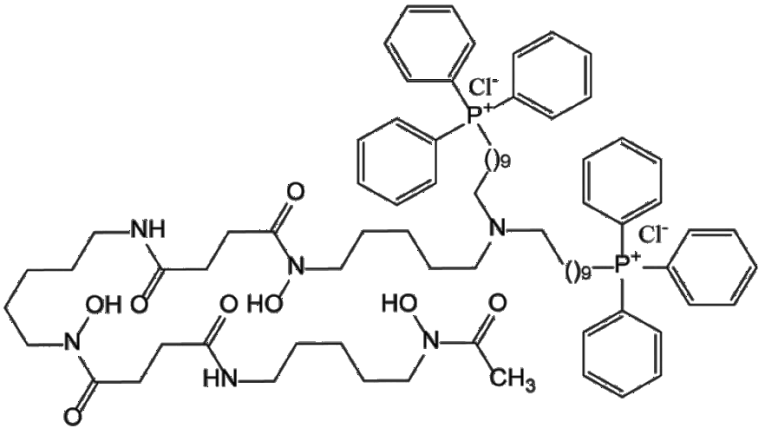

Illustration 2: Schematic picture of mitoDFO. The structure of mitoDFO consists of DFO bound to two molecules of TPP^+. Adapted from [37].

1.2. The role of iron in immune response

Iron has a dual nature, being a necessary, yet potentially toxic element. On one side it is vital for mitochondrial metabolism and DNA replication and further metabolic processes, on the other side it can generate toxic ROS. Therefore, iron recycling, absorption, storage, and regulation within an organism must be tightly controlled. Alterations in this process may contribute to carcinogenesis [5]. Recycling iron from red blood cells (RBCs), where iron is found in the form of haemoglobin, is important for maintaining systemic iron homeostasis in the body. Approximately 95% of the iron is dependent on macrophage haem-iron recycling [38].

Macrophages phagocytize senescent or damaged RBCs and then degrade haemoglobin to release haem. Iron metabolism within macrophages is a complex process involving multiple molecules and proteins, which participate in the acquisition, utilization, storage, and release of iron [39, 40]. In turn, iron is involved in macrophage polarization and function. Macrophages can be polarized into pro-inflammatory M1 or

anti-inflammatory M2 phenotypes. Activated M1 macrophages stimulate Th1 adaptive response, while alternatively activated M2 macrophages are involved in Th2 immune response, termination of the inflammatory immune response, tissue development, wound healing, immunological self-tolerance, immune suppression, and tumour promotion [41]. The polarization is dependent on the cytokine profile. Classical activation to M1 phenotype is achieved by lipopolysaccharides and interferon-γ and is characterized by the induction of major histocompatibility complex class II molecules, the expression of pro-inflammatory cytokines, e.g. tumour necrosis factor α, as well as ROS and reactive nitrogen species formation. Activation to M2 phenotype is typically achieved by interleukin (IL)-4 and IL-13, transforming growth factor (TGF)-β, and glucocorticoids [42].

Iron handling by macrophages is closely associated with their polarization. M1 polarization generally favours an iron storage phenotype, with high expression of ferritin, decreased expression of ferroportin (FPN) and changes in hepcidin and transferrin receptor protein 1. M2 cells are characterized by high expression of scavenger receptors (e.g. haemoglobin scavenger receptor), low expression of ferritin, and high expression of FPN. This phenotype displays an iron-release mode [43]. Near the tumour, in the tumour microenvironment, there are tumour associated macrophages. These type of macrophages exhibits M2 phenotype and can promote cancer growth by releasing iron into their environment [42].

In addition to the role of iron on macrophage function, this trace element is also critical for the proper function of T and B lymphocytes. T lymphocytes, together with antibody-producing B lymphocytes, are the main components of the adaptive immune system. T lymphocytes are divided into two major subtypes named according to the presence of surface proteins CD8 or CD4: $CD8^+$ cytotoxic and $CD4^+$ helper T lymphocytes. $CD8^+$ T lymphocytes can directly kill infected or cancer cells by releasing cytotoxic mediators such as perforin or granzyme, while $CD4^+$ T lymphocytes influence B lymphocytes and innate immune cells through the release of various cytokines and chemokines. The maturation of T, as well as B, lymphocytes to perform their effector function are energy expensive and iron-dependent processes [44]. Besides, a recent study has been demonstrated that iron can directly participate in inflammatory responses by promoting proinflammatory cytokine production in the T lymphocytes and negatively affect autoimmune diseases [45]. Conversely, iron deficiency might cause impairment of proliferative responses in B lymphocytes connected with attenuation of antigen-specific

antibody production. It might cause marginal or insufficient antibody response after immunization with a vaccine in iron-deprived individuals [46]. Another recent study has been shown that iron deficiency induced by hepcidin, which is an iron control hormone, might impair effector and memory immune responses to immunization [47].

Another and probably not the last role of iron in the immune system is the induction of immunogenic cell death (ICD). ICD is any type of cell death that induce an immune response by releasing a series of immunostimulatory damage-associated molecular patterns (DAMPs). These molecules represent so-called "eat me" signals for professional phagocytes that remove dead cells. Among the most important DAMPs, which are exposed to the cell surface or secreted into the extracellular environment during ICD, belong calreticulin, heat shock proteins (HSP70 and HSP90), the non-histone chromatin-binding nuclear protein high mobility group box 1 (HMGB1), nucleic acids, and small metabolites such as ATP, as well as type I interferons. Calreticulin is an endoplasmic reticulum (ER) chaperone, which gets exposed on the cell surface in the early stages of ICD, even before shuffling of phosphatidylserine between the inner and outer leaflet of the plasma membrane [48]. Iron-dependent ICD (ferroptosis) is caused by the accumulation of iron ions within cells followed up by the Fenton reaction, which generates ROS. The elevated amounts of ROS may promote ferroptosis by extensive peroxidation of lipids and subsequent damage of plasma membrane [49]. Ferroptosis activation has been confirmed to be associated with calreticulin translocation on the plasma membrane as well as with releasing ATP and HMGB1 [50, 51]. Induction of ferroptosis may be blocked by iron chelators [52]. Also, hypoxia may induce ER stress response, and calreticulin exposition on the cell surface and modulation of immune response [53].

1.3. NDRG1

1.3.1. NDRG superfamily

NDRG1 belongs to the N-myc downstrem regulated (NDRG) protein family, consisting of 4 members, NDRG1, NDRG2, NDRG3, and NDRG4. These proteins share 57-65% homology and are characterised by the presence of the NDR domain, consisting of an esterase-/lipase-/thioesterase-active-site serine and an α/β-hydrolase fold of approximately 220 amino acids [54, 55]. Thanks to the catalytic motif, NDRG family members belong to the α/β-hydrolase superfamily, however, none of them has hydrolytic

activity [56]. The differences between particular members are located in the N- and C-terminal regions. On the basis of phylogenetic analysis, they might be divided into two subgroups – one containing NDRG1 and NDRG3, and another composed of NDRG2 and NDRG4 [55].

NDRG1, NDRG2, NDRG3, and NDRG4 are located on 8q24.2, 14q11.2, 20q11.23 and 16q21, respectively. While NDRGs share high sequence identity and have similar functions, they differ in tissue distribution. NDRG1, which is the most described NDRG protein, is ubiquitously expressed in all tissues, while NDRG2-4 are highly expressed in the brain. Moreover, NDRG2 is expressed in skeletal muscle and heart, NDRG3 in testis, and NDRG4 in the heart [55]. All of them are involved in cell proliferation, apoptosis, differentiation, tissue development and its maintenance, and stress response. In multiple cancer types, NDRGs can act as suppressors by decreasing proliferation rate, and inhibiting invasion and metastasis. Nevertheless, depending on the cancer type, NDRGs may act as oncogenes and thus promote cancer growth [57-67].

1.3.2. NDRG1 structure and genetics

NDRG1, also known as CAP43, DRG1, RIT42, and PROXY1, is mapped on the long arm of chromosome 8 (8q24.2), a region commonly amplified in some tumours [68]. It encodes an mRNA of about 3 kb, which is translated into a 43 kDa protein with 394 amino acids [69, 70]. NDRG1 consists of three unique 10 amino acid tandem repeats (GTRSRSHTSE) at the C-terminal region and a phosphopantetheine attachment site (PPAS) motif within the α/β hydrolase fold, that have not been observed in other NDRGs. Other structural features, that are specific for NDRG1, are a helix-turn-helix (HTH) near the N-terminus of the protein and a cap-like domain within the α/β hydrolase fold (Illustration 3) [55, 71].

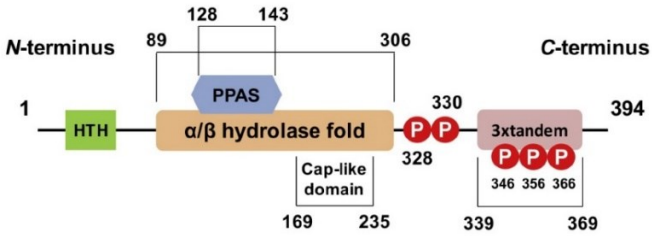

Illustration 3: General structure of NDRG1 protein. The full-length NDRG1 protein is composed of 394 amino acids and it contains multiple structural motifs: helix-turn-helix (HTH) near the N-terminus, α/β hydrolase fold, phosphopantetheine attachment site (PPAS) and cap-like domain within the hydrolase fold, and three tandem repeats at the C-terminus. The NDRG1 protein contains multiple phosphorylation sites including Thr^{328}, Ser^{330}, Thr^{346}, Thr^{356}, and Thr^{366}, which are all phosphorylated by the serum- and glucocorticoid-induced kinase 1(SGK1). Taken from [72].

Several post-translational modifications occur on the NDRG1 protein, including sumoylation, phosphorylation, and truncation near its N-terminus. The sumoylation mediated by small ubiquitin-like modifier 2 (SUMO-2) decreases NDRG1 stability and promotes its ubiquitinylation, leading to proteasomal-dependent degradation. Moreover, SUMO-2 modification inhibits the induction of p21, the cyclin-dependent kinase inhibitor 1, by NDRG1 [73].

NDRG1 can be phosphorylated at multiple sites by various kinases. The phosphorylation mediated by serum- and glucocorticoid-induced kinase 1 (SGK1) at Thr^{346}, Thr^{356} and Thr^{366} within unique decapeptide repeat, as well as at Thr^{328} and Ser^{330}, the two residues conserved in all four family members, prime NDRG1 for subsequent phosphorylation by glycogen synthase kinase 3 (GSK3) at Ser^{342}, Ser^{352} and Ser^{362} also within the tandem repeat [74, 75]. The phosphorylation by both kinases simultaneously may lead to NDRG1 degradation mediated by the 26S-proteasome [76]. NDRG1 was also described to serve as a good substrate for protein kinase A, less potently for protein kinase C, calmodulin kinase-II, and casein kinase II, however, this remains unclear and probably the activity of individual kinases may vary depending on the cell type [77, 78].

Although NDRG1 is described primarily as a 43 kDa protein, some recent studies identified multiple NDRG1 bands varying in molecular weight [72, 79, 80]. These different isoforms have been described as 41 kDa, 46 kDa and, 47 kDa. Previous investigations examining different cell types suggested that different primary antibodies used to detect NDRG1 result in two distinct bands by immunoblotting and the higher band is thought to be result of phosphorylation [30, 77, 81-85]. A more recent study described the 46 kDa NDRG1 as a full-length unmodified protein, whose molecular weight was not result of the phosphorylation or glycosylation. Also, according to this study the 41 kDa protein is probably a result of proteolytic cleavage of full-length protein at the N-terminus specifically in prostate cancer cells, but not in non-malignant counterparts [80]. The following study has come with 47 kDa isoform of NDRG1 [72]. The 47 kDa NDRG1 isoform may be processed by the proteasome to generate the 46 kDa NDRG1 isoform, which can be further degraded by the lysosome. In addition, the 47 kDa NDRG1 can be cleaved *via* an independent and unknown mechanism leading to the 41 kDa NDRG1 isoform. Moreover, all these NDRG1 isoforms were demonstrated to be, at least in part, phosphorylated [86]. The exact function of these different isoforms is not clear yet, but it is suggested that they may affect cellular distribution, which may result in different protein functions.

1.3.3. Cellular and tissue distribution of NDRG1

In contrast with other NDRGs, NDRG1 is ubiquitously expressed at mRNA level in most human tissues, however, many of them do not contain detectable protein levels. The absence of NDRG1 protein was observed in the heart, brain and skeletal muscle, whereas high NDRG1 was found in epithelial cells.

NDRG1 is mostly a cytoplasmic protein, but its subcellular localization differs depending on the cell type. For instance, in intestinal epithelia and lactating breast it is connected with the plasma membrane, while in glandular epithelia of prostate it is associated with the nucleus, and in the kidney, NDRG1 displays mitochondrial localization [87]. *In silico* analysis by PSORTII software predicted NDRG1 localization in the cytoplasm, nucleus, and mitochondria with probabilities 47.8 %, 26.1 %, and 8.7 %, respectively. According to this software, NDRG1 is also predicted to be localized in vacuoles, cytoskeleton, peroxisomes, and plasma membrane with probabilities of 4.3 % each [88]. However, using another software led to different values. WolfPSORT predicts NDRG1 localization in the nucleus with 17% probability, 16.5% for cytoplasmic and nuclear localization, 10% for cytoplasm, 1% for mitochondria, peroxisomes, and plasma membrane each, moreover, this tool suggested 2% probability for extracellular secretion [89].

Although NDRG1 can be localized in the nucleus, it does not contain any nuclear localisation signal in its sequence [87]. Furthermore, NDRG1 can be translocated from cytoplasm to nucleus upon DNA damage suggesting a possible role of NDRG1 in DNA repair [90]. This nuclear translocation might be caused by NDRG1 phosphorylation and/or NDRG1 interaction with nuclear proteins. There is one recent report showing that the full-length NDRG1 phosphorylated at Ser^{330} localises mainly in the nucleus, whereas the truncated NDRG1 and NDRG1 phosphorylated at Thr^{346} are mainly cytosolic [72]. In mast cells, NDRG1 can interact with HSP70, which is a nuclear protein, allowing it to enter the nucleus [91].

Similarly to the lack of the nuclear localisation sequence, NDRG1 does not contain any mitochondrial targeting sequences necessary for its translocation into mitochondria [87]. Nonetheless, it has a potential cytochrome c family haem-binding motif and a phosphopantetheine attachment motif, which are compatible with mitochondrial localization. In addition, NDRG1 has been shown to interact with mitochondrial proteins such as voltage-dependent anion channel 1 and cytochrome

c oxidase subunit II and ATPase subunit 6 [91] which might be a way how it gets indirectly into mitochondria [87].

The membrane-associated NDRG1 was predominantly found adjacent to the adherent junction and desmosomes within the cytoplasm, as well as the intermediate and microfilament bundles, which insert into these structures [87]. Of note, the expression of NDRG1 correlates with the expression of E-cadherin, a protein involved in cell-cell adhesion [92]. Moreover, NDRG1 seems to participate in E-cadherin recycling, stabilizing it [93].

1.3.4. Physiological functions of NDRG1

NDRG1 has pleiotropic functions in vital processes within cells, such as stress response, induction of differentiation, lipid metabolism, myelinisation and vesicular protein transport.

Cell differentiation is a process through which an unspecialized cell evolves into a specialized cell, reaching its mature form and gaining different functions. The process of differentiation is driven by a plethora of molecules and factors, and NDRG1 is one of them. Its involvement in the differentiation of trophoblast [94], placental development [95], maturation of several immune cells (e.g. mast cells, dendritic cells, and macrophages) [96-98] and terminal differentiation of Schwann cells during nerve regeneration [99] has been described so far. Of note, a mutation in the *NDRG1* gene, resulting in a truncated isoform, causes the hereditary motor and sensory neuropathy known as Charcot-Marie-Tooth disease type 4D identified in the Gypsy community of Lom, a small town in northwest Bulgaria. This neuropathy is linked with loss of Schwann cell differentiation and axonal survival [100].

Concerning axonal survival, NDRG1 is implicated in lipid metabolism, which is a crucial step of myelinisation. Insights into how NDRG1 regulates myelinisation suggest that it regulates lipid transport. Upon NDRG1 silencing in epithelial cells using small interfering RNA, uptake of low-density lipoprotein (LDL) was decreased by decreasing LDL receptor at the plasma membrane. Furthermore, NDRG1-silenced oligodendrocytes showed downregulation of oligodendrocyte lineage transcription factor 2. This protein is necessary for the genesis of oligodendrocytes and is an important regulator of oligodendrocyte differentiation and myelination by controlling vesicular trafficking from oligodendrocyte body to distant myelin sheath [101]. In addition to its role in myelination,

NDRG1 has been suggested to play a role in the regulation of high-density lipoprotein cholesterol (HDL)-C level by its interaction with apolipoprotein A-I and -II, the two main molecules composing HDL [102].

Using global gene expression profiling in cells with manipulated NDRG1 expression, it was found that NDRG1 can affect a number of genes involved in ER, Golgi apparatus, endosomes or vesicular transport between these compartments. Thus, NDRG1 might facilitate a downregulation of several genes encoding proteins in the ER to endosome axis. Under stressful conditions with lack of energy, such as hypoxia or during ER-stress, the downregulation of some activities in the secretory and/or endocytic pathway of the cell might conserve energy and therefore contribute to restoring cellular homoeostasis [103]. Moreover, NDRG1 overexpression can enhance exocytic response in mast cells [104] and regulate vesicular trafficking within glial cells [101].

NDRG1 expression is induced in response to many different cytotoxic molecules, such as heavy metal ions (Ni^{2+}, Co^{2+}, Fe^{2+}), vitamin D3, phorbol myristate acetate, retinoids, intracellular Ca^{2+}, or DNA damaging agents (e.g. mitomycin C, doxorubicin) [90, 105-107]. These findings together with nuclear localization of NDRG1 suggested its potential role in response to cellular stress. One of the important proteins linked with the stress response is p53, which acts as the sensor of DNA damage and can promote cell cycle arrest followed by DNA repair or apoptosis. Interestingly, it was shown that the p53 protein can directly induce NDRG1 expression after DNA damage. Using RNA interference and inducible gene expression approaches it was suggested that NDRG1 is necessary but not sufficient for p53-mediated caspase activation and apoptosis. [90, 108]. Nonetheless, NDRG1 was also described as the microtubule-associated protein localised in the centrosomes and spindle esters in p53-deficient tumour cells, where, upon overexpression, it drives inhibition of polyploidy development after disruption of the spindle checkpoint, increasing the cell population arrested in mitosis. Loss of NDRG1 in normal cells results in loss of astral microtubule and hardly detectable dividing spindle fibre formation. Therefore, NDRG1 can play a role in the regulation of microtubule dynamics and the maintenance of genomic euploidy [109]. Furthermore, NDRG1 phosphorylation by SGK1 is increased in p53-deficient cells and is temporally and spatially controlled during the cell cycle, suggesting its involvement in successful mitosis [84]. Additionally, NDRG1 is involved in ER stress response, which is caused by the accumulation of unfolded or misfolded proteins. ER stress activates several cytoprotective mechanisms to restore and maintain homeostasis or to induce apoptosis.

NDRG1 regulates main ER stress pathways to increase cytoprotective mechanisms by (1) increasing the expression of three major chaperones (binding-immunoglobulin protein, calreticulin, and calnexin), (2) suppressing the protein kinase R-like endoplasmic reticulum kinase (PERK), (3) inhibiting the inositol-requiring kinase 1, and (4) increasing the cleavage of activating transcription factor 6 [110].

1.4. NDRG1 in cancer

1.4.1. NDRG1 expression in cancer

The expression of NDRG1 is highly altered in many cancers in comparison with its expression in normal tissues, suggesting its involvement in cancer development and progression. In addition, the NDRG1 level can negatively correlate with tumour grade, with higher tumour grade and poorly differentiated tumours expressing less NDRG1 [111]. *NDRG1* expression at the mRNA level is also lower in metastatic cancer cells compared to their primary cancer counterparts [92]. This difference between malignant and non-malignant cells are probably the result of genetic and epigenetic modulations.

1.4.2. Regulation of NDRG1 expression in cancer

Myc oncoproteins belong to the family of so-called “super transcription factors”, because of their ability to regulate transcription of more than 15 % of all genes. The expression of Myc proteins is strictly controlled under normal circumstances. Yet, Myc is frequently deregulated in human cancers. Excess Myc expression can be induced upon retroviral promoter insertion, chromosomal translocation or amplification, activation of super-enhancers within the *MYC* gene, and/or mutation of upstream signalling pathways that enhance Myc stability [112, 113]. N-myc and c-myc suppress the *NDRG1* expression at the transcriptional level by recruiting histone deacetylase, an enzyme removing acetyl groups from histones and making DNA more inaccessible for transcription factors [114]. Besides, the NDRG1 promoter contains multiple CpG sites, forming a large CpG island that can be silenced upon the promoter’s methylation [115, 116].

On the other hand, the expression of NDRG1 is stimulated in response to several stimuli including cytotoxic agents mentioned above and hypoxia [105]. Hypoxia is one of the hallmarks of cancers and occurs when tumour cells are deprived of oxygen. Oxygen tension regulates cytoplasmic subunit of hypoxia inducible transcription factor (HIF)-1α. In normoxia, HIF-1α is hydroxylated by prolyl hydroxylases. This modification enables

it to be ubiquitinylated by E-3 ubiquitin protein ligase with the cooperation of the Von Hippel-Lindau complex and further degraded in the proteasome [117, 118]. Prolyl hydroxylases are not active in hypoxic environments, thus HIF-1α is accumulated and translocates into the nucleus, where it dimerises with HIF-1β subunit, whose expression is not dependent on oxygen level, to form an active transcription factor. HIF-1 complex activates transcription of hypoxia-related genes, including *NDRG1*, by binding to hypoxia responsive elements (HRE) within promoters of hypoxia-related target genes [119]. *NDRG1* has three HIF-1-binding sites, one in the promoter and two in the 3´ untranslated region [120]. Additionally, putative HREs upstream of the promoter at -1376 bp and -7503 bp are involved in its regulation by acting as a transcriptional enhancer for efficient *NDRG1* transactivation [121].

1.4.3. The function of NDRG1 in cancer

Cancer cells share several features driving the transformation of normal cells to cancer cells (Illustration 4) [122, 123]. NDRG1 affects most of these hallmarks of cancer cells. It plays an important role in the main steps promoting primary tumour growth, metastasis, epithelial-to-mesenchymal transition (EMT), migration and invasion of cancer cells, tumour angiogenesis, ER stress and autophagy.

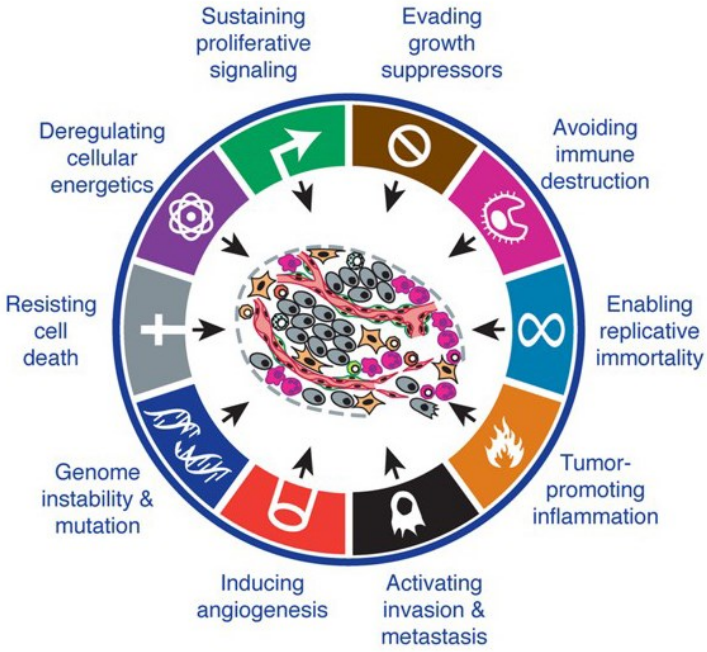

Illustration 4: Hallmarks of cancer cells. Hallmarks of cancer cells proposed by Douglas Hanahan and Robert Weinberg representing several characteristics that are important for the transformation of healthy cells into malignant ones. Adapted from [122].

Tumours are characterised by uncontrolled rapid growth independent of external factors and deregulated cell cycle. At this point, enhanced expression of NDRG1 was found to inhibit cancer proliferation and tumour growth in a number of *in vitro* and *in vivo* studies. NDRG1 can stabilize p21, a universal cell cycle inhibitor, by decreasing its ubiquitination, and therefore induces G0/G1 arrest [124]. In addition, it can upregulate the expression of thiamine-triphosphatase that is involved in hydrolysing thiamine triphosphate, an important energy currency molecule [125]. Therefore, thiamine triphosphatase upregulation by NDRG1 may decrease the available energy as thiamine triphosphate is decreased, leading to reduced growth [126].

Metastasising is a process of spreading cancer cells from the place of origin to distant sites within the body, often by way of lymphatic or blood vessels. It includes several successive steps accompanied by biochemical and morphological changes, beginning with EMT, intravasation, transit in the lymphatic and blood system, and extravasation followed by growth at the new site. NDRG1 can attenuate EMT by inhibiting the TGF-β signalling pathway resulting in maintaining of E-cadherin and β-catenin, two molecules mediating cell-cell adhesion, on the plasma membrane, and inhibiting expression of the EMT marker, vimentin [81]. Moreover, it reduces tumour cell migration and invasion by lowering cell motility, suppressing actin-filament polymerization, stress fibre assembly and formation [127] and formation of focal adhesions [128]. Additionally, NDRG1 suppresses the level of matrix metalloproteinase (MMP)-2 and MMP-9. MMP-2 and MMP-9 degrade components of basement membrane and extracellular matrix, and thus facilitate movement of cells through tissues [82, 129].

Similar to non-malignant cells, tumour cells require oxygen and nutrient supply for their growth. This is achieved through angiogenesis, the process where new blood vessels develop from a pre-existing vascular network. In addition, tumour vasculature facilitates dissemination of cancer cells [130]. NDRG1 decreases *in vitro* expression of several pro-angiogenic factors, such as vascular endothelial growth factor (VEGF), IL-8, and MMP-2 and MMP-9 [82, 129, 131]. Also, it may decrease expression of CXC chemokines by suppressing nuclear factor kappa-light-chain-enhancer of activated B cell (NF-κB) signalling pathway [83]. *In vivo* studies have shown decreasing vascular density in mice with reduced expression of VEGF and IL-8 upon NDRG1 overexpression [82].

Tumour cells are exposed to several extrinsic and intrinsic factors, which alter normal cell homeostasis and trigger a variety of adaptive mechanisms to support cell transformation and promote the acquisition of characteristics necessary for cancer

progression. Extrinsic signals, such as hypoxia, nutrient deprivation, acidosis, alter the normal function of ER. Intrinsic factors, e.g. oncogenic activation, alteration in chromosome number and impaired secretory capacity cause high demand for protein production. Taken together, all these factors result in ER stress, a cellular condition caused by the accumulation of misfolded proteins at the ER lumen [132]. In established cancers, ER stress can initiate autophagy, a process maintaining normal cell homeostasis through the removal of oncogenic protein substrates, toxic unfolded proteins and damaged organelles, mediated by the PERK signalling pathway to support cancer cell survival and growth [133, 134]. NDRG1 overexpression suppresses the stress-induced autophagic response in cancers through suppression of the PERK pathway [134].

1.4.4. NDRG1 and main signalling pathways

All biological functions contributing to cell development and homeostasis are driven by several molecular pathways and their crosstalk. These signalling pathways are often genetically altered in cancer cells, which is one of the main characteristics of cancers. Understanding molecular mechanisms driving tumour progression is essential for cancer treatment and prevention of cancer recurrence. NDRG1 targets the key oncogenic pathways, including NF-κB signalling pathway, phosphoinositide 3-kinase (PI3K)/ protein kinase B (AKT)/mechanistic target of rapamycin (mTOR), mitogen-activated protein kinase (MAPK)/extracellular signal-regulated kinase (ERK), Wnt family member (WNT)/β-catenin, cellular Src kinase (c-Src)/Ras-related C3 botulinum toxin substrate 1 (Rac1) and Rho associated coiled-coil-containing protein kinase 1 (ROCK1)/phosphorylated myosin light chain 2 (pMLC2), to name the most important ones [135].

1.4.4.1. NDRG1 and NF-κB signalling pathway

NF-κB represents a family of inducible transcription factors, which regulates a large number of genes involved in innate and adaptive immune responses that can accelerate cell proliferation, inhibit apoptosis, promote cell migration and invasion, and stimulate angiogenesis and metastasis. Activation of this signalling pathway may be induced by viral and bacterial infections, necrotic cell products, DNA damage, oxidative stress and pro-inflammatory cytokines. In many cancer types, NF-κB is constitutively active, and rarely is this activation caused by genetic alteration [136].

NF-κB family is composed of five related members, including p50 (NF-κB1), p52 (NF-κB2), p65 (RelA), RelB and c-Rel, which mediate transcription of target genes by binding to a specific site within promoters or NF-κB enhancers, as various homodimers or heterodimers [137]. The NF-κB proteins are normally sequestered in the cytoplasm by IκB inhibitory proteins [138]. When the signalling becomes activated, it exerts its downstream effects through the classical (canonical) pathway initiated by p50 and an alternative (non-canonical) pathway initiated by p52 (Illustration 5). The canonical pathway involves activation of the IκB kinase (IKK) complex including IKKα, IKKβ and IKKγ (NEMO). Activation of the IKK leads to phosphorylation of IκB and initiation of proteasome-mediated IκB degradation, which results in rapid and transient nuclear translocation of canonical NF-κB members, predominantly the p50/RelA and p50/c-Rel heterodimers. Contrary to the canonical pathway, the non-canonical NF-κB pathway does not involve IκBα degradation, but rather relies on the processing of the p52 precursor protein, p100. Then, the cleaved p52 protein binds to RelB and translocates into the nucleus. In the nucleus, RelA/p50 and RelB/p52 are modified and bind the promoters of genes whose products are important in metastasis, including *HIF-1*, *c-MYC*, signal transducers and activators of transcription (*STAT*), *SNAIL* and *TWIST* [139-141].

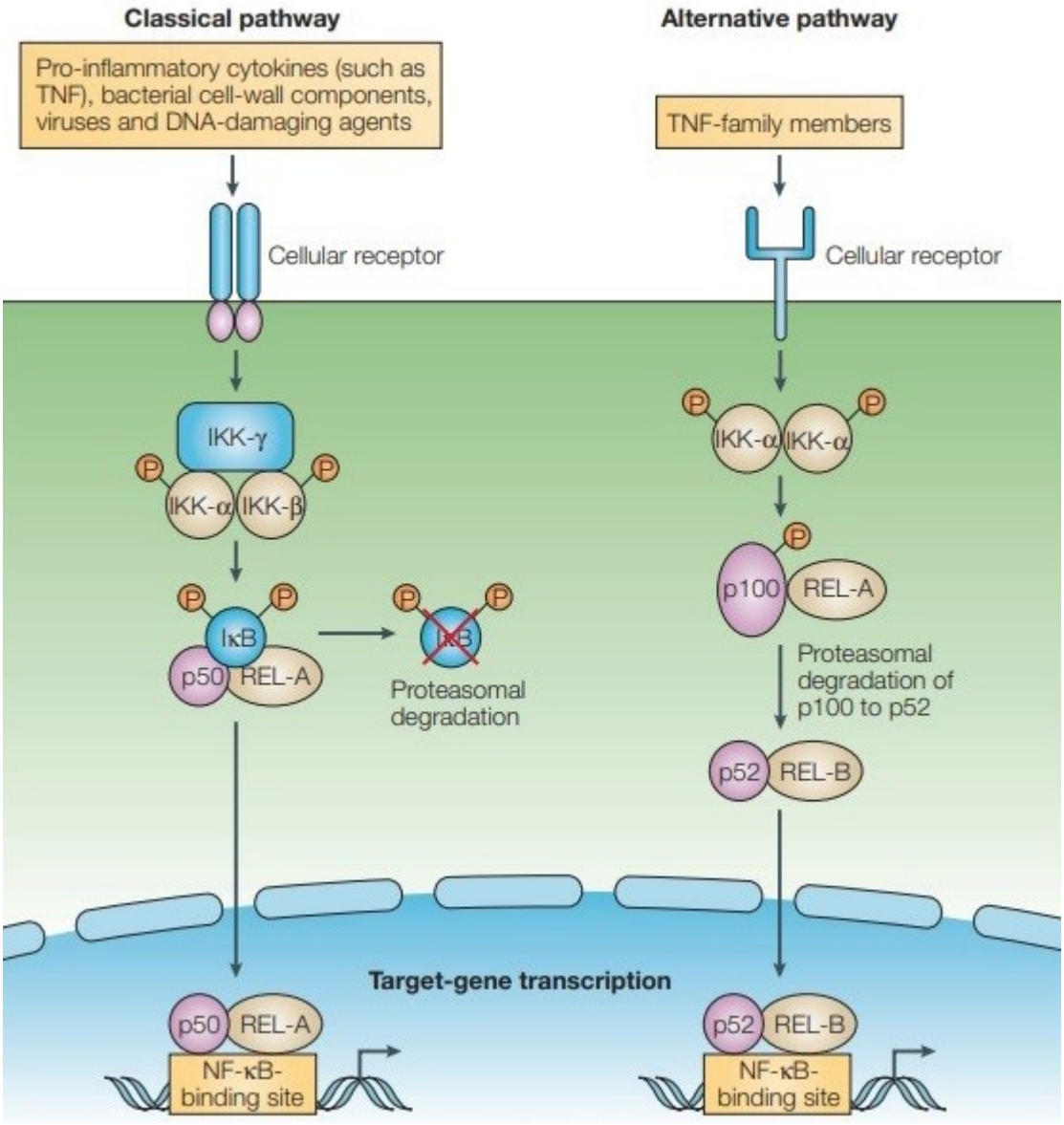

Illustration 5: Classical (canonical) pathway and an alternative (non-canonical) pathway. Classical and alternative pathways lead to the activation of NF-κB transcription factors. Activation of the classical NF-κB signalling leads to IKK-dependent phosphorylation of NF-κB-bound IκB resulting in their proteasomal degradation, and liberating of NF-κB dimers to enter the nucleus. Upon triggering of alternative NF-κB pathway, p100 is phosphorylated by IKK-α and processed by the proteasome to p52, which results in nuclear translocation of p52/RelB dimers. Taken from [142].

NDRG1 can attenuate NF-κB signalling *via* several mechanisms. At first, it may reduce the level of NF-κB activation complex by downregulation of NEMO and IKKα levels, but not IKKβ. Furthermore, NDRG1 overexpression may inhibit the activation of IKKα/β by decreasing its activating phosphorylation. Secondly, NDRG1 overexpression may increase total NF-κB inhibitor, IκBα, and simultaneously decrease IκBα phosphorylation. Thus, NDRG1 may prevent nuclear translocation of NF-κB heterodimer. Finally, NDRG1 can reduce the level of the p65 subunit [143].

1.4.4.2. NDRG1 and TGF-β pathway

Under physiological conditions, the TGF-β signalling pathway plays a role in regulating critical cellular activities, such as cell growth, differentiation, and development. In cancers, TGF-β plays a dual role. While in the early stages of cancer development, TGF-β acts as a tumour suppressor, in late stages it supports invasion and metastasis by modulating the immune system and tumour microenvironment. The TGF-β signalling is triggered by the binding of TGF-β ligand to its specific receptor with intrinsic serine/threonine kinase activity. TGF-β receptors include two major types - TGF-β type I receptors (TβRI) and TGF-β type II receptors (TβRII). Binding of TGF-β ligand to TβRII recruits and phosphorylates the TβRI subunit. Then, phosphorylated TβRI induces signal transduction via canonical or non-canonical pathways. The canonical pathway involves the activation of mothers against decapentaplegic homolog (SMAD) 2 and 3. In turn, activated SMAD2 and SMAD3 can interact with SMAD4 to form a trimeric complex, which can be translocated into the nucleus to regulate the expression of TGF-β target genes [144].

NDRG1 overexpression inhibits the canonical TGF-β/SMAD pathway through reduced expression of SMAD2 and pSMAD3, thus preventing TGF-β-induced SLUG expression, a nuclear transcriptional repressor, which is responsible for the down-regulation of E-cadherin during the EMT. E-cadherin forms complexes with β-catenin and together mediate cell-cell adhesion. *NDRG1* knock-down confirmed this effect by loss of membrane E-cadherin and increased migration and invasion [81].

In connection with the previous signalling pathway, IKKα can even affect the TGF-β-mediated SMAD-dependent signalling pathway by forming a complex with transcription factors SMAD2/3 and regulating the transcription of SMAD-dependent genes (eg. *SLUG* and *SNAIL*, which both are E-cadherin repressors) [143].

1.4.4.3. NDRG1 and EGFR

EGFR is the RTK, which can bind several ligands. Ligands for EGFR include epidermal growth factor (EGF), TGF-α, amphiregulin, epiregulin, β-cellulin, and heparin-binding EGF. Upon activation, EGFR undergoes a transition from an inactive monomeric form to an active homo/heterodimer resulting in phosphorylation of specific tyrosine residues within its cytoplasmic tail. Phosphorylated tyrosine residues act as binding sites for proteins containing Src-homology 2 domains, which in turn activate downstream

signalling pathways including MAPK/ERK, STAT3, STAT5 and PI3K/AKT/mTOR (Illustration 6). Dysregulation of EFGR may lead to tumour initiation, progression, and metastasis [145].

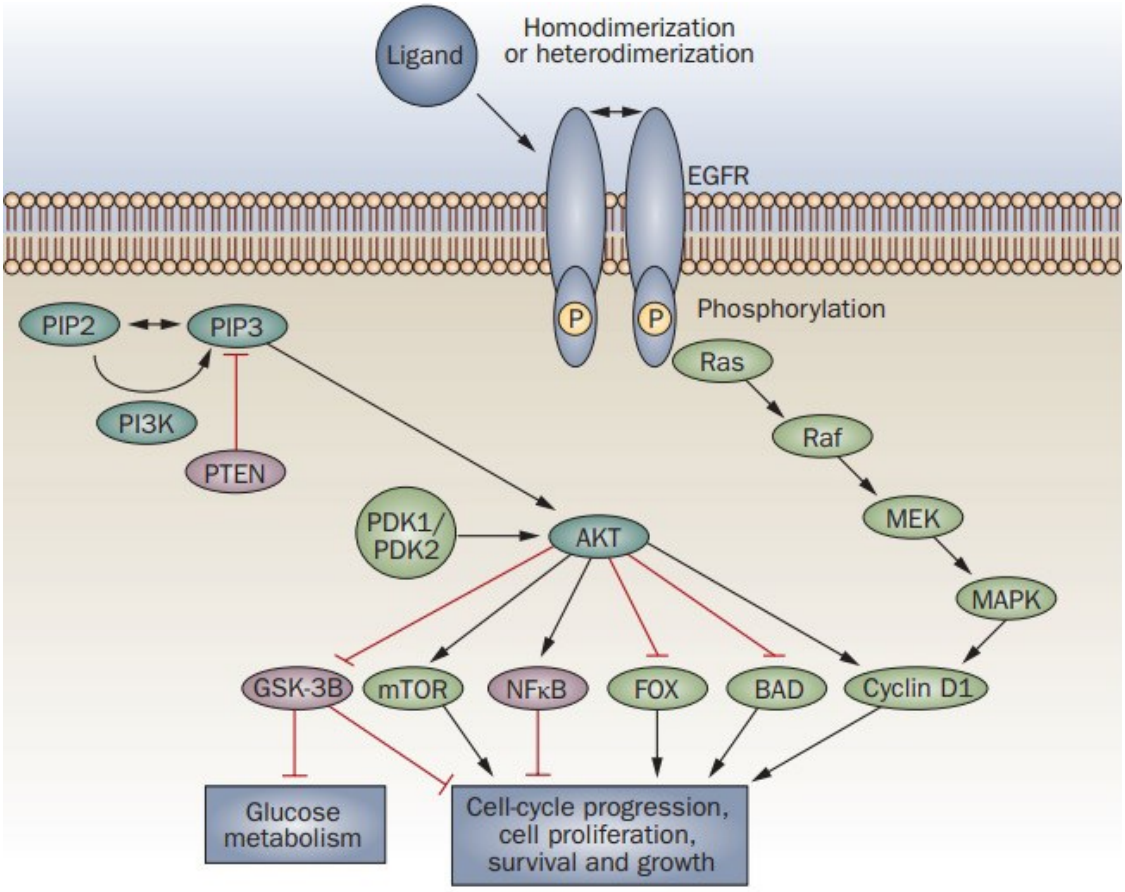

Illustration 6: The EGFR signalling. EGFR activation by its ligand results in a conformational change of the receptor and its dimerization with a second EGFR. Dimerization is essential for receptor function and autophosphorylation on key cytoplasmic residues. Activated receptor triggers downstream proteins and initiates a signalling cascade, including activation of the MAPK pathway or PI3K/AKT. Taken from [146].

In pancreatic and colon cancer cells, NDRG1 significantly downregulates EGFR protein level, but not its mRNA level. NDRG1 also attenuates phosphorylation of EGFR at various sites, including Tyr^{1068}, Tyr^{1086} and Tyr^{1148} [32]. The molecular mechanism behind the NDRG1-mediated EGFR downregulation includes increased expression of mitogen-inducible gene 6, which inhibits EGFR and facilitates its lysosomal processing and degradation [147].

1.4.4.4. NDRG1 and c-MET

c-MET, also known as hepatocyte growth factor receptor, is a high-affinity tyrosine kinase receptor for hepatocyte growth factor (HGF) (Illustration 7). It is a disulfide-linked

heterodimer made of 45 kDa α- and 145 kDa β-subunits. β-subunit of c-MET contains five catalytic tyrosines in its cytoplasmatic part. Interaction of c-MET with HGF results in autophosphorylation at the tyrosines, which can recruit several downstream signalling components, including its direct target GRB2-associated-binding protein 1 (GAB1). Phosphorylation at Tyr^{1003} is essential for c-MET degradation. Phosphorylation of $Tyr^{1234/1235}$ in the c-MET kinase domain upregulates kinase activity and results in autophosphorylation of Tyr^{1349} and Tyr^{1356}, leading to binding of an adaptor protein GAB1 and other signalling molecules. The canonical c-MET activation triggers MAPK/ ERK, PI3K, and the PKB/AKT. Aberrant activation of c-MET is associated with proliferation, invasion, and metastasis of cancer cells [148].

NDRG1 silencing has been shown to upregulate c-MET expression [31]. Concerning pancreatic cancer cells (PaCa), it was shown that c-MET induces secretion of sonic hedgehog from PaCa cells, which activates myofibroblast-like cells to secrete HGF and other growth factors, thus creating a positive feedback loop. NDRG1 was demonstrated to inhibit this cross-talk between cancer cells and stromal cells [149].

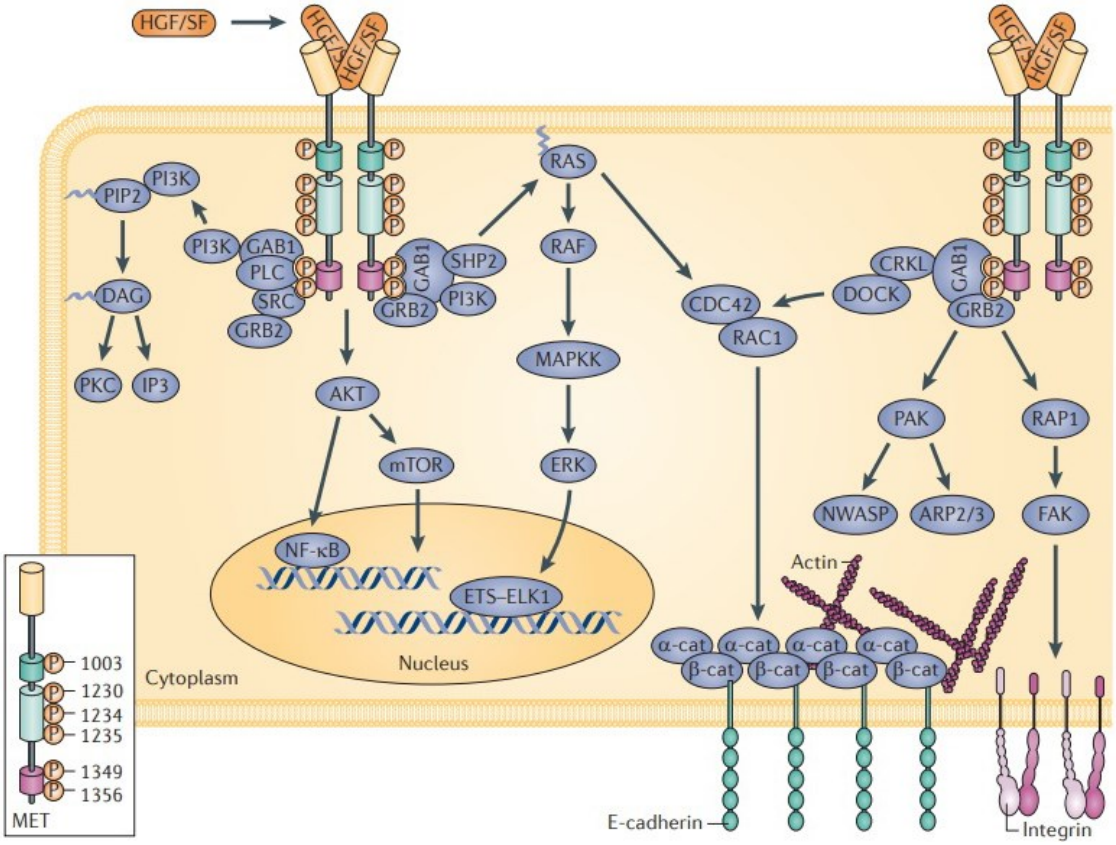

Illustration 7: Signalling pathways activated by HGF/SF and c-MET. Ligand-induced c-MET dimerization activates the tyrosine kinase by phosphorylation of tyrosine residues within the cytoplasmic domain. Phosphorylation (P) sites of c-MET are indicated. Activated receptor phosphorylates GAB1 that is bound to c-MET and can attract further docking proteins, which activate various downstream signalling cascades. Taken from [150].

1.4.4.5. NDRG1 and c-Src

c-Src is a non-receptor protein tyrosine kinase that transmits signals from stimulated receptors (e.g. EGFR) to the nucleus. It is encoded by the *c-src* gene, which belongs to a family of nine similar genes and occurs only in multicellular animals. It is one of the best-studied tyrosine kinases because it was the first cancer-causing gene that was discovered and its protein product was the first identified tyrosine kinase. c-Src is often overexpressed or hyperactivated in various types of tumours [151]. The c-Src activity is regulated by an inhibitory phosphorylation site at Tyr^{527} located in the carboxy-terminal tail and an activation loop bearing a positive-regulatory phosphorylation site at Tyr^{416} [152].

NDRG1 inhibits c-Src phosphorylation at Tyr^{416} resulting in a decrease of c-Src enzymatic activity and attenuation of p130Cas/CrkII/Rac1 mediated cellular migration [153].

1.4.4.6. NDRG1 and RhoA/ROCK1 signalling pathway

The signalling pathway mediated by ROCK1 is involved in the polymerisation of actin filaments (F-actin) and stress fibres formation, which affect the cell motility and migration. This signalling involves activation of Rho proteins by guanine nucleotide exchange factors. RhoA-GTP subsequently activates ROCK1 that has a broad range of substrates and is responsible for diverse cellular responses. One of its targets is MLC phosphatase, which is blocked by ROCK1, leading to increased phosphorylation of the pMLC2. In turn, phosphorylated MLC2 drives cell motility by stress fibre contraction [154].

NDRG1 inhibits cell motility *via* targeting the ROCK1 pathway, however, the precise mechanism is not known so far [127].

2. Aims

The overall aim of this thesis was to assess, whether the anti-cancer effect of mitochondrially targeted iron chelators also involves NDRG1 upregulation, besides the block of cellular respiration, inhibition of Fe-S cluster assembly and haem biogenesis, since NDRG1 upregulation has been described for non-targeted iron chelators. Further, we set to investigate whether the observed induction of NDRG1 could be an important molecular mechanism that has a direct impact on the potency of the iron chelators to inhibit the growth of cancer cells and whether signalling pathways modulated by NDRG1 may play a part in the effect. Answering these questions could lead to a deeper understanding of the effect of NDRG1 in carcinogenesis. Particular aims are described below:

- To characterise the expression of NDRG1 at mRNA and protein level in MCF7 and MRC5 cells after treatment with the targeted and non-targeted iron chelators.
- To evaluate the effect on the selected signalling pathways (EGFR, c-MET, NF-κB) in MCF7 and MRC5 cells after treatment with targeted iron chelators.
- To generate *NDRG1* knock-out MCF7 cells.
- To characterise *NDRG1* knock-out clones and assess the effect of *NDRG1* deletion on the ability to respond to targeted iron chelators.
- To assess immunogenic cell death by detection of calreticulin on the surface of MCF7 cells after exposition to targeted iron chelators.

2. Materials and methods

3.1. Methods

3.1.1. Cell culture

Human breast cancer cell line MCF7 and human fibroblasts MRC5 were used in all experiments. Both cells were cultured in complete Dulbecco's modified eagle medium (DMEM) under standard conditions (5% CO_2 humidified atmosphere, 37 °C). Cells were passaged as needed, approximately twice a week, and regularly checked for the presence of mycoplasma infection (MycoAlert Plus detection kit; Lonza). Both cell lines were authenticated by STR analysis (Generi Biotech)

3.1.2. RNA isolation

Cells were seeded into 60 mm plates and cultivated under standard cultivation conditions (5% CO_2 atmosphere, 37 °C) until they reached approximately 60-80 % of confluence. Then, they were treated with mitochondrially targeted and non-targeted compounds for 24 h. Next day, cells were washed two times with phosphate buffer saline (PBS), lysed with 500 µl RNAzol and transferred into 1.5 ml Eppendorf tubes. 200 µl of sterile RNase-free water and 2 µl of glycogen were added and the cell lysate was vortexed for 15 seconds. After 10 minutes of incubation at room temperature, samples were spun at 12,500×g for 15 minutes at room temperature, and the supernatant was transferred into a new sterile Eppendorf tube with 3 µl of 4-bromoanisole added beforehand. The content was vortexed for 10 seconds, incubated for 5 minutes at room temperature and spun at 12,500×g at room temperature. After that, the supernatant was transferred into a new sterile Eppendorf tube and an equal volume of ice-cold isopropanol was added. The content was carefully mixed until full homogenization and left at -20 °C overnight. Next day, the content was spun at 14,000×g at 4 °C for 15 min. The supernatant was discarded and the pellet was washed two times with 800 µl of 80% ethanol. Finally, all ethanol was removed, the pellet was dried in a heating block set to 55 °C for 1-2 minutes and approximately 30-50 µl (according to the pellet size) of RNase-free water was added to dissolve the pellet. After solubilisation, the concentration of isolated RNA was measured at 260 nm by using absorbance reader NanoDrop.

3.1.3. Reverse transcription

The reverse transcription was performed by using Revert Aid cDNA First Strand Synthesis Kit from ThermoFisher Scientific. 1 µl of 2× diluted Random primers was pipetted into 0.2 ml strips. Then, 500 ng of RNA and RNAse-free water were added so the total volume was 6 µl. Samples were then incubated in a polymerase chain reaction (PCR) cycler at 65 °C for 5 min and cooled down to 4 °C to ensure disruption of RNA secondary structures. After that, 4 µl of prepared RT mastermix mix containing 2 µl of 5x Reaction buffer, 0.5 µl of RiboLock RNase inhibitor, 1 µl of 10 mM dNTP and 0.5 µl of RevertAid M-MuLV Reverse Transcriptase (200 U/µl) per one reaction was added to the samples and incubated in PCR cycler with the following program: 45 °C 60 min, 75 °C 5 min, 10 °C indefinitely. Prepared complementary DNA (cDNA) was kept at -20 °C until need.

3.1.4. Quantitative PCR

Quantitative PCR (qPCR) was performed using HOT FIREPol® EvaGreen® qPCR Mix Plus kit from Solis Biodyne. Mastermix containing EVA Green, specific primers and water was prepared as follows: 1.58 µl of 5× EVA GREEN Mastermix, 0.20 µl of 10 µM forward/reverse primers (Table 1), and 3.48 µl of RNase-free water per reaction well. 5 µl of this mastermix was mixed with 10 ng cDNA in 2.5 µl of RNase-free water in appropriate well plates (384 white plates). The plate with samples was tightly covered with transparent optical tape and run in PCR cycler BioRad CFX384 on following protocol: 95 °C 12 minutes (initial denaturation), then 38× 95 °C for 10 seconds (denaturation), 60 °C for 20 seconds (annealing) and 72 °C for 20 seconds (extension and measurement in the SYBR/FAM channel). All data was analysed by ΔΔ Ct method using GeneEx 6, a qPCR data analysis software by MultiD.

Gene	**Manufacturer**	**Primer**
NDRG1	Generi Biotech	F 5'-CCAACAAAGACCACTCTCCTC-3' R 5'-CCATGCCCTGCACGAAGTA-3'
RPLP0	Invitrogen	F 5'-ATCACAGAGGAAACTCTGCATTCTCG-3' R 5'-GATAGAATGGGGTACTGATGCAACAGTT-3'

Table 1: List of primers for qPCR.

3.1.5. Whole cell lysate preparation

1×10^6 cells were seeded into 60 mm plates and cultured under normal conditions until they reached around 60-80 % of confluence. Then, 10 ml of fresh media was added together with different concentrations of mitochondrially targeted and non-targeted iron chelators. After 24 h of incubation, the medium was removed and cells were washed on ice with ice-cold PBS. Then, cells were gently scraped using a plastic cell scraper in 100 µl of ice-cold PBS and the cell suspension was transferred into a pre-cooled 1.5 ml Eppendorf tube. Cells were spun at 350×g for 5 min at 4 °C, the supernatant was removed and the pellet was resuspended in 70 µl of ice-cold lysis solution radioimmunoprecipitation assay (RIPA) with protease and phosphatase inhibitors. Cell lysates were mixed on ice on a shaker for 30 min and spun 11,000×g for 5 min at 4°C. Finally, the supernatant was transferred into new pre-cooled Eppendorf tubes and stored at -80 °C until use.

3.1.6. Isolation of nuclear and cytosolic fractions

Nuclear and cytosolic fractions were isolated using the Nuclear Extraction Kit from Active Motif. 1×10^6 cells were seeded into 100 mm plates and cultured under normal conditions until they reached around 60-80 % of confluence. Then, 10 ml of fresh media was added together with different concentrations of mitochondrially targeted and non-targeted iron chelator. After 24 h of incubation, the medium was removed and cells were washed twice on ice with ice-cold PBS. Then, cells were gently scraped using plastic cell scraper in 200 µl of 1× hypotonic buffer with protease/phosphatase inhibitors and the cell suspension was transferred into the pre-cooled 1.5 ml Eppendorf tube. After 15 min of incubation on ice, 10 µl of detergent was added to the suspension and mixed thoroughly by vortexing. Lysates were spun at 14,000×g for 30 seconds at 4°C. The supernatant, which represents the cytosolic fraction, was transferred into a new pre-cooled Eppendorf tube and the pellet was resuspended in 1× hypotonic buffer with protease/phosphatase inhibitors and spun again at 14,000×g for 30 seconds at 4°C. This step was repeated several times to clear the nuclear fraction from cytosolic. Then, the pellet was resuspended in approximately 50 µl RIPA supplemented with protease and phosphatase inhibitors. After 30 min incubation on ice with agitation, samples in RIPA were vortexed and spun at 14,000×g for 10 min at 4°C. The supernatant representing the nuclear

fractions was transferred into a pre-cooled microcentrifuge tube. Both, cytosolic and nuclear fraction, were stored at -80 °C until use.

3.1.7. Protein concentration assessment

Protein concentration was assessed using Pierce BCA Protein Assay Kit (Thermo Fisher Scientific) with bovine serum albumine (BSA) as the protein standard. This method is based on the reduction of cupric ions (Cu^{2+}) to cuprous ions (Cu^{1+}) by peptide bonds, known as the biuret reaction, and followed by the chelation of one Cu^{1+} with two molecules of bicinchoninic acid (BCA). Resulted purple-coloured complex of this reaction has a peak absorbance at 562 nm [155]. Albumin standards were prepared by diluting one BSA standard ampule at the concentration of 2 mg/ml into several Eppendorf tubes, using distilled water as the diluent. The final BSA standard concentrations were: 2,000, 1,000, 750, 500, 250 and 125 mg/ml. 20 µl of each BSA standard solution was pipetted in duplicates into a 96 well plate. In addition, 1 µl and 2 µl of each sample and 19 µl and 18 µl of water were pipetted into the plate. 200 µl of the BCA solution, which was prepared by mixing 50 parts of BCA Reagent A with one part of BCA Reagent B, was added to each well. The plate was incubated at 37 °C for 20 min and the absorbance was measured on TECAN at 562 nm. The amount of protein in each sample was calculated by interpolating from the standard BSA curve.

3.1.8. Sodium dodecylsulphate - polyacrylamide gel electrophoresis (SDS-PAGE) and Western blotting

30 µg of protein in each sample were mixed with 4×loading buffer and RIPA to achieve 1x SDS-PAGE loading buffer and 3 µg/µl concentration of proteins. The samples were incubated at 95 °C for 5 minutes. After the denaturation step, a prepared SDS-PAGE gel was loaded with samples and 10 µl of protein ladder was added to one lane (Spectra™ Multicolor Broad Range Protein Ladder from Thermo Scientific). Electrophoresis was run at 80 V for the first 15 min and 110 V for the rest of the run.

After electrophoresis, a Western blot transfer “sandwich” was prepared. Separated proteins were blotted onto PVDF membrane at constant 30 V, maximum of 200 mA per membrane, 4 °C, for 120 min. After blotting, the membrane was washed three times with TBS/T buffer and blocked for 1 h in 5% milk (w/v) dissolved in TBS/T buffer or, in the case of phosphorylated proteins, 5% BSA (w/v) dissolved in TBS/T buffer. After

blocking, the membrane was washed three times with TBS/T buffer. The primary antibody (Table 2) was diluted according to the manufacturer's instructions in 5% BSA (w/v) in TBS/T buffer. The membrane was incubated with the primary antibody overnight at 4 °C on a roller. Next day, the membrane was washed three times for 10 min with TBS/T buffer, incubated for 1 h with the corresponding secondary antibody (Table 3), which was diluted in 1% milk (w/v) in the TBS/T buffer or, in the case of phosphorylated proteins, in 1% BSA) in TBS/T buffer protected from light, and then washed three times for 10 min with the TBS/T buffer. Proteins were visualised by using chemiluminescent substrate WesternBright Sirius (Advansta, highly sensitive substrate) or Clarity western ECL (BioRad, normal substrate). Chemiluminiscent signal was detected by using CCD camera Azurec600.

Antibody	Dilution	Manufacturer	Catalogue number
NDRG1	1:1000	Thermo Scientific	42-6200
p-NDRG1 Ser^{330}	1:1000	Cell Signaling Technology	#3506
p-NDRG1 Thr^{346}	1:1000	Cell Signaling Technology	#5482
NDUFA9	1:7000	Abcam	ab14713
p-NF-κB Ser^{536}	1:1000	Cell Signaling Technology	3033P
NF-κB	1:1000	Cell Signaling Technology	8242P
p-IKKα/β $Ser^{176/180}$	1:1000	Cell Signaling Technology	2697P
IKKα	1:1000	Cell Signaling Technology	11930P
IKKβ	1:1000	Cell Signaling Technology	8943P
p-IκBα Ser^{32}	1:1000	Cell Signaling Technology	2859P
IκBα	1:1000	Cell Signaling Technology	4814P
p-MET Tyr^{1003}	1:1000	Cell Signaling Technology	#3135
p-MET $Tyr^{1234/1235}$	1:1000	Cell Signaling Technology	#3077
p-MET Tyr^{1349}	1:1000	Cell Signaling Technology	#3133
c-MET	1:1000	Cell Signaling Technology	#8198
GAB1	1:1000	Cell Signaling Technology	#3232
p-GAB1 Tyr^{307}	1:1000	Cell Signaling Technology	#3234
LDH-A	1:1000	Santa Cruz Biotechnology	sc-137243
Laminin B	1:1000	Santa Cruz Biotechnology	sc-6216
EGFR	1:1000	Santa Cruz Biotechnology	sc-373746
Actin-HRP	1:10 000	Santa Cruz Biotechnology	Sc-47778 HRP

Table 2: List of primary antibodies.

Antibody	Dilution	Manufacturer	Catalogue number
anti-rabbit IgG-HRP	1:10 000	MERCK/Sigma	AP132P
anti-mouse IgG-HRP	1:10 000	Invitrogen	31439

Table 3: List of secondary antibodies.

3.1.9. Vector digestion for CRISPR cloning

500 ng of 55 pX AsCpf1-Venus expression vector (Illustration 8), a kind gift of Bjorn Schuster (Institute of Molecular genetics, Czech Academy of Sciences), was digested with 1 µl FastDigest BpiL in reaction mixture together with 1 µl FastAP, 2 µl 10× FastDigest Green Buffer adjusted to the total volume of 20 µl with dH_20. The digestion product was run on 1% agarose gel in 1× TAE. The digestion backbone band was then visualised under UV, cut out and placed into a 1.5 ml microcentrifuge tube. Thereafter, ssDNA was extracted from the agarose gel using Zymoresearch DNA Clean & Concentrator kit and agarose dissociating buffer (ADB) according to the manufacturer's instructions. Vector DNA was stored at -20 °C until use.

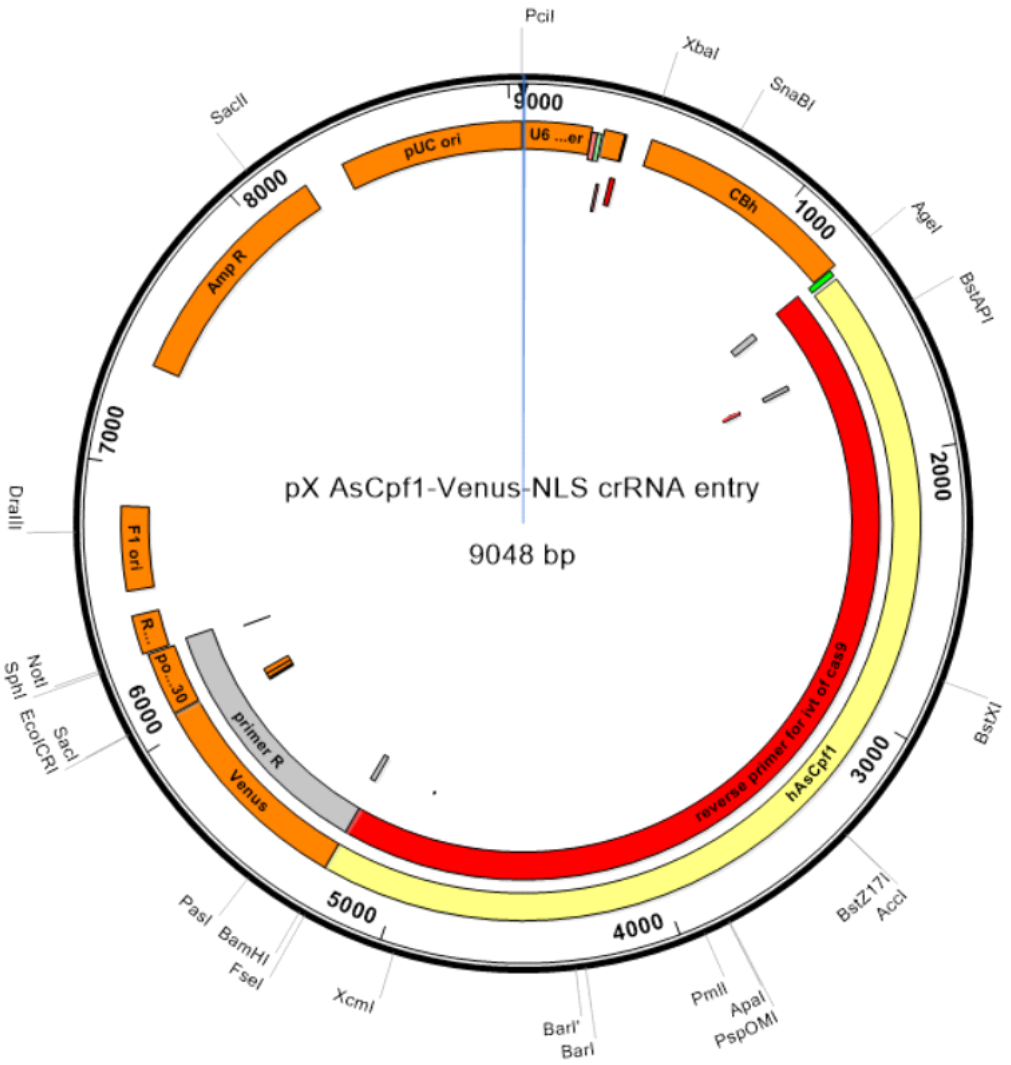

Illustration 8: Venus expression cloning vector.

3.1.10. Phosphorylation and annealing of oligos

Lyophilized oligos targeting exon 4 and adjacent introns within the *NDRG1* sequence are listed in the List of primers for targeting NDRG1 exon4 by CRISPR/*AsCpf1* (Table 4). Oligos contain the three sgRNA sequences which are underlined (Table 4). Oligos were diluted with RNAse-free water to a 100 µM stock. Then, the reaction containing 1 µl of each 100 µM oligos, 1 µl 10× T4 Ligation buffer, 6.5 µl dH_2O and 0.5 µl T4 Polynucleotide Kinase was prepared. The reaction run in thermocycler at 37 °C for 30 min, 95 °C for 5 min and then it was cooled down to 25 °C at 5 °C/min. Annealed and phosphorylated oligos were stored at -20 °C until use.

Name	Manufacturer	Primer sequence
NDRG1 CPF1 ex 4 F	Generi Biotech	5'-AGATCGCCACTCTCTTGGGAACCGGCTAATTTCTACTCTTGTAGATCCTTGGGAGTCCCACACAGCGTGAATTTCTACTCTTGTAGATAGGAAGCTCTCTTCTCATCTGGC-3'
NDRG1 CPF1 ex 4 R	Generi Biotech	5'-AAAAGCCAGATGAGAAGAGAGCTTCCTATCTACAAGAGTAGAAATTCACGCTGTGTGGGACTCCCAAGGATCTACAAGAGTAGAAATTAGCCGGTTCCCAAGAGAGTGGCG-3'

Table 4: List of primers for targeting NDRG1 exon 4 by CRISPR/*AsCpf1*.

3.1.11. Ligation and heat shock transformation of *E. coli* with plasmid DNA

The ligation reaction was prepared by mixing 50 ng of digested plasmid, 1 µl of diluted, annealed and phosphorylated oligo duplex (1:200), 1 µl of 10× T4 Ligation Buffer and dH_20 up to 10 µl subtotal and finally of 1 µl T4 DNA Ligase. Ligation was performed at room temperature for 30 minutes. Then, 2.5 µl of the ligation reaction were mixed with 50 µl competent bacterial cells (*E. coli,* TOP10 strain) in a microbiology test tube on ice. After 15 min of incubation on ice, the mixture was heat shocked by placing the tube into a 42 °C for 45 sec and then 2 min on ice. Then, 500 µl SOC media was added and kept for 1 h at 37 °C. After the incubation, the cells were pelleted and transferred to an agar plate supplemented with ampicillin and pre-heated at 37°C. Plates were placed upside down and incubated at 37 °C overnight.

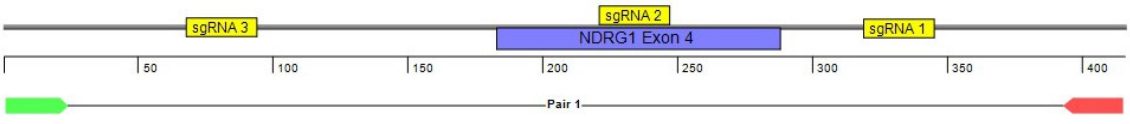

Illustration 9: Map of sgRNA binding sites and primers for sequencing and PCR amplification of the targeted locus.

3.1.12. Colony PCR after transformation

The colony PCR is a method used for colony screening to ensure that the DNA construct is actually present in these clones. Firstly, the bacterial plate from the previous day was checked for colonies and some of them were marked. Then, PCR mastermix containing 3 µl of 5× HotStart Master mix, 0.03 µl of F/R 100 µM primers (Table 5), 0.75 of µl

dimethylsulfoxide (DMSO), 0.15 of µl 10% Tween-20 and 11.07 of RNase-free water per reaction was prepared and aliquoted into a 96-well plate.

Name	Manufacturer	Primer sequence
PXPR	Generi Biotech	F 5'-GGACTATCATATGCTTACCGTAACTTGAAAG-3' R 5'-CCACTTTTTCAAGTTGATAACGGACTAGC-3'

Table 5: List of primers for colony PCR amplifying transfected vector.

Using a sterile pipette tip, one marked colony was picked, streaked onto a new agar plate and the pipette tip was transferred into the respective well containing the colony PCR mastermix. The agar plate was placed upside down into an incubator and incubated at 37 °C overnight to obtain bacterial streaks for inoculation and generation of plasmid DNA. Colony PCR was run in a Biometra thermocycler with the following protocol: 95 °C for 12 minutes (polymerase activation), 98 °C for 2 min (DNA denaturation), then 35× 95 °C for 10 seconds (denaturation), 60 °C for 30 seconds (annealing) and 72 °C for 35 seconds (elongation), and finally 72 °C for 4 minutes and 10 °C indefinitely. Meanwhile, 2% agarose gel in 1× TAE with GelRed dye (1:50,000) was prepared and 2-log DNA ladder and PCR products were loaded into particular wells. Electrophoresis was run at 70 V until the front reached the end of the agarose gel and then it was checked under UV and photographed. Selected clones that contained the insert were inoculated into 15 ml conical centrifugation tubes with 1 ml LB medium supplemented with ampicillin and kept growing at 37 °C with continuous shaking until cloudy. Afterwards, 100-200 µl of the bacterial starter culture was added to a new Erlenmeyer flask with 50 ml of LB supplemented with 200 µg/ml ampicillin and cultured at 37 °C with continuous shaking overnight. The grown bacterial culture was used for plasmid isolation with MIDI PREP.

3.1.13. Plasmid purification and sequencing

Plasmid isolation was performed by NucleoBond® Xtra Midi prep kit from Macherey-Nagel according to the manufacturer's instructions. Briefly, bacterial cells were pelleted in a centrifuge tube at 6,000×g for 10 min at 4 °C. Then, the pellet was resuspended in 8 ml Resuspension Buffer and lysed with 8 ml Lysis Buffer, which was added directly to the suspension. The mixture was gently mixed and incubated 5 min at room temperature followed by the addition of 8 ml Neutralization Buffer. The lysate was thoroughly mixed by inverting the tube until blue samples turned colourless. Then, the suspension was

loaded on NucleoBond® Xtra Column Filter and washed with 5 ml of Equilibration Buffer, followed by washing with 8ml Wash Buffer. Subsequently, plasmid DNA was eluted with 5 ml Elution Buffer and precipitated by adding 3.5 ml cold isopropanol. The precipitate was centrifuged at 15,000×g for 30 min at 4 °C. Then, the pellet was washed with 2 ml room-temperature 70% ethanol, centrifuged, dried at room temperature for 10-15 minutes and reconstituted in 150-300 µl TE buffer (according to the pellet size). After solubilisation at 55°C for 15 minutes, the concentration of isolated DNA was measured on NanoDrop. Then, 500 ng of isolated plasmid were diluted with sterile DNase-free water to the final volume of 9.75 µl in 1.5 ml Eppendorf tubes. After adding 0.25 µl of 100 µM sequencing primer, the Eppendorf tube was labelled with a barcode sticker (Eurofins Genomics Company, Light run barcodes) and sent for sequencing. Obtained sequences were analysed by DNASTAR software (data not shown).

3.1.14. Transfection

For transfection, 1×10^5 MCF7 cells were seeded into 6-well plates and let to attach overnight. Next day, 200 µl Opti-MEM medium per one reaction was mixed with 2.5 µl PLUS Reagent and 2,500 ng plasmid in one Eppendorf tube and 200 µl Opti-MEM medium with 5 µl Lipofectamine LTX in a second Eppendorf tube. After a 5 min incubation at room temperature, both solutions were mixed and incubated for 20 min. During the incubation phase, plasmid DNA should form complexes with Lipofectamine. Subsequently, 400 µl of the DNA-lipid complex was added to one well and incubated for 6 h (5% CO_2, 37 °C). After the incubation, the Opti-MEM medium was replaced by complete DMEM without ATB and cells were incubated for two days under standard conditions. Afterwards, cells were prepared for single cell sorting. Briefly, the cells were harvested by trypsinization, resuspended in medium with no fetal bovine serum (FBS) and sorted into 96 well plates in medium containing 20% FBS. Plates were regularly checked for the presence of clones. Selected clones were validated by Western blotting.

3.1.15. Genomic DNA (gDNA) isolation for CRISPR testing

Cells were harvested by trypsinisation and spun down at 350 ×g for 5 min at 4 °C. The Supernatants were aspirated and discarded, pellets were resuspended with 1 ml of DNazol by pipetting up and down, and left at 4 °C for 2 days to allow degradation of contaminating RNA. After that, lysates were spun down at 10,000 ×g for 10 min.

Supernatants were aspirated, pellets were mixed with 500 µl of absolute ethanol and left 30 min on rotating platform at room temperature. After subsequent spinning down at 10,000 ×g for 10 min, supernatants were discarded and pellets containing precipitated gDNA was washed twice with 70% ethanol. The precipitates were dried at 55 °C for several minutes and dissolved in 200 µl of 8mM NaOH and left 15 minutes at 55 °C followed by 15 min incubation at room temperature. The concentration of isolated DNA was measured at 260 nm by using absorbance reader NanoDrop. gDNA was stored at 4 °C until use.

3.1.16. Polymerase chain reaction

50 ng of genomic DNA was mixed with 5× HOT FIREPol® Blend Master Mix Ready to Load from Solis BioDyne and specific primers to gain 1x Master Mix with the template and primers (Table 6) and subsequently amplified in PCR cycler on following protocol: 98 °C 2 minutes, 95 °C 12 minutes, then 35× 98 °C 2 seconds, 60 °C 30 seconds, 72 °C 1 minutes, and finally 72 °C 5 minutes. The location of the primers is shown in the Illustration 9.

Gene	Manufacturer	Primer
NDRG1 seq ex 4	Generi Biotech	F 5'-AACAGCCCCAGGAAGTCCCAGG-3' R 5'-CCTAGCCCTGGTCCTTGGAGTGG-3'

Table 6: List of primers for PCR for agarose gel electrophoresis.

3.1.17. Agarose gel electrophoresis

For visualisation of PCR products, DNA agarose gel electrophoresis was run. 2% agarose gel with Gel Red dye (1:50,000) was prepared by agarose dissolving in 1× tris-acetate-ethylenediaminetetraacetic acid (EDTA) (1×TAE). Then, prepared agarose gel was loaded with PCR products and a molecular weight ladder was added to one line. Electrophoresis was run at 75 V as long as needed. Bands were visualized using CCD camera ChemiBis.

3.1.18. Assessment of cellular and mitochondrial level of reactive oxygen species

To assess the cellular ROS state, the cell/permeant probe dichlorofluorescein diacetate (DCF-DA) was used. The probe diffuses into the cell, where it is deacetylated by cellular esterases to a non-fluorescent impermeable compound, which is then oxidized by ROS into a highly fluorescent product dichlorofluorescein (DCF) [156]. 1×10^5 cells/ml were seeded into a 12-well plate and left to attach overnight (5% CO_2, 37 °C). The following day, cells were treated with DCF-DA at a final concentration of 5 µM. After 20 min of incubation, cells were washed two times with PBS, then 100 µl of warm trypsin was added into each well. Once the cells were detached, 400 µl of warm media was added into each well and the suspension was transferred into 1.5 ml Eppendorf tubes. Cells were pelleted at 500×g for 5 min, 4 °C. Then, the supernatant was removed and the pellet was resuspended in 100 µl of PBS and transferred into flow cytometry tubes. The fluorescence of DCF was measured at 504 nm excitation and 524 nm emission in LSR Fortessa. The acquired data were analysed using the FlowJo software.

For the evaluation of the mitochondrial level of ROS, the cell-permeable MitoSOX dye was used. The positively charged MitoSOX is rapidly targeted to the mitochondria, where is oxidized by superoxide and exhibits red fluorescence [157]. Cells were processed in the same way as in the case of cellular ROS, but instead of DCF-DA, MitoSOX was added at a final concentration of 2.5 µM. Mitochondrial ROS was measured at 510 nm excitation and 580 nm emission in LSR Fortessa.

3.1.19. Assessment of mitochondrial transmembrane potential ($\Delta\psi_m$)

To estimate the mitochondrial transmembrane potential, the tetramethyl rhodamine methyl ester (TMRM) dye was used. Cell permeant TMRM accumulates in highly negatively charged mitochondria with intact membrane potentials. The fluorescence intensity is proportional to the membrane potential. 1×10^5 cells/ml were seeded into a 12-well plate and left to attach overnight (5% CO_2, 37 °C). The following day, cells were treated with TMRM at a final concentration of 50 nM. After 20 min of incubation, cells were washed two times with PBS, then 100 µl of warm trypsin was added into each well. Once the cells were detached, 400 µl of warm media was added into each well and the suspension was transferred into 1.5 ml Eppendorf tubes. Cells were pelleted at 500×g for 5 min, 4 °C. Then, the supernatant was removed and the pellet was resuspended in 100

µl of PBS with 50 nM TMRM and transferred into flow cytometry tubes. The fluorescence of TMRM was measured at 548 nm excitation and 574 nm emission in LSR Fortessa. The acquired data were analysed using the FlowJo software.

3.1.20. Assessment of cell cycle

To evaluate the cell cycle, the Click-iT™ Plus EdU Flow Cytometry Assay Kit and Vybrant™ DyeCycle™ Violet Stain were used. 1×10^5 cells/ml were seeded into 6-well plates and cultured for two days (5% CO_2, 37 °C). After, the 5-ethynyl-2′-deoxyuridine (EdU) was added to each well at a final concentration of 10 µM. After 90 min of incubation at 37 °C, the cells were harvested by trypsinization and washed once with 1 ml of 1% BSA in PBS, spun down and the supernatant was removed. In the next step, the pellet was dislodged by adding 50 µl of Click-iT™ fixative and mixed well. After 15 of incubation at room temperature (protected from light), the cells were washed with 1 ml of 1% BSA in PBS, pelleted by centrifugation and the supernatant was removed. Then, the cell pellet was resuspended in 100 µl of 1× Click-iT™ permeabilization and wash reagent and incubated for 15 min at room temperature (protected from light). Meanwhile, Click-iT™ Plus reaction cocktail was prepared as follows: 438 µl PBS, 10 µl Cooper protectant, 2.5 µl Fluorescent dye picolyl azide and 50 µl Reaction Buffer Additive per one reaction. After incubation, 500 µl of the reaction cocktail was added to each well and incubated for another 30 min at room temperature (protected from light). After finishing the incubation, the cells were washed with 1 ml of 1% BSA in PBS, centrifuged and the supernatant was removed. Finally, the cell pellet was resuspended in 200 µl PBS with 20 µl Vybrant® DyeCycle™ Violet Stain and incubated 20 min at 37 °C. The cell cycle was measured in Flow Cytometer LSR Fortessa at 405 nm excitation and 437 nm emission for Vybrant dye and 410 nm excitation and 455 nm emission for picolyl azide. Analysis of the data was performed by the FlowJo software.

3.1.21. Real-time cell monitoring

Cells were seeded into a 96-well plate at 2.000 cells/well and let them attach overnight. Next day, they were added with 1µM mitoDFO and SYTOX green was added (0.5 µM final concentration; ThermoFisher Scientific), an impermeable nucleic acid stain detecting dead cells. Afterwards, images were acquired using Lumascope Etaluma720 placed in an incubator (37°C, 5% CO2). Phase contrast and green (SYTOX) fluorescence

images were captured every 3 hours for 93 h. Analyses (cell proliferation and cell count) were performed using the Lumaview Software and shown as a percentage of confluence and number of dead cells. The higher variability is an inherited feature of the assay since it depends on the corresponding amount of cells per selected field of view on each well, which are not uniform and sometimes differ quite significantly.

3.1.22. Confocal microscopy

Cells were seeded into a 12-well plate with coverslips on the bottom at 100.000 cells/well and let them attach overnight. Next day, cells were treated with compounds for 24 h. When incubation finished, cells were fixed with 4% paraformaldehyde for 15 min at room temperature and washed three times with PBS. Then, cells were permeabilized with permeabilization buffer for 10 min at room temperature with agitation of 50 rpm. After permeabilization, cells were washed three times with PBS and blocked with 5% BSA in PBS for 1 h at room temperature. Subsequently, cells were incubated with primary antibody (1:200; NDRG1 from Thermo Scientific, 42-6200) diluted in 5% BSA in PBS for 1 h, washed three times with PBS and incubated with secondary antibody (1:2,000; goat anti-rabbit AF488 from Life Technologies, A11034) and Hoechst 33342 (0.25 µl/ml) diluted in 5% BSA in PBS for 1 h at room temperature, protected from light. Then, cells were washed three times with PBS and placed in a microscope glass with 10 µM of mounting media. Finally, fluorescence was visualized on Leica SP8 confocal microscopy with using an immersion objective. Blue colour represents nuclei, green colour represents NDRG1.

3.1.23. Extracellular immunostaining for flow cytometry

The procedure was modified from [158] and [159]. Cells were seeded into a 6-well plate at 200.000 cells/well and let them attach overnight. Next day, cells were treated with compounds for 24 h. When incubation finished, cells were prepared by trypsinization and incubated with primary antibody (1:100; Calreticulin from Abcam, ab92516) diluted in Hank's balanced salt solution (HBSS) + 2% FBS for 1 h at room temperature. Then, cells were washed two times with HBSS + 2 mM glycine and incubated with secondary antibody (1:2,000; goat anti-rabbit AF488 from Life Technologies, A11034) diluted in HBSS + 2% FBS for 1 h at room temperature. Finally, cells were washed two times with HBSS + 2 mM glycine and resuspended in 100 µl of PBS. Propidium iodide (PI) was

added to each flow cytometry tube immediately before measuring to a final concentration of 0.5 µg/ml. The fluorescence was measured at 504 nm excitation and 524 nm emission for AF488 and 534 nm excitation and 617 nm emission for PI in LSR Fortessa. The acquired data were analysed using the FlowJo software.

3.2. Solutions

Separating gel

375 mM	Tris-HCl (pH 8.8)
0.1%	sodium dodecylsulphate (SDS)
8% or 10%	acrylamide/bis-acrylamide
0.05%	tetramethyl ethylenediamine (TEMED)
0.05%	ammonium persulfate (APS)

The solution was completed by adding dH_2O to obtain desired final concentrations. Polymerization reagents, TEMED and APS, were added just before gel pouring and mixed thoroughly.

Stacking gel

125 mM	Tris-HCl (pH 6.8)
0.1%	SDS
4%	acrylamide/bis-acrylamide
0.06%	TEMED
0.06%	APS

The solution was completed by adding dH_2O to obtain desired final concentrations. Polymerization reagents, TEMED and APS, were added before just gel pouring and mixed thoroughly.

Running buffer (10×)

250 mM	Tris
1.92 M	Glycine
34.7 mM	SDS

The solution was completed to a final volume of 1,000 ml with dH_20. 1× Running buffer was prepared by adding 100 ml of 10× Running buffer to 900 ml of dH_20.

SDS-PAGE loading buffer (4×)

250 mM	Tris-HCl (pH 6.8)
40%	Glycerol
8%	SDS
20%	β-mercaptoethanol
0.02%	bromphenol blue

The solution was completed to a final volume of 10 ml with dH_20.

Transfer buffer (10×)

250 mM	Tris
1.92 M	Glycine

The solution was prepared in 1,000 ml with dH_20. 1× Transfer buffer was prepared by adding 100 ml of 10× Transfer buffer to 700 ml of $dH_20$and subsequently adding 200 ml of methanol.

Tris buffer saline (TBS, 20×)

3 M	NaCl
0.4 M	Tris

The solution was prepared in 1,000 ml of dH_2O and pH was adjusted to 7.55. 1× TBS/Tween (TBS/T) was prepared by adding 50 ml of TBS and 500 µl of Tween-20 to 950 ml of dH_2O.

Complete DMEM media for cell cultivation

500 ml	DMEM (Sigma; D6429)
100 µg/ml	Streptomycin
100 U/ml	Penicillin
2 mM	L-glutamine
10%	FBS

RIPA lysis buffer

150 mM	NaCl
50 mM	Tris (pH 8)
1%	NP-40
0.1%	SDS
1 mM	EDTA
0.5%	Na-Deoxycholate

The solution was completed to a final volume of 200 ml with dH_20.

SOC medium

2.5 mM	KCl
10 mM	$MgCl_2$
10 mM	$MgSO_4$
20 mM	Glucose

All reagents were dissolved in 50 ml dH_2O. Then, solutions were added to LB media to desire final concentrations.

Electrophoresis Buffer (TAE, 50×)

2 M	Tris free base
50 mM	Disodium EDTA
1 M	Acetic Acid

At first, Tris and EDTA were dissolved in 700 ml dH_2O. Then, Acetic Acid was added and the buffer was made up to 1000 ml. 1× TAE was prepared by adding 20 ml of 50× TAE to 980 ml of dH_20.

TE buffer

10 mM	Tris
1 mM	EDTA

The solution was prepared in 50 ml of dH_2O and pH was adjusted to 8.

Permeabilization Buffer

100 mM	Glycine

Glycine was dissolved in 200 ml PBS. Then, 150 µl of Tween-20 and 150 µl of Triton X-100 were added. The solution was filtered before use.

Molecular weight ladder

30 µg/ml	2-log DNA ladder
1×	TAE
0.5×	Fast digest buffer
0.5×	DNA loading dye

The solution was completed with dH20.

3.3. Iron chelators

3.3.1. Dp44mT

Dp44mT with molecular weight 285.37 was dissolved to the desired concentration in DMSO.

3.3.2. DFO

DFO with the molecular weight 560.68 was dissolved to the desired concentration in DMSO.

3.3.3. DFX

DFX with the molecular weight 373.4 was dissolved to the desired concentration in DMSO.

3.3.4. mitoDFO

mitoDFO with the molecular weight 1434.67 was dissolved to the desired concentration in DMSO.

3.3.5. mitoDFX

mitoDFX with the molecular weight 809.39 was dissolved to the desired concentration in DMSO.

4. Results

4.1. Mitochondrially targeted iron chelators increase *NDRG1* mRNA

It was already shown in several reports that standard iron chelators as well as novel thiosemicarbazones can markedly induce *NDRG1* expression, which subsequently suppresses pro-oncogenic cellular mechanisms within cancer cells. The novel class of chelators, mitochelators, including mitoDFO and mitoDFX are currently studied in our laboratory. Both mitochondrially targeted iron chelators have shown enhanced anti-tumour efficiency against breast cancers as well as other cancer types. The effects of mitoDFO on cancer cells has been described in our recent publication with reported inhibitory concentration $IC_{50} = 1.4 \pm 0.2$ for MCF7 and $IC_{50} = 6.6 \pm 1.3$ for MRC5 [37]. The second compound, mitoDFX, is under pending patent application and is even more effective, yet, due to the proprietary nature of this research, full experimental data regarding its efficacy and its structure are not shown. Nevertheless, although there is solid evidence showing that mitoDFO affects mitochondrial respiration, Fe-S cluster assembly and haem biosynthesis and induces mitophagy, there still might be additional mechanisms that underlie the biological effect of these chelators that have not been fully understood yet. In this study, we focused on investigating a new potential mechanism of mitochondrially targeted iron chelators and defining the link between these agents and NDRG1.

As an experimental model for our research, we chose MCF7 breast cancer cell line. MCF7 is a widely studied human epithelial cancer cell line derived from breast adenocarcinoma and has characteristics of differentiated mammary epithelium. The main characteristic of MCF7 cell line is its responsiveness to oestrogen in form of oestradiol, thus it is classified as an oestrogen receptor (ESR) positive cell line. It is also progesterone-receptor positive and HER2 negative. Besides, MCF7 is a poorly aggressive and non-invasive cell line with low metastatic potential [160]. MCF7 cells are sensitive to mitoDFO in *in vitro* settings and to express *NDRG1* upon hypoxia or pseudohypoxia [161]. To compare malignant cells with their non-malignant counterparts we used MRC5 fibroblasts derived from human lung tissue [162].

To investigate whether mitoDFO and mitoDFX are able to increase transcription of the *NDRG1*, we isolated mRNA from MCF7 breast cancer cells and MRC5 fibroblast pre-treated for 24 h with increasing concentrations of mitoDFO or mitoDFX ranging from

30 nM to 3 μM. It has been reported that mitoDFO has a primarily cytostatic effect in this concentration range, meaning that it inhibits cell cycle and division, but does not activate cell death [37]. mitoDFX has a similar effect on malignant cells, however it is more potent (unpublished data). Dp44mT was used as a positive control. Then, quantitative PCR was performed to assess the amount of *NDRG1* mRNA (Figure 1).

As we expected, Dp44mT markedly increased expression of *NDRG1* mRNA in a dose-dependent manner in MCF7 cells (Figure 1A). In MRC5 cells, *NDRG1* was also significantly induced at higher concentrations of Dp44mT, however, the highest measured expression occurred at 1 μM concentration and at 3 μM of Dp44mT the mRNA expression was slightly decreased (Figure 1B). MCF7 cells as well as MRC5 treated with mitoDFO for 24 h did not show any change in relative *NDRG1* expression (Figure 1C, D). Conversely, mitoDFX significantly increased the level of *NDRG1* mRNA in MCF7 cells in the highest tested concentration and slightly increased it in MRC5 (Figure 1E, F).

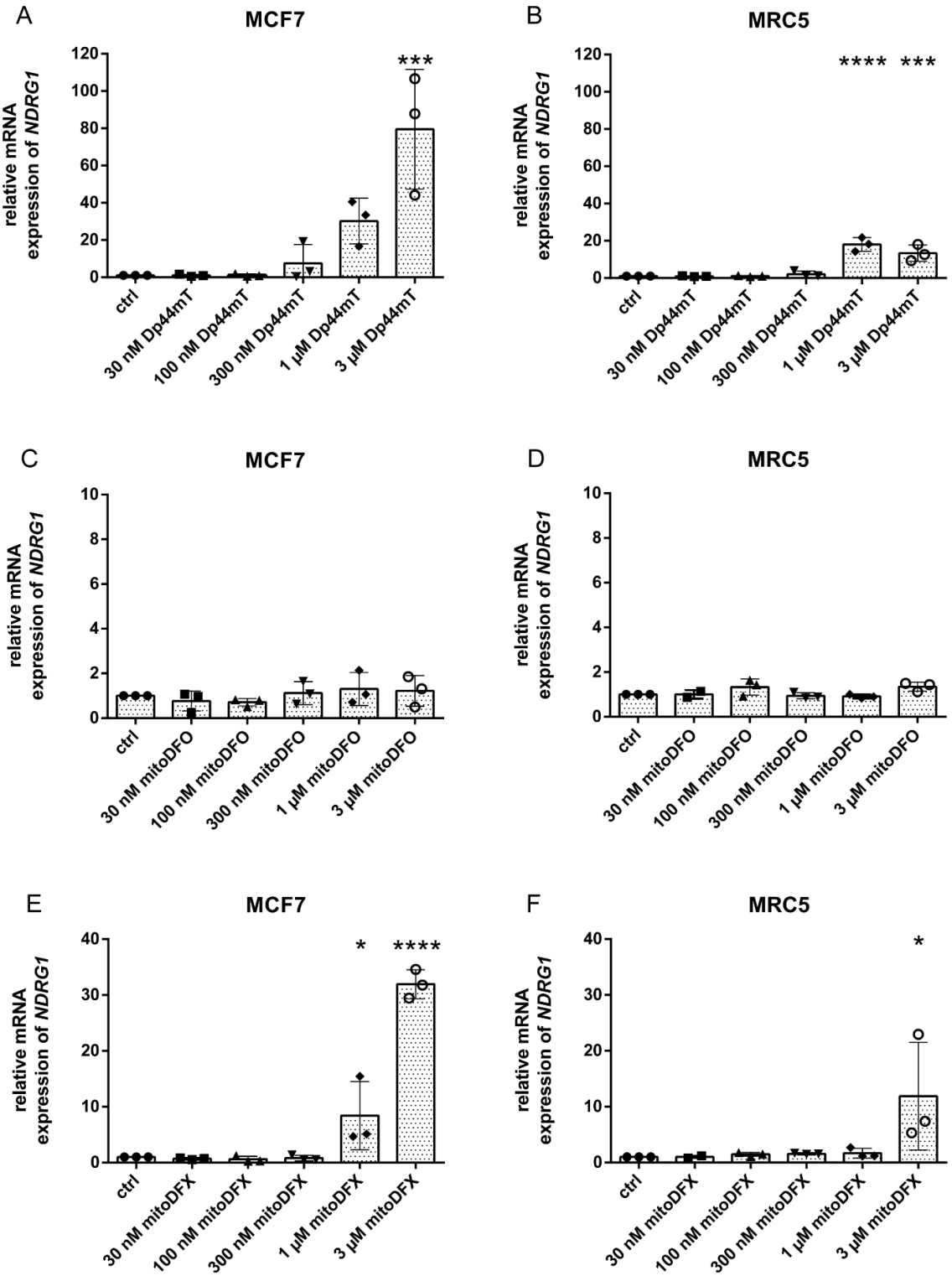

Figure 1: Relative expression of *NDRG1* mRNA after 24 h exposition to iron chelator Dp44mT and mitochondrially targeted iron chelators. Expression of *NDRG1* in (A, C, E) MCF7 and (B, D, F) MRC5 cells was analysed by qPCR. *NDRG1* expression was normalised to the human ribosomal large protein P0 gene (*RPLP0*). Data are shown as relative expression of *NDRG1* and represent the mean ± SD of three independent replicates. Statistical significance was determined by one-way ANOVA using GraphPad PRISM software, where the values obtained from the treated cells were compared to the control values; * $p < 0.05$, ** $p < 0.01$, *** $p < 0.001$, **** $p < 0.0001$.

4.2. Mitochondrially targeted chelators increase NDRG1 at the protein level and affect its phosphorylation

In the previous section, we demonstrated the expression of the *NDRG1* gene in MCF7 and MRC5 cells after treatment with selected iron chelators. Therefore, we next assessed the total protein level of NDRG1 and the level of its phosphorylated forms at Ser^{330} and Thr^{346} (Figure 2, Figure 3).

We observed increased expression of total NDRG1 as well as both its phosphorylated forms after 24 h incubation with Dp44mT in MCF7 and MRC5 cells, which is consistent with qPCR results (Figure 2A, B). In MRC5 cells, as with mRNA, we saw an increased protein level of NDRG1 and its phosphorylated forms starting at 1 μM concentration (Figure 2B). Treating MCF7 cells with mitoDFO showed an increasing level of total NDRG1 protein with increasing concentration of the compound, but the extent of induction is much smaller. Similarly, there was an increase in p-NDRG1 Thr^{346}, whereas there was no change in p-NDRG1 Ser^{330} (Figure 2C). In MRC5 cells, the levels of all NDRG1 forms were unchanged by mitoDFO. NDUFA9, a subunit of the enzyme NADH dehydrogenase that is destabilised under iron deprivation, was decreased with increasing concentrations of mitoDFO (Figure 2D), which suggested that mitoDFO was indeed active [37]. After treatment with mitoDFX for 24 h, all NDRG1 variants were significantly increased in MCF7 and MRC5 cells in a dose-dependent manner (Figure 2E, F).

In order to compare the effect of the mitochondrially targeted iron chelators and their parental non-targeted counterparts, we incubated cells with several concentrations of each chelator (Figure 3). The comparison of mitochondrially targeted and non-targeted chelators showed that mitoDFO was the least potent in induction of NDRG1 in malignant (MCF7) and non-malignant cell lines (MRC5). Non-targeted DFO was, on the other hand, able to induce NDRG1 and its phosphorylated forms in MCF7 as well as MRC5 cells. mitoDFX at 3 μM concentration increased the expression of NDRG1 much more than 3 μM concentration of its non-targeted counterpart in the MCF7 cell line and was more effective in malignant cells. Dp44mT served as positive control and induced NDRG1 significantly in both malignant and non-malignant cells. Subsequently, the levels of NDRG1 protein upon induction were confirmed by using confocal microscopy (Figure 4, Figure 5, Figure 6, Figure 7). Confocal images showed the same trend in NDRG1 induction in malignant and non-malignant cells as immunoblotting. However, these two

lines differed in the subcellular distribution of the NDRG1 protein. In MCF7 cells, upon iron chelation, NDRG1 localization showed a punctate pattern, often near the nucleus, which was best visible for non-targeted DFO (Figure 4, Figure 5). In contrast, MRC5 cells showed a more diffuse pattern of NDRG1 staining for all compounds (Figure 6, Figure 7).

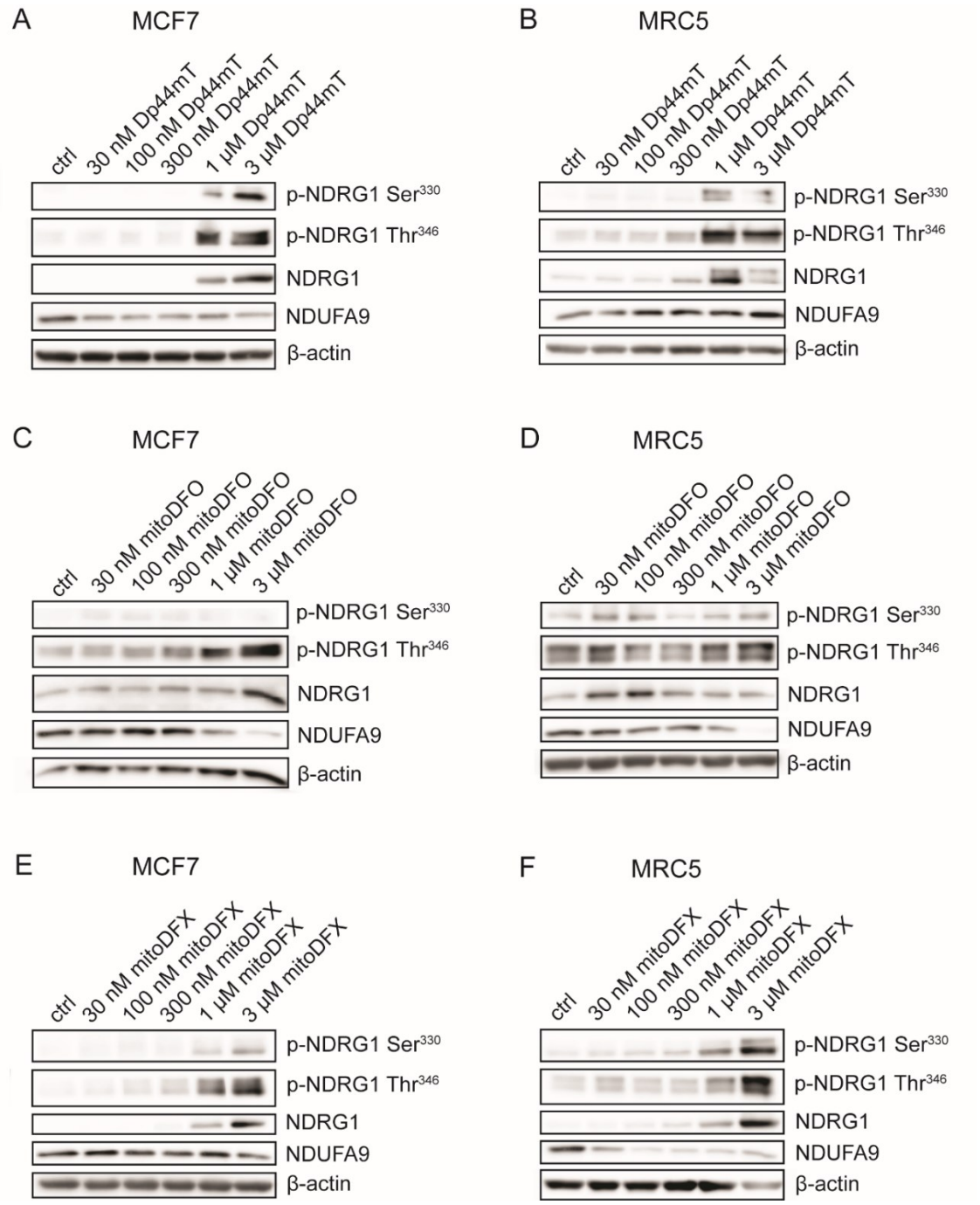

Figure 2: Protein level of NDRG1 after 24 h exposition to iron chelator Dp44mT and mitochondrially targeted iron chelators. Protein levels of NDRG1 in (A, C, E) MCF7 and (B, D, F) MRC5 cells were analysed by western blotting. MCF7 and MRC5 cells were treated with different concentrations of Dp44mT, mitoDFO or mitoDFX. After 24 h of incubation, cells were harvested and whole cell lysates were prepared. Equal amounts (30 µg of proteins) of cell lysates were separated onto 10% bis-acrylamide gel, then transferred onto PVDF membrane. The membrane was immunoblotted with NDRG1, p-NDRG1 Ser^{330}, p-NDRG1 Thr^{346} and NDUFA9 antibodies overnight. Then, membrane was washed and incubated with anti-rabbit or anti-mouse secondary antibody for 1 h. Detection of proteins expression was performed using enzyme-linked chemiluminescence or fluorescence. β-actin was used as a loading control.

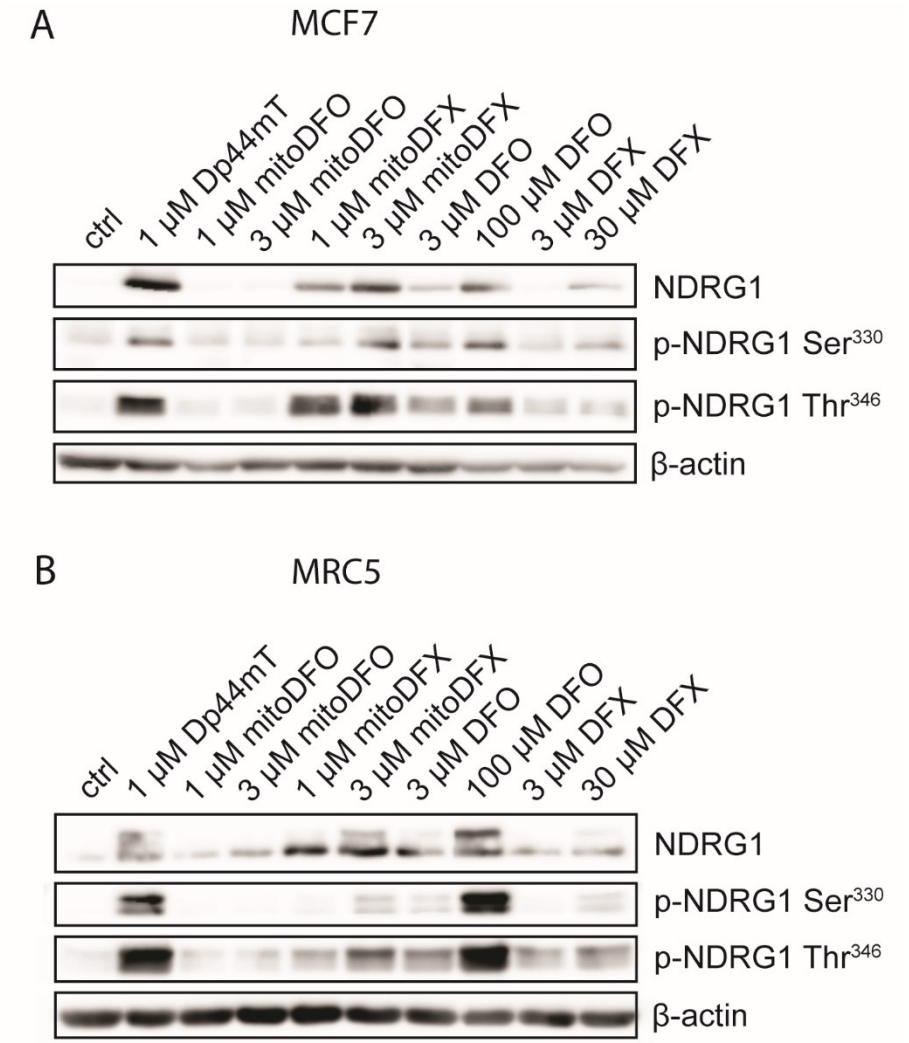

Figure 3: Comparison of NDRG1 protein level after 24 h exposition to mitochondrially targeted or non-targeted iron chelators. Protein levels of NDRG1 in (A) MCF7 and (B) MRC5 cells were analysed by western blotting. MCF7 and MRC5 cells were treated with different concentrations of Dp44mT, mitoDFO, mitoDFX, DFO or DFX. After 24 h of incubation, cells were harvested and whole cell lysates were prepared. Equal amounts (30 µg of proteins) of cell lysates were separated onto 10% bis-acrylamide gel, then transferred onto PVDF membrane. The membrane was immunoblotted with NDRG1, p-NDRG1 Ser^{330} and p-NDRG1 Thr^{346} antibodies overnight, and then washed and incubated with anti-rabbit or anti-mouse secondary antibody for 1 h. Detection of proteins expression was performed using enzyme-linked chemiluminescence system. β-actin was used as a loading control.

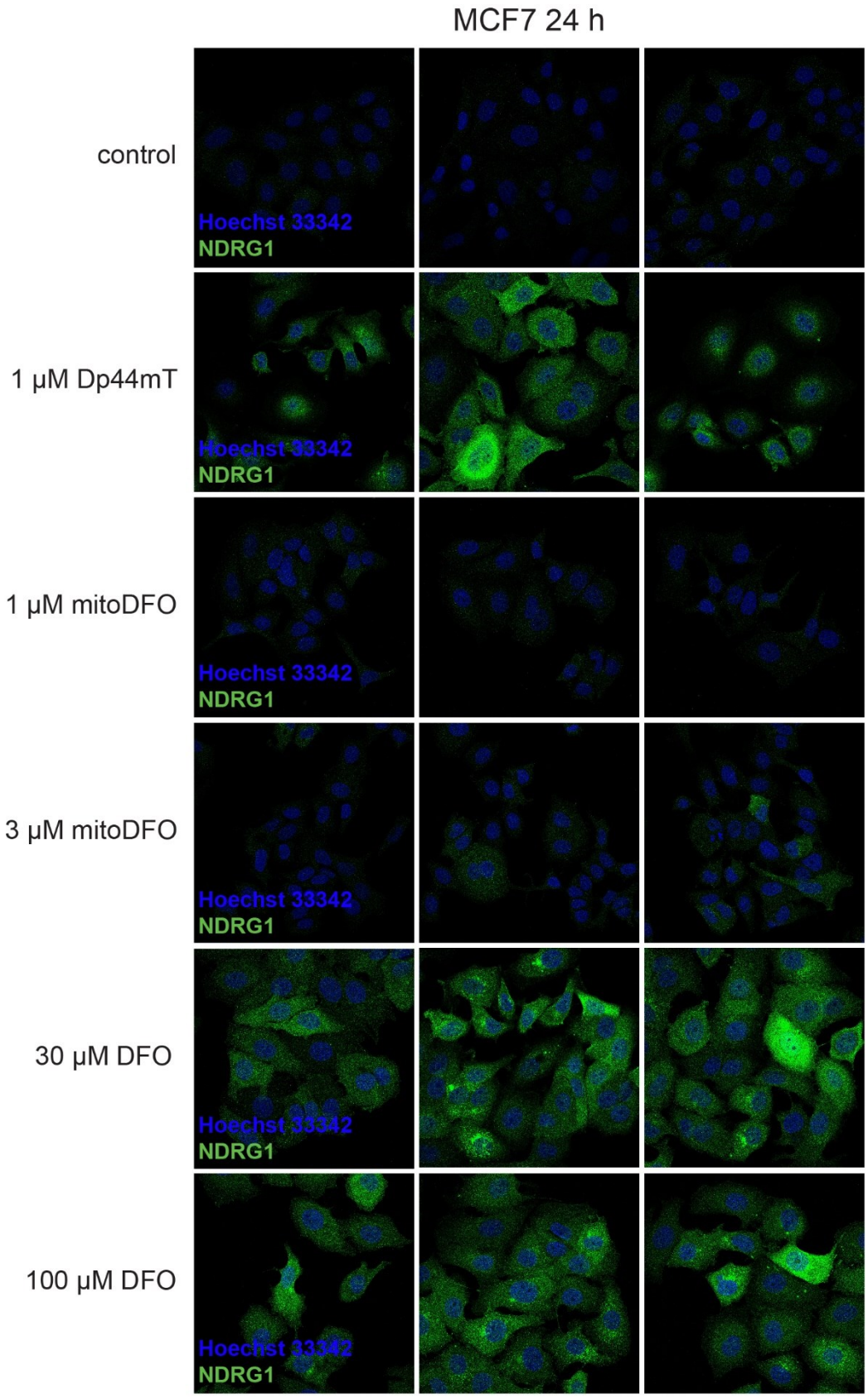

Figure 4: Comparison of NDRG1 protein level after 24 h exposition to mitochondrially targeted or non-targeted iron chelators in MCF7 by confocal microscopy. Representative confocal immunofluorescence images demonstrate staining for NDRG1 (green) and Hoechst 33342 for nuclei (blue).

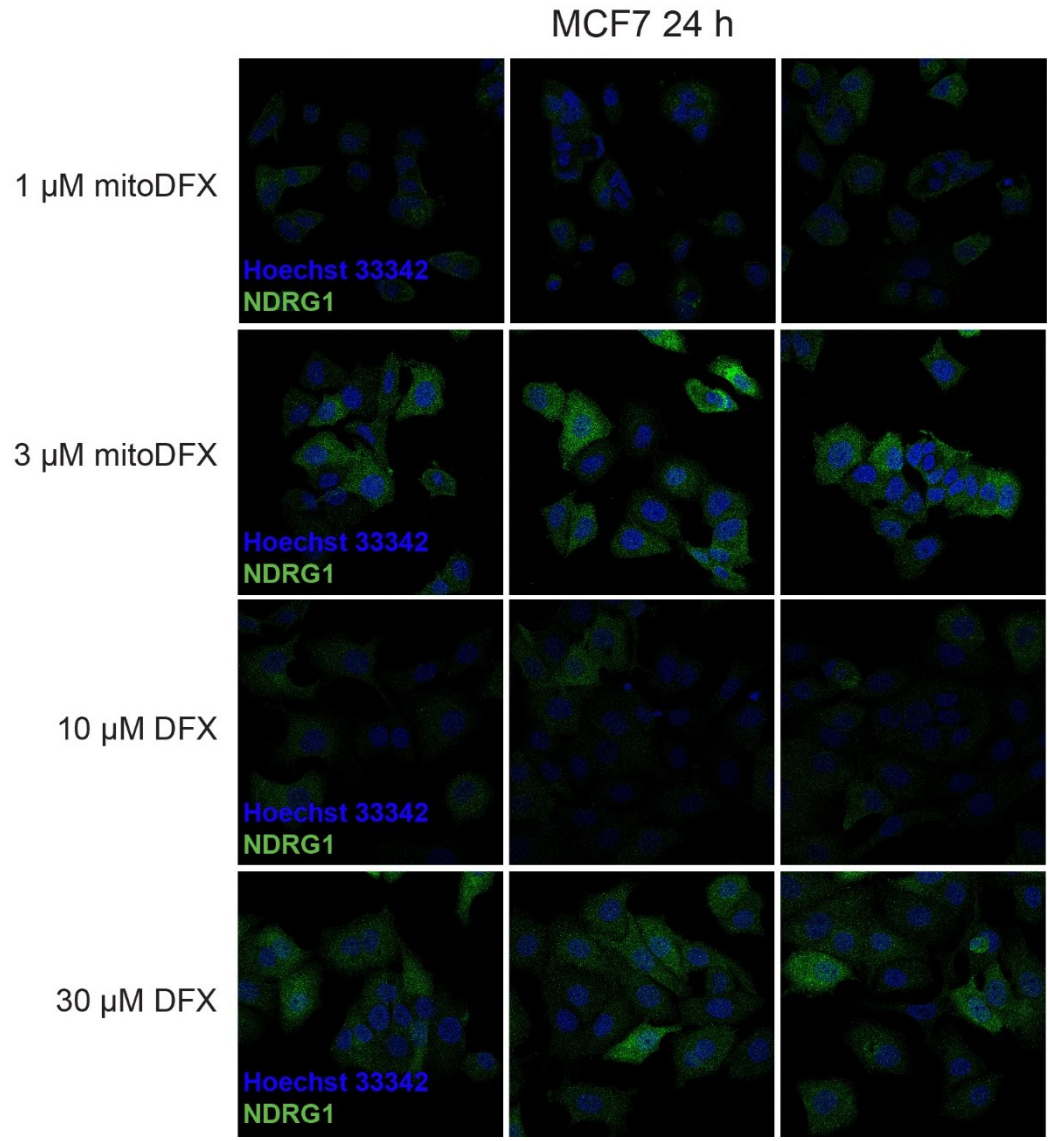

Figure 5: Comparison of NDRG1 protein level after 24 h exposition to mitochondrially targeted or non-targeted iron chelators in MCF7 by confocal microscopy. Representative confocal immunofluorescence images demonstrate staining for NDRG1 (green) and Hoechst 33342 for nuclei (blue).

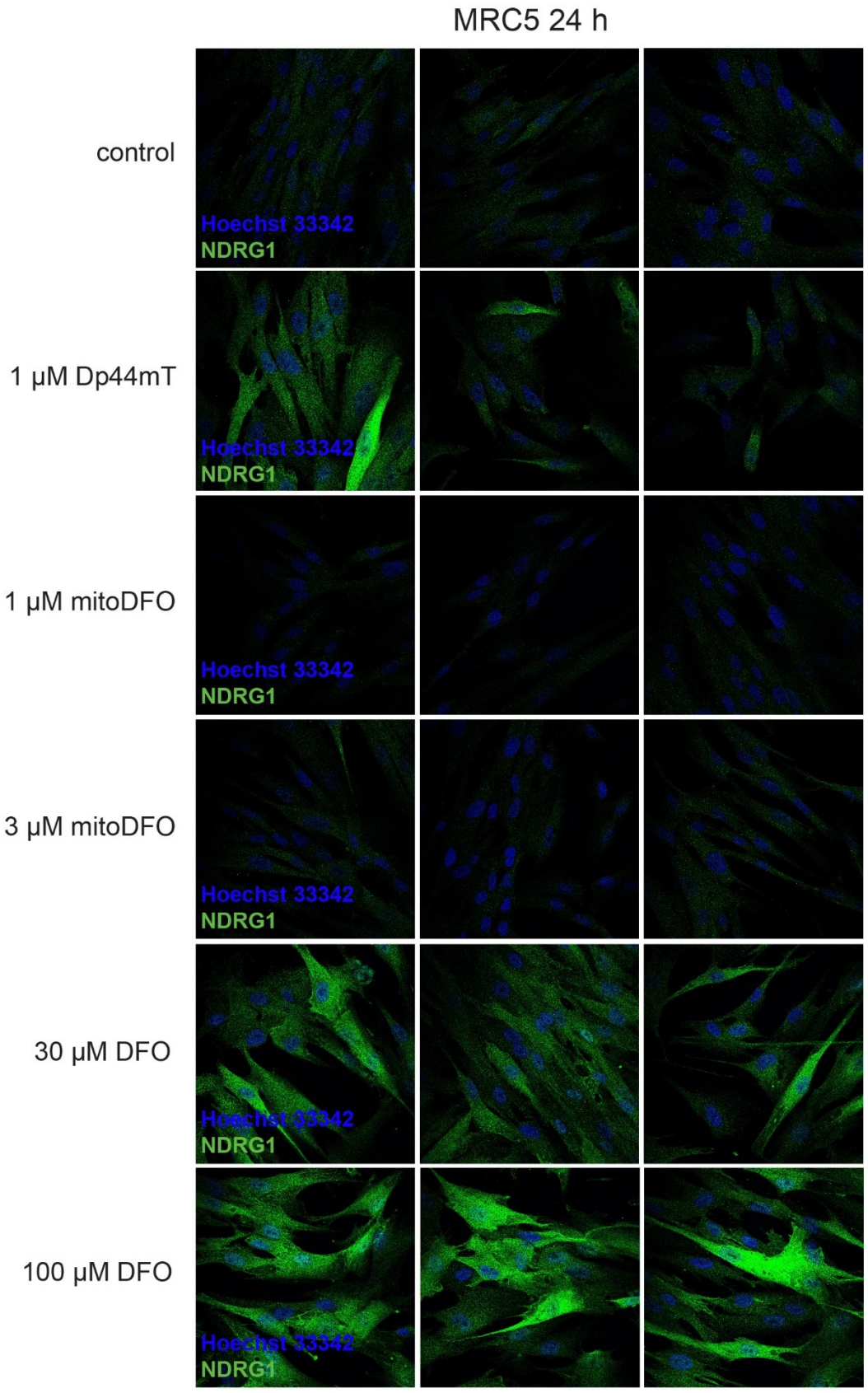

Figure 6: Comparison of NDRG1 protein level after 24 h exposition to mitochondrially targeted or non-targeted iron chelators in MRC5 by confocal microscopy. Representative confocal immunofluorescence images demonstrate staining for NDRG1 (green) and Hoechst 33342 for nuclei (blue).

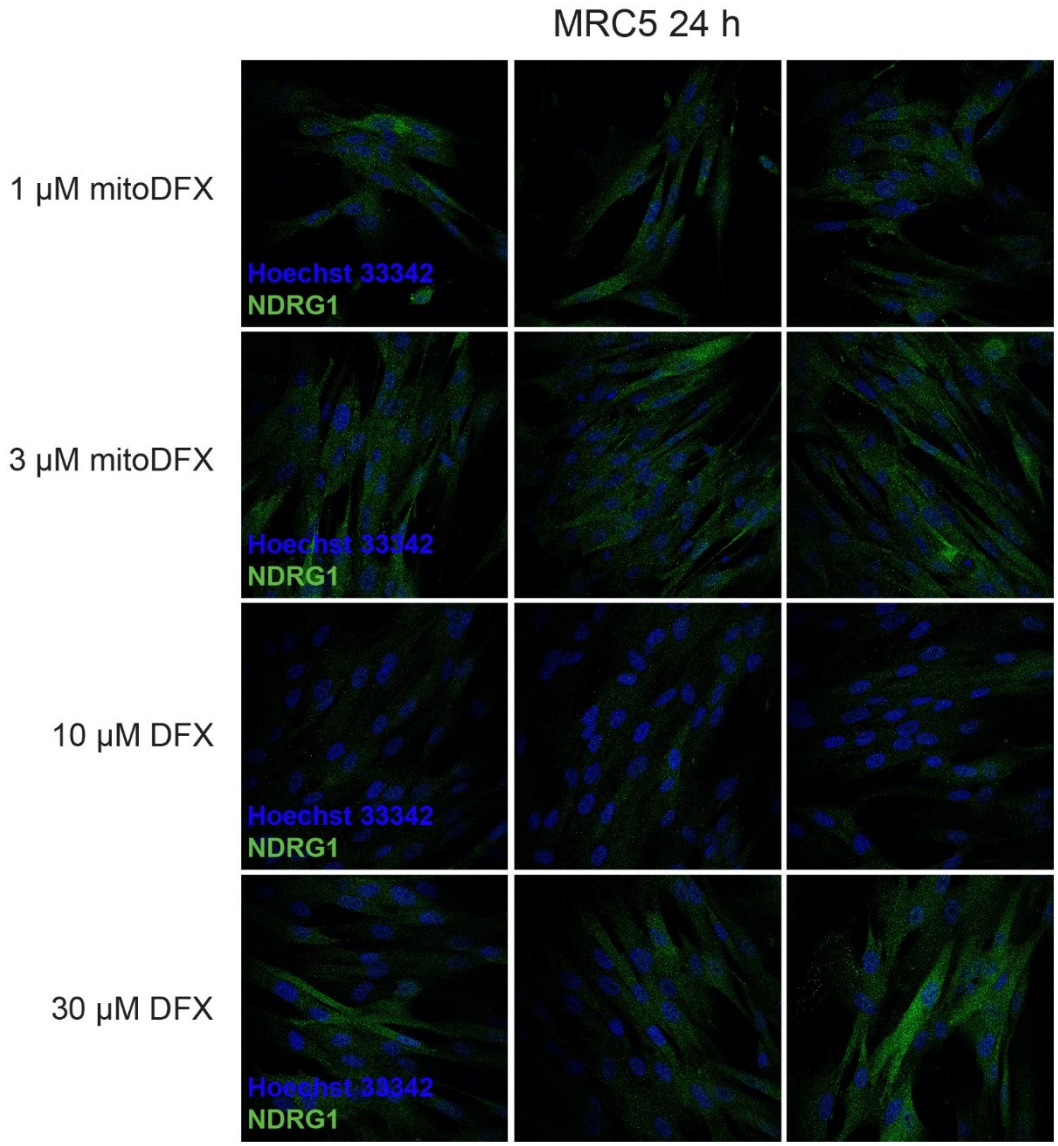

Figure 7: Comparison of NDRG1 protein level after 24 h exposition to mitochondrially targeted or non-targeted iron chelators in MRC5 by confocal microscopy. Representative confocal immunofluorescence images demonstrate staining for NDRG1 (green) and Hoechst 33342 for nuclei (blue).

4.3. The effect of iron chelation on the NDRG1 downstream signalling pathways: c-MET

Increased level of proto-oncogene c-MET, its phosphorylation and downstream effector, GAB1, have been shown in human prostate cancer cells DU145 and human hepatocellular carcinoma Huh7 cells upon *NDRG1* silencing the. Moreover, Dp44mT has been shown to decrease c-MET expression *via* an NDRG1 independent mechanism [31]. We asked if mitochondrially targeted deferoxamine or deferasirox would also affect this proto-oncogenic signalling pathway in MCF7 cells. To answer this question, we cultivated cells in the presence of iron chelating compounds for 24 h and then the relevant proteins were detected by western blotting.

In MCF7 cells, Dp44mT significantly increased the total level of c-MET, however, it did not affect the level of any p-MET residues. Also, Dp44mT increased total GAB1 and its phosphorylated form. We observed a similar effect for 3 μM mitoDFO, where total c-MET, GAB1 and p-GAB1 Tyr^{307} were slightly increased. mitoDFX did not affect the expression of c-MET or its adaptor protein (Figure 8A).

In MRC5 cells, Dp44mT had an opposite effect on c-MET expression than in MCF7 cells. The treatment with Dp44mT for 24 h markedly reduced total c-MET, GAB1 and p-GAB1 Tyr^{307}. The levels of p-MET were not changed. The same effect on the reduction of c-MET and its adaptor protein was observed after exposition to mitoDFX, where the lower band disappeared at 3 μM concentration. mitoDFO did not affect the expression of c-MET in MRC5 cells (Figure 8B).

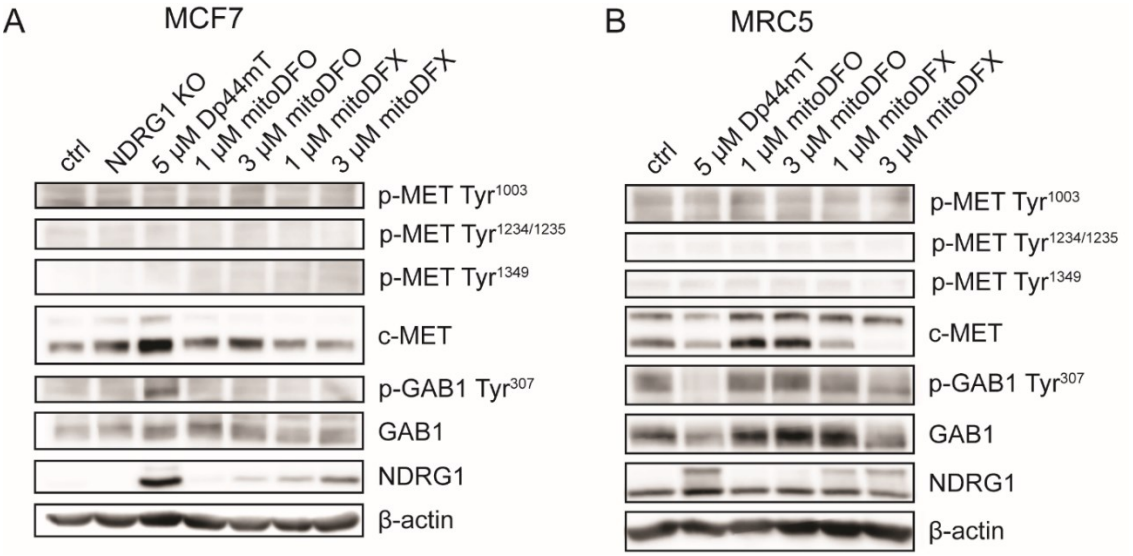

Figure 8: Effect of iron chelation on c-MET in MCF7 and MRC5 cells. Protein level of c-MET, its direct target GAB1 and NDRG1 were analysed by western blotting. MCF7 or MRC5 cells were treated with different concentrations of Dp44mT, mitoDFO and mitoDFX. After 24 h of incubation, cells were harvested and whole cell lysates were prepared. Equal amounts (50 µg of proteins) of cell lysates were separated onto 8% bis-acrylamide gel, then transferred onto PVDF membrane. The membrane was immunoblotted with c-MET, p-MET Tyr^{1003}, p-MET Tyr$^{1234/1235}$, p-MET Tyr^{1349}, GAB1, p-GAB1 Tyr^{307} and NDRG1 antibodies overnight, and then washed and incubated with anti-rabbit or anti-mouse secondary antibody for 1 h. Detection of proteins expression was performed using enzyme-linked chemiluminescence system. β-actin was used as a loading control.

4.4. The effect of iron chelation on the NDRG1 downstream signalling pathways: NF-κB

NDRG1 has already been described as a comprehensive inhibitory protein of the NF-κB signalling pathway in pancreatic cancer cells [143]. Treating with different iron chelators for 24 h did not affect total level of NF-κB in cytosol fraction as well as its nuclear localization. The level of cytosolic p-NF-κB Ser^{536} was slightly increased for 3 μM concentration of mitoDFO in comparison with untreated control cells, while 1 μM concentration of mitoDFO, both concentrations of mitoDFX, and Dp44mT remained unchanged. Concerning the nuclear localisation of p-NF-κB Ser^{536}, it was slightly decreased in 5 μM concentration of Dp44mT and in 3 μM concentration of mitoDFO and mitoDFX. There was no change in total level of NF-κB and p-NF-κB Ser^{536} in *NDRG1* knockout (KO) clone, which was used as a negative control that lacks NDRG1. Regarding the activating kinase IKK, the level of the IKKα subunit was not affected after treatment with the iron chelating compounds or in response to the *NDRG1* deletion in the cytosol, however the level of the kinase α subunit was reduced in 5 μM concentration of Dp44mT in the nuclear fraction. IKKβ was not detected and the level of phosphorylated IKKα/β was almost undetectable and unchanged in all concentrations and treatments used in MCF7 cells, in the *NDRG1* KO cells as well. Protein levels of IκBα and p-IκBα were not changed in MCF7 cells as well as in *NDRG1* KO clone (Figure 9).

In MRC5 cells, iron chelation by Dp44mT and mitoDFO did not change the level of total NF-κB protein, while treating with mitoDFX slightly decreased the total NF-κB in the cytosolic and nuclear fraction. Interestingly, treating with 5 μM Dp44mT, 1 μM mitoDFO and 1 μM mitoDFX for 24 h markedly increased the level of p-NF-κB Ser^{536} in cytosolic fraction compared to untreated controls and MRC5 cells treated with 3 μM mitoDFO or mitoDFX . The levels of both subunits of IKK kinase were not affected by the presence of Dp44mT and both mitochondrially targeted iron chelators. However, iron chelation by mitoDFO and mitoDFX, but not Dp44mT, increased the phosphorylation of IKKα/β at $Ser^{176/180}$. The total level of inhibitor IκBα was slightly increased in the presence of 5 μM Dp44mT and 3 μM mitoDFO, while in MRC5 cells treated with 1 μM mitoDFO or mitoDFX remained unchanged. The negative phosphorylation of IκBα resulting in releasing of NF-κB was greatly increased in MRC5 cells incubated with 5 μM concentration of Dp44mT. In mitoDFO or mitoDFX-treated cells, the levels of p-IkBα Ser^{32} protein were also increased compared to untreated controls (Figure 10).

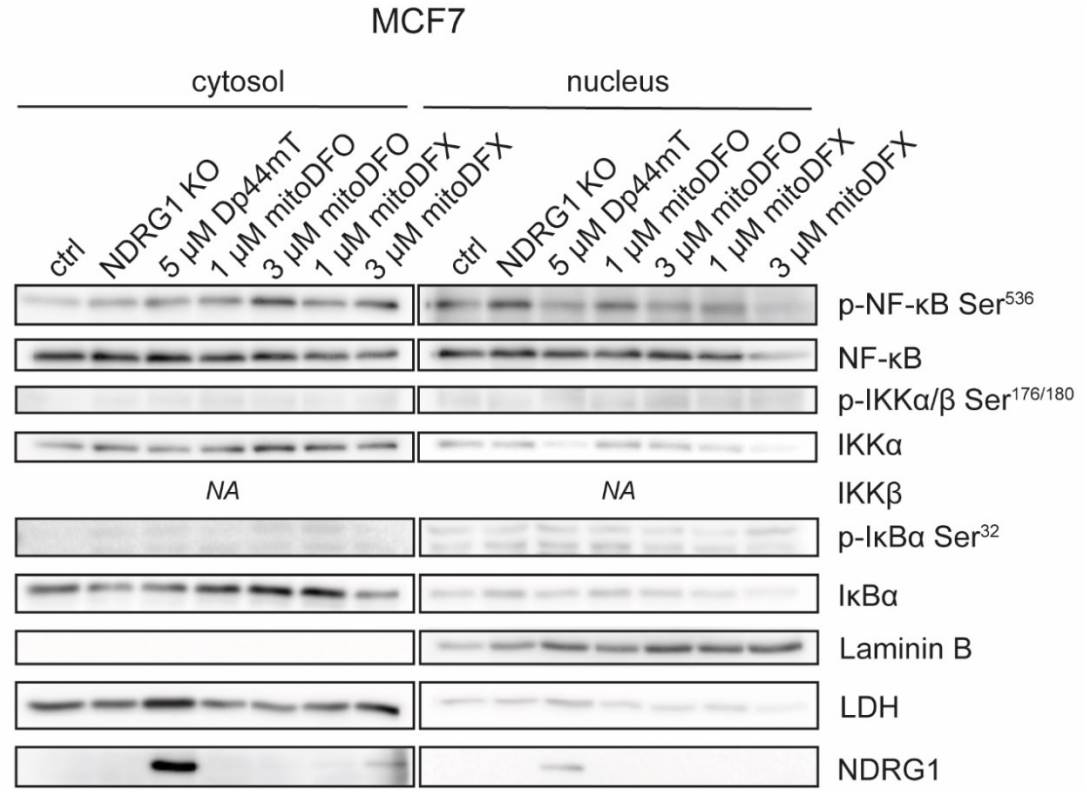

Figure 9: Effect of iron chelators on NF-κB signalling pathway in MCF7 cells. Protein level of components of the NF-κB signalling pathway and NDRG1 was analysed by western blotting. MCF7 cells were treated with different concentrations of Dp44mT, mitoDFO and mitoDFX. After 24 h of incubation, cells were harvested and cell lysates from cytosolic and nuclear fractions were prepared. Equal amounts (50 µg of proteins) of lysates were separated onto 10% bis-acrylamide gel, then transferred onto PVDF membrane. The membrane was immunoblotted with NF-κB, p-NF-κB Ser^{536}, IKKα, IKKβ, p-IKKα/β $Ser^{176/180}$, IκBα, p-IκBα Ser^{32} and NDRG1 antibodies overnight, and then washed and incubated with anti-rabbit or anti-mouse secondary antibody for 1 h. Detection of proteins expression was performed using enzyme-linked chemiluminescence system. LDH and Laminin B were used as a loading control. *NA* indicates undetectable protein.

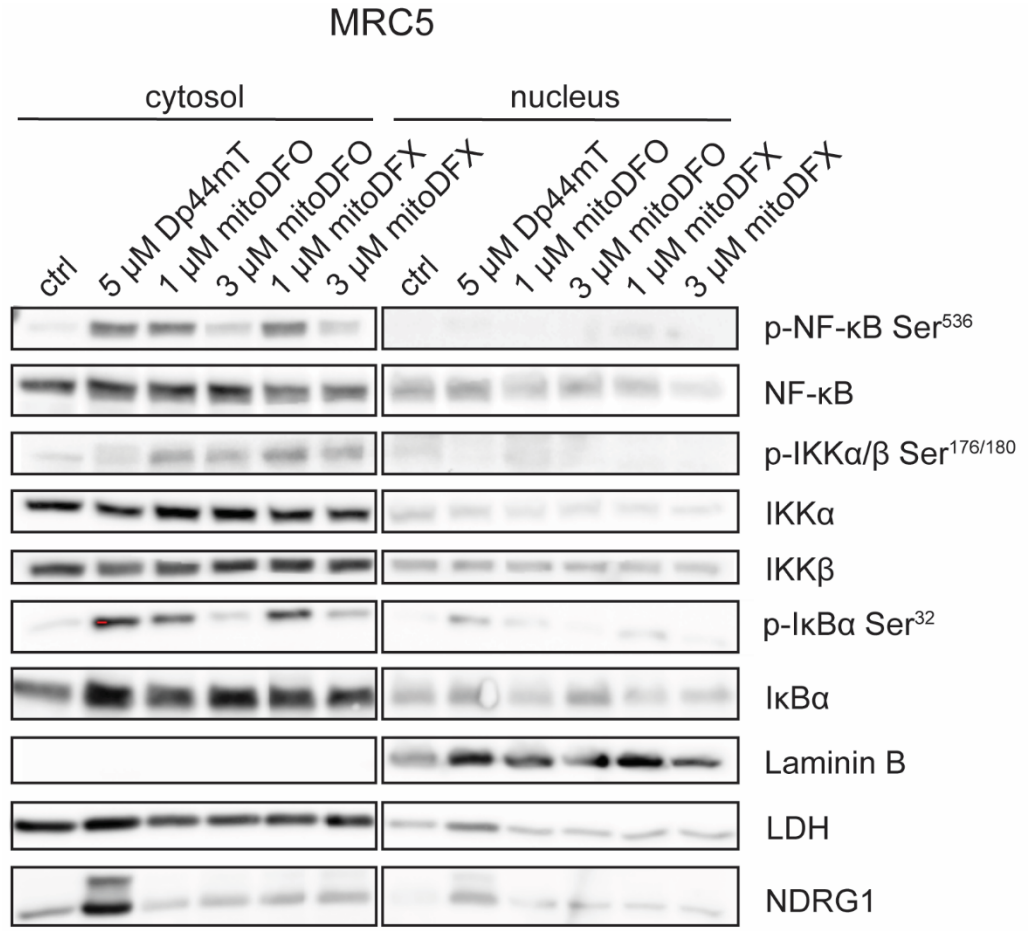

Figure 10: Effect of iron chelators on NF-κB signalling pathway in MRC5 cells. Protein level of components of the NF-κB signalling pathway and NDRG1 was analysed by western blotting. MR5C cells were treated with different concentrations of Dp44mT, mitoDFO and mitoDFX. After 24 h of incubation, cells were harvested and cell lysates from cytosolic and nuclear fractions were prepared. Equal amounts (50 μg of proteins) of lysates were separated onto 10% bis-acrylamide gel, then transferred onto PVDF membrane. The membrane was immunoblotted with NF-κB, p-NF-κB Ser^{536}, IKKα, IKKβ, p-IKKα/β $Ser^{176/180}$, IκBα, p-IκBα Ser^{32} and NDRG1 antibodies overnight, and then washed and incubated with anti-rabbit or anti-mouse secondary antibody for 1 h. Detection of proteins expression was performed using enzyme-linked chemiluminescence system. LDH and Laminin B were used as a loading control.

4.5. The effect of iron chelation on the NDRG1 downstream signalling pathways: EGFR

Recently, it was demonstrated that NDRG1 over-expression in pancreatic and colon cancer cells downregulates EGFR protein level [32]. Therefore, in this study, we also looked at whether mitochondrially targeted iron chelators are able to reduce EGFR expression similar to Dp44mT. In MRC5 cells, 5 μM Dp44mT markedly decreased expression of EGFR and the same effect was observed after exposition to mitoDFO and mitoDFX, where EGFR was decreased in a dose-dependent manner. However, in MCF7 cells the EGFR was undetectable (Figure 11).

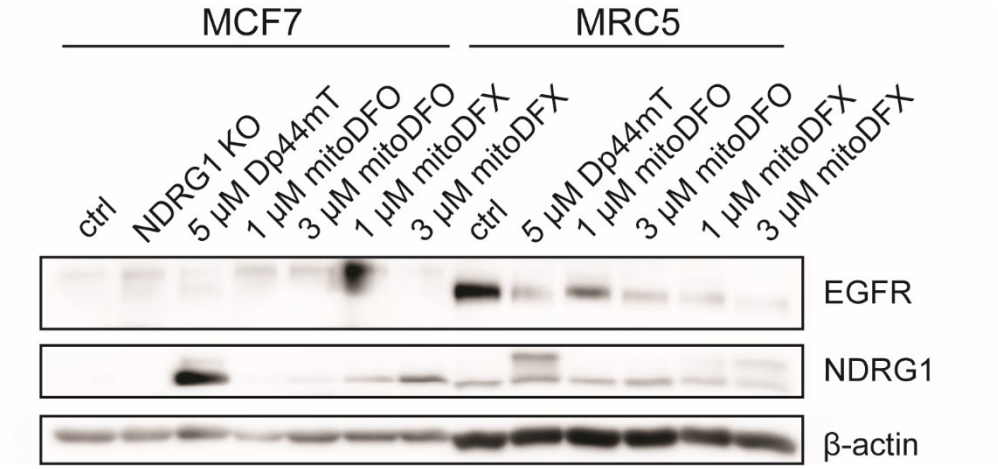

Figure 11: Effect NDRG1 on EGFR in MCF7 and MRC5 cells. Protein level of EGFR and NDRG1 was analysed by western blotting. MCF7 and MR5C cells were treated with different concentrations of Dp44mT, mitoDFO and mitoDFX. After 24 h of incubation, cells were harvested and whole cell lysates were prepared. Equal amounts (50 μg of proteins) of lysates were separated onto 8% bis-acrylamide gel, then transferred onto PVDF membrane. The membrane was immunoblotted with EGFR and NDRG1 antibodies overnight, and then washed and incubated with anti-rabbit or anti-mouse secondary antibody for 1 h. Detection of proteins expression was performed using enzyme-linked chemiluminescence system. β-actin was used as a loading control.

4.6. Generation of *NDRG1* knock out MCF7 cells and their validation

In order to test the role of NDRG1 in the response to iron chelators, we decided to construct MCF7 *NDRG1* knockout cells to see the effect of the gene deletion on cancer cell and its responsiveness to iron chelation.

We used the 55 pX AsCpf1-Venus-NLS crRNA entry vector with three cloned sgRNAs targeting exon 4 of *NDRG1*; one sgRNA inside the exon and two outside, and transfected the plasmid by Lipofectamine LTX into MCF7 cells. After single cell sorting of transfected cells on flow cytometer, we obtained several potential *NDRG1* knockout clones. Further examination of the length of the PCR product amplifying the targeted *NDRG1* exon 4 from isolated genomic DNA was performed. The clones showed relatively high variability in the length of *NDRG1* PCR products, but several of them showed truncated version of the targeted exon (Figure 12). We preferentially selected clones with exon 4 deletion in all alleles (2C11 and 3F5) and added three possible heterozygous clones (1F9, 2F4, 3C3) and tested them by western blotting and immunofluorescence (Figure 13, Figure 14). In order to assess the NDRG1 protein level, we pre-incubated clones with 1 μM Dp44mT to induce NDRG1 expression. None of the selected clones demonstrated NDRG1 expression, confirming they are *NDRG1* KO (Figure 13). Furthermore, these results were recapitulated by confocal microscopy, where the induction of NDRG1 protein was not visible in the KO clones (Figure 14).

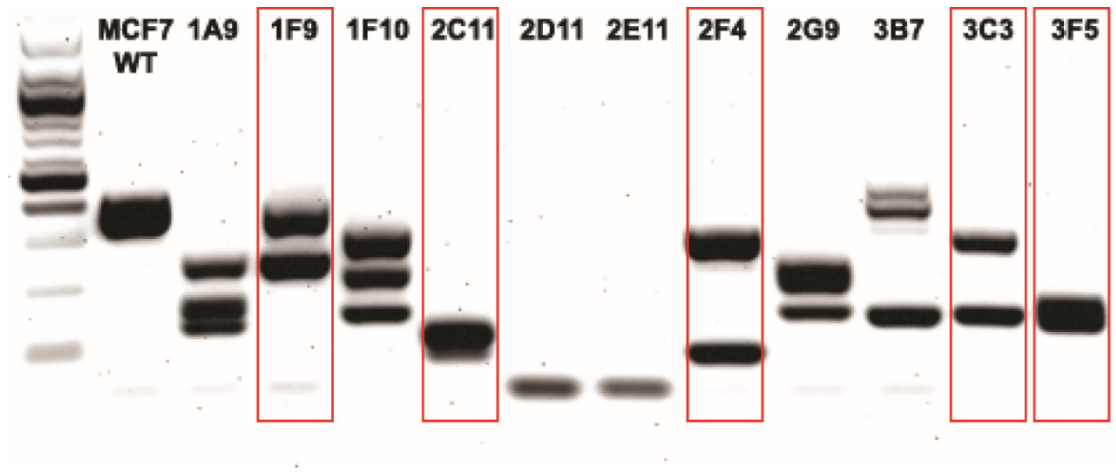

Figure 12: Validation of *NDRG1* KO clones. DNA-PCR analysis of obtained MCF7 *NDRG1* KO cells for the presence of full NDRG1 exon 4 on a 2% agarose gel.

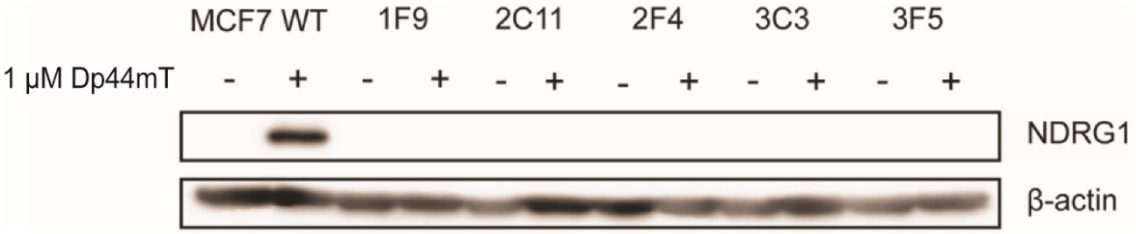

Figure 13: Validation of *NDRG1* KO clones. NDRG1 western blot analysis of selected MCF7 *NDRG1* KO cells pre-treated with 1 μM Dp44mT for 24 h or left untreated as indicated.

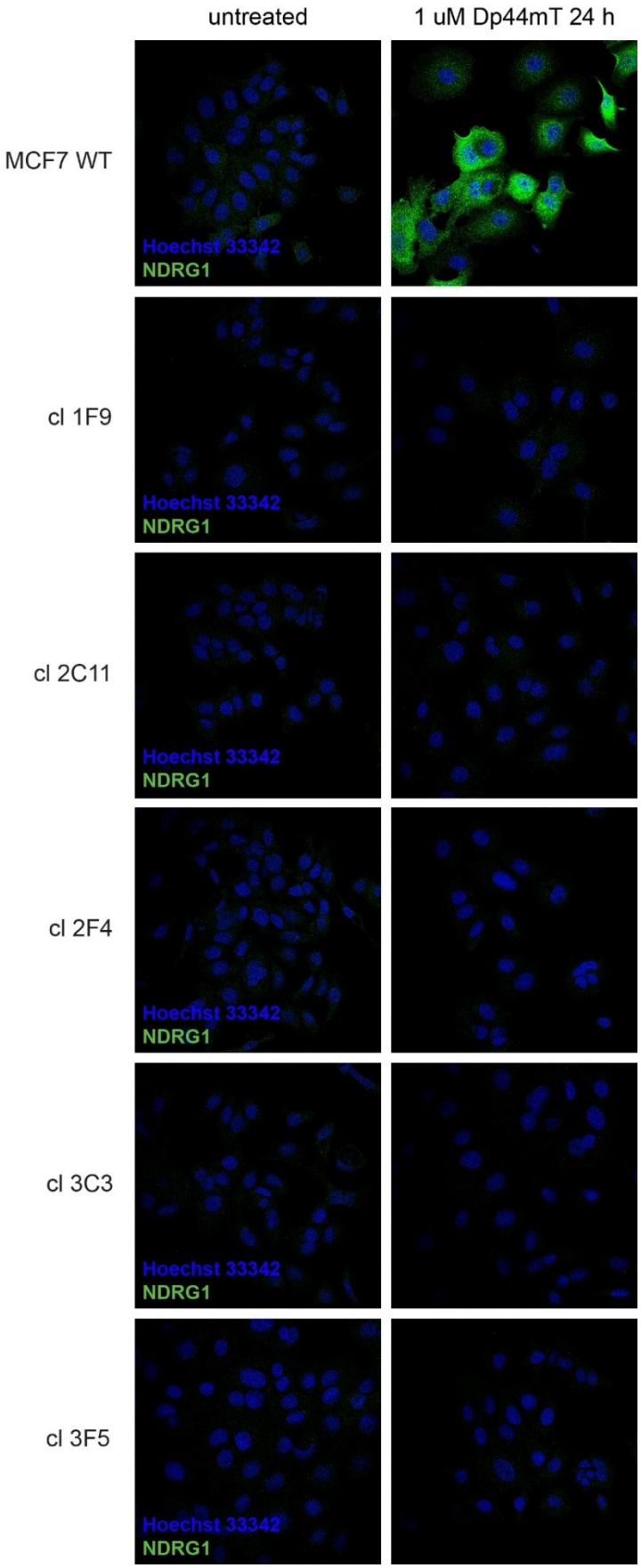

Figure 14: Validation of *NDRG1* KO clones by confocal microscopy. Confocal immunofluorescence images of selected MCF7 *NDRG1* KO cells treated with 1 µM Dp44mT or left untreated as indicated demonstrate staining for NDRG1 (green) and Hoechst 33342 for nuclei (blue).

4.6. Evaluation of ROS production and mitochondrial transmembrane potential in *NDRG1* KO cells

To assess the effect of *NDRG1* knockout on cancer cell metabolism, we used our MCF7 *NDRG1* knockout clones and measured cellular and mitochondrial ROS, and mitochondrial inner membrane potential. Analysis of cellular ROS production by DCF probe showed slightly higher relative fluorescence intensity in all MCF7 *NDRG1* KO clones compared to control MCF7 cells except for clone 2F4, where the fluorescence was slightly lower (Figure 15). Further analysis of mitochondrial ROS production by MitoSOX probe showed almost no change in fluorescence for clones 2C11 and 2F4, while for clones 1F9 and 3C3 the relative MitoSOX fluorescence was slightly lower. Clone 3F5 had significantly decreased mitochondrial ROS production (Figure 16). At last, evaluation of transmembrane potential showed decreasing of TMRM signal in all clones. The decrease in fluorescence was significant only in clone 3C3 (Figure 17).

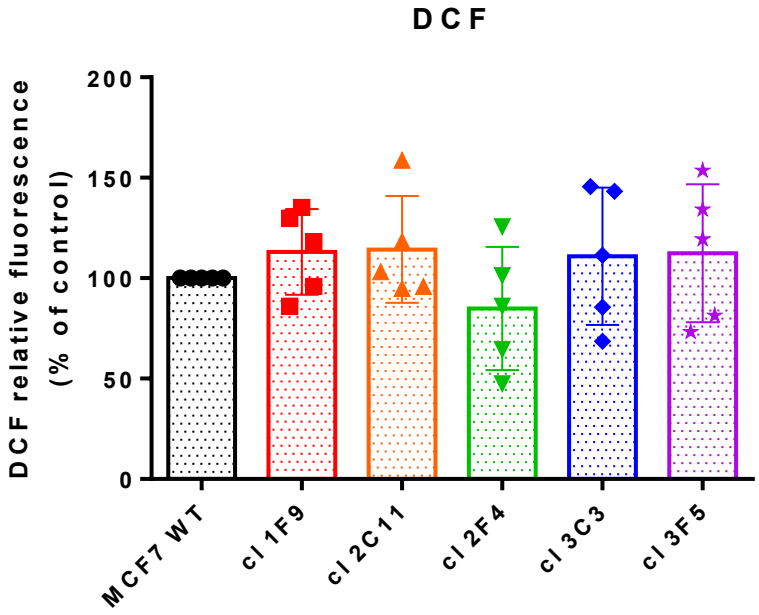

Figure 15: Evaluation of cellular ROS in *NDRG1* KO clones using DFC-DA as a probe. Cells were treated with 5 µM DCF-DA and incubated for 20 min. The fluorescence of DCF was measured at 504 nm excitation and 524 nm emission in LSR Fortessa. Data are shown as relative fluorescence of DCF and represent the mean ± SD of five independent replicates. Statistical significance was determined by one-way ANOVA using GraphPad PRISM software, where the values obtained from the treated cells were compared to the control values; * $p < 0.05$, ** $p < 0.01$, *** $p < 0.001$, **** $p < 0.0001$.

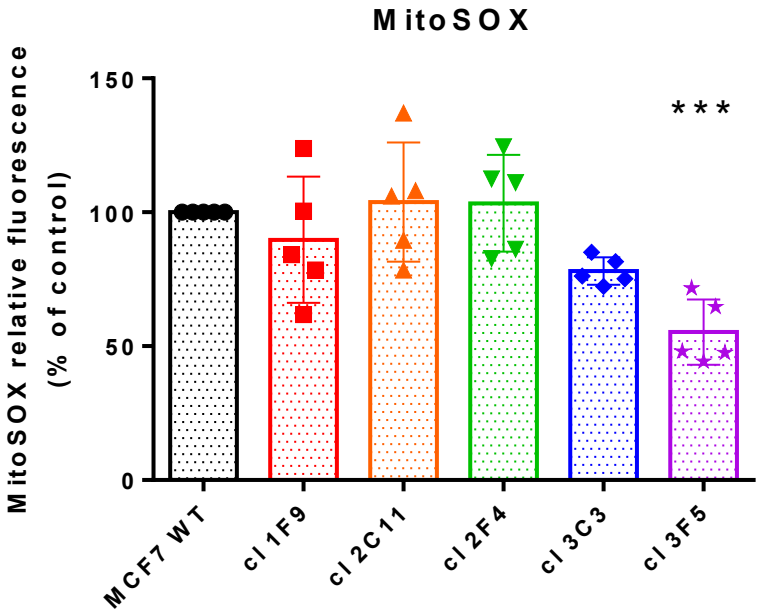

Figure 16: Evaluation of mitochondrial ROS in *NDRG1* KO clones using MitoSOX as a probe. Cells were treated with 2.5 µM MitoSOX and incubated for 20 min. MitoSOX was measured at 510 nm excitation and 580 nm emission in LSR Fortessa. Data are shown as relative fluorescence of MitoSOX and represent the mean ± SD of five independent replicates. Statistical significance was determined by one-way ANOVA using GraphPad PRISM software, where the values obtained from the treated cells were compared to the control values; * $p < 0.05$, ** $p < 0.01$, *** $p < 0.001$, **** $p < 0.0001$.

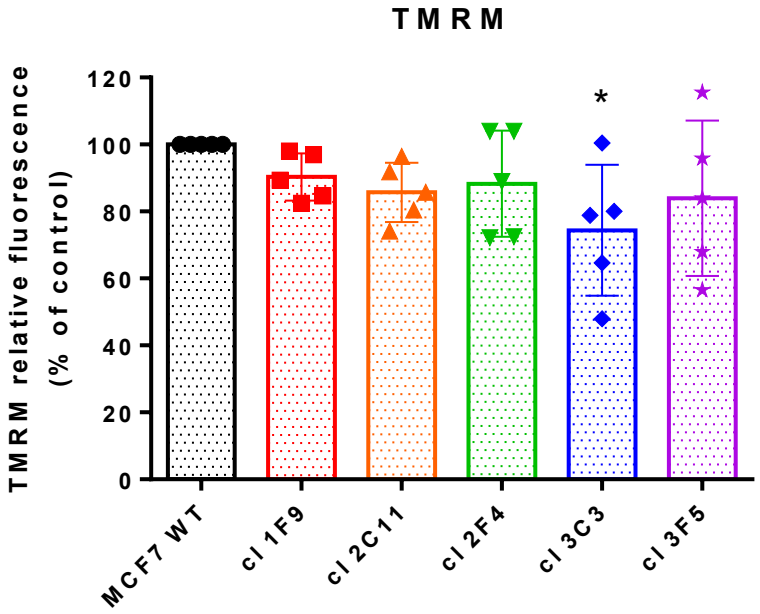

Figure 17: Evaluation of mitochondrial transmembrane potential in *NDRG1* KO clones using TMRM as a probe. Cells were treated with TMRM at a final concentration of 50 nM and incubated for 20 min. The fluorescence of TMRM was measured at 548 nm excitation and 574 nm emission in LSR Fortessa. Data are shown as relative fluorescence of TMRM and represent the mean ± SD of five independent replicates. Statistical significance was determined by one-way ANOVA using GraphPad PRISM software, where the values obtained from the treated cells were compared to the control values; * $p < 0.05$, ** $p < 0.01$, *** $p < 0.001$, **** $p < 0.0001$.

4.7. Evaluation of the cell cycle in MCF7 *NDRG1* KO cells

Evaluation of cell cycle should provide us with another important characteristic of *NDRG1* knockout clones. Ideally, upon knocking out a tumour suppressor gene, cells should divide faster, and it should be also visible on their cell cycle. If the cell cycle dysregulation occurs, the proportions of the individual phases should be changed in favour of G1 or G2.

Analysis of the cell cycle in clones, which lack *NDRG1*, showed a significant increase in G1 phase in clones 1F9, 2F4 and 3C3. Clone 3C3 also has a significantly reduced proportion of cells occurring in the S phase of the cell cycle compared to wild type (WT) cells, and clone 2F4 has a lower percentage of cells in the G2 phase. The proportions of cells in the individual phases of the cell cycle remained almost unchanged for the clones 2C11 and 3F5 (Figure 18). The relative values obtained by averaging two replicates of the cell percentages in the individual phases of the cell cycle obtained from the individual experiments are shown in the Table 7 for illustration.

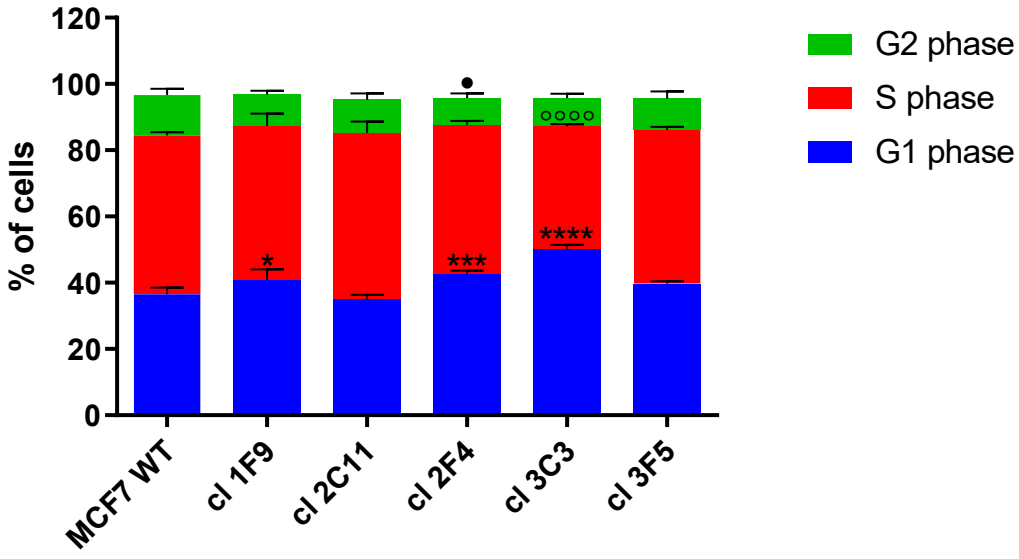

Figure 18: Cell cycle phases in the *NDRG1* KO clones. The cell cycle was analysed by flow cytometry using Vybrant dye and EdU as probes. Cells were harvested and incubated for 90 min with EdU to allow incorporation into newly synthesized DNA. Then, cells were incubated with picolyl azide for 30 min followed by incubation with Vybrant dye for 20 min. The cell cycle was measured in Flow Cytometer LSR Fortessa at 405 nm excitation and 437 nm emission for Vybrant dye and at 410 nm excitation and 455 nm emission for picolyl azide. Data are shown as the percentage of cells and represent the mean ± SD of two independent experiments. Statistical significance was determined by two-way ANOVA using GraphPad PRISM software; * $p < 0.05$, ** $p < 0.01$, *** $p < 0.001$, **** $p < 0.0001$. * indicates statistical significance for G1 phase, ○ for S phase and ● for G2 phase.

	G1 phase		S phase		G2 phase	
replicate	**1st**	**2nd**	**1st**	**2nd**	**1st**	**2nd**
MCF7 WT	36.1	37.0	47.4	48.4	12.9	11.6
cl 1F9	39.0	42.5	49.2	44.1	8.9	10.2
cl 2C11	33.9	36.0	53.2	47.4	8.6	11.6
cl 2F4	43.2	41.9	46.1	44.2	6.8	9.2
cl 3C3	50.5	49.9	36.5	37.6	8.0	8.7
cl 3F5	40.0	39.7	46.8	46.0	8.6	10.3

Table 7: Percentages of individual phases of the cell cycle from particular replicates. Each number represents the average of two measured values, which are written as percentages of cells.

4.8. Proliferation rate of *NDRG1* KO cells

Since *NDRG1* is mostly described as a tumour suppressor gene, we hypothesised that deletion of the *NDRG1* gene should affect the proliferative rate of cancer cells. Thus, we carried out time lapse live cell imaging to examine the differences in proliferation rate between parental and *NDRG1* KO clones.

We observed almost no change in proliferation rate for clones 1F9, 2C11, 2F4 and 3F5 compared to MCF7 WT cells. There is a trend of KO clones to grow slower, with clone 3C3 proliferating the least, however, this result is not significant (Figure 19). Calculation of the area under curve (AUC), which represent the integral of curve over the interval between the first and final time point, also showed reduced AUC for clone 3C3 without any statistical significance (Figure 20A). However, additional analysis of the slope, which represent linear part of the curve, showed a significant decrease of proliferation rate for all clones with the highest significance for the clone 3C3 (Figure 20B).

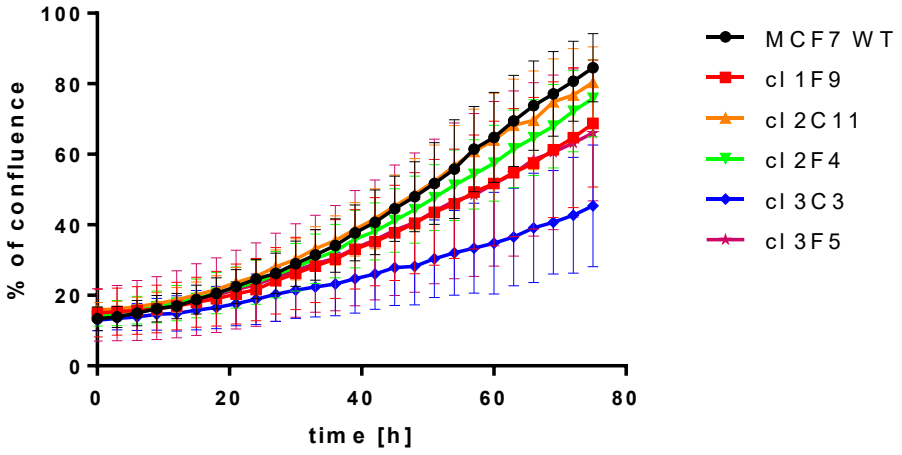

Figure 19: Effect of *NDRG1* deletion on cellular proliferation. MCF7 control cells and *NDRG1* knockouts were seeded in 96-well plate at 2.000 cells per well. Brightfield images were captured every 3 hours for 75 h. Analyses were performed using the Lumaview Software. Data are shown as a percentage of confluence and represent the mean ± SD of three independent experiments.

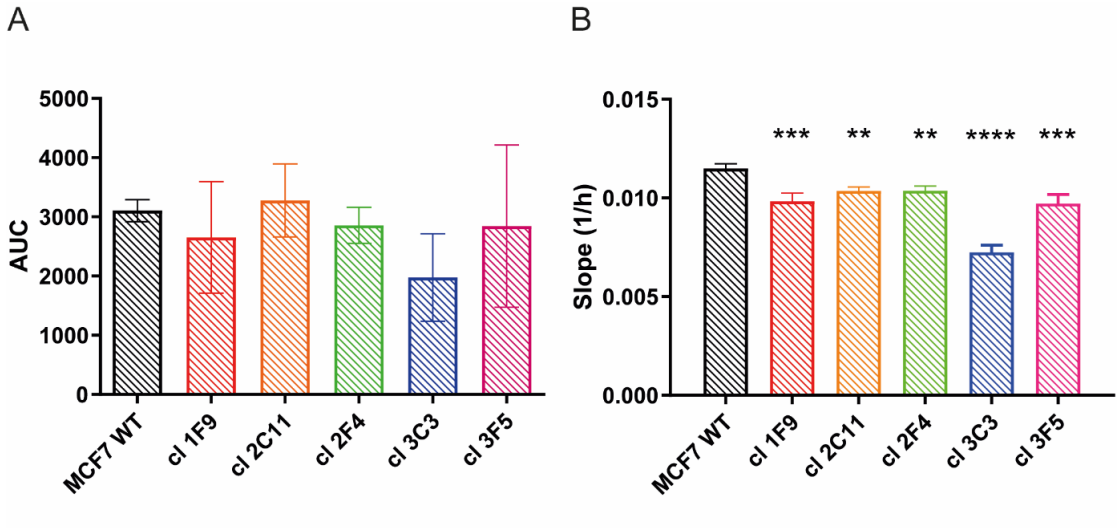

Figure 20: Effect of NDRG1 deletion on cellular proliferation. A) AUC of shown curves calculated in GraphPad PRISM; B) slopes of shown curves calculated in GraphPad PRISM. Data are shown as mean ± SD of three independent experiments. Statistical significance was determined by one-way ANOVA using GraphPad PRISM software, where the values obtained from clones were compared to the control values; * $p < 0.05$, ** $p < 0.01$, *** $p < 0.001$, **** $p < 0.0001$.

4.9. Responsiveness of *NDRG1* knockout clones to iron chelation

We also analysed if our *NDRG1* knockout clones are able to differently respond to iron chelation. Thus, we treated them with the lowest concentration of mitoDFX, which had been previously show to induce NDRG1 in MCF7 cells. However, our results show that deletion of *NDRG1* does not effect on the responsiveness to the treatment with 30 nM concentration of mitoDFX (Figure 21). Measurement of the number of dead cells after

application of mitoDFX using SYTOX green fluorescent dye showed that the increase in the number of dead cells occurred about 20 h after the addition of 30 nM concentration of mitoDFX, only for clone 3F5 there was an increase later after about 40 h. In clones 1F9, 2C11 and 3F5 the increase in the number of dead cells was slower, linear, on the contrary in clones 2F4 and 3C3 it was faster, almost exponential (Figure 22).

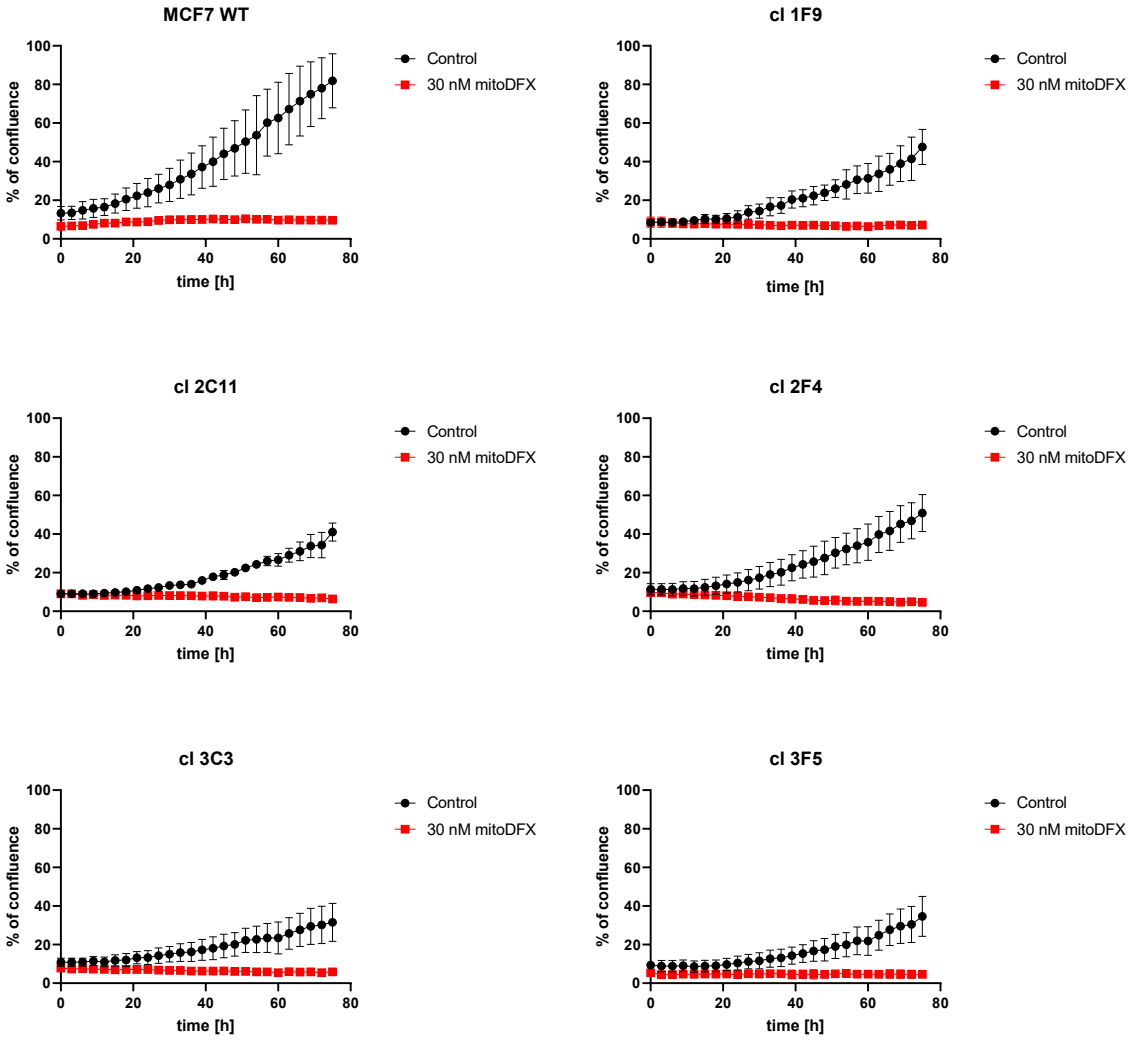

Figure 21: Responsiveness of *NDRG1* knockout clones to iron chelation. MCF7 WT cells and *NDRG1* KO clones were seeded in 96-well plate at 2.000 cells per well. Next day, they were treated with 30 nM concentration of mitoDFX. Phase contrast images were captured every 3 hours for 75 h. Analyses were performed using the Lumaview Software. Data are shown as the percentage of confluence ± SD of five replicates from one experiment.

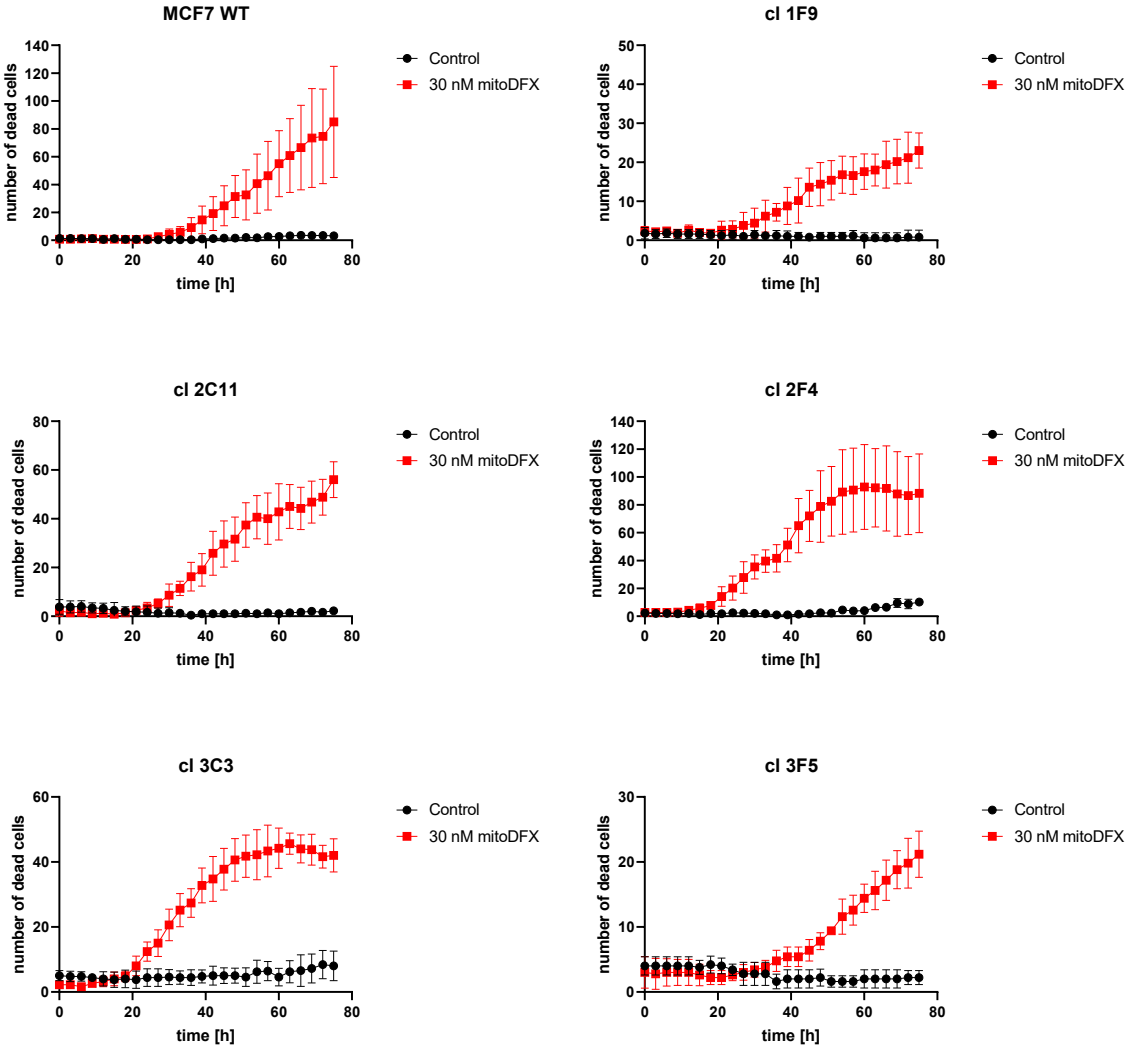

Figure 22: Responsiveness of *NDRG1* knockout clones to iron chelation. MCF7 WT cells and *NDRG1* KO clones were seeded in 96-well plate at 2.000 cells per well. Next day, they were treated with 30 nM concentration of mitoDFX and 0.5 µM SYTOX green. Green fluorescence images were captured every 3 hours for 75 h. Analyses were performed using the Lumaview Software. Data are shown as the number of dead cells ± SD of five replicates from one experiment.

4.10.Induction of immunogenic cell death

Several anti-cancer treatments are able to induce immunogenic cell death, which may be beneficial during cancer treatment [158, 159]. Thus, we tested if mitochondrially targeted iron chelators can activate immune response against death cancer cells by exposing the calreticulin on their surface based on the fact that its effect is much stronger in immunocompetent mice. MCF7 cells were treated with three different concentrations of each mitochondrially targeted iron chelators, tunicamycin and staurosporine were used as a positive control according to already published data [158].

The analysis of calreticulin-positive non-permeabilised cells showed that after 24 h incubation of MCF7 cells with tunicamycin there was no significant increase in percentage of calreticulin-positive cells, while 4 hours of incubation with staurosporine increased the number almost 8-fold. Treating malignant cells with 1 μM concentration of mitoDFO did not affect the proportion of calreticulin-positive cells, while the higher 5 μM concentration slightly increased this number. In contrast, we observed 2-fold increase in calreticulin-positive cells in 0.5 μM concentration of mitoDFX and 2 μM concentration increased the percentage of positive cells almost 4-fold. Dp44mT also slightly increased the percentage of calreticulin-positive cells (Figure 23A). However, different analysis of these results by excluding dead, PI-positive cells, and including live, PI-negative cells, did not show significant changes in the cell surface calreticulin exposure and showed a very low percentage of calreticulin-positive/PI-negative cells (Figure 23B).

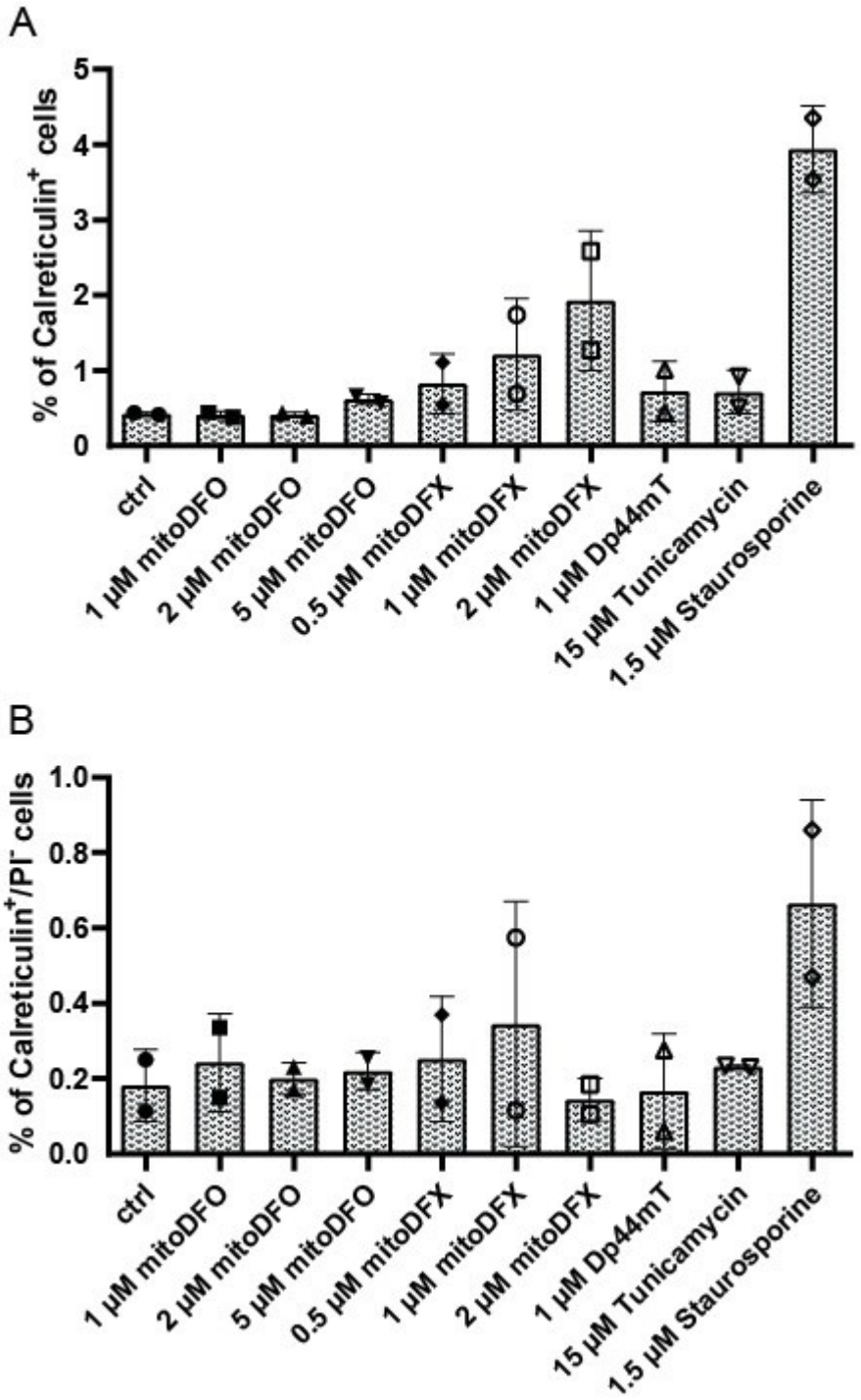

Figure 23: Induction of immunogenic cell death in MCF7 cells after exposition to iron chelators. MCF7 cells were treated with different concentrations of mitoDFO, mitoDFX, Dp44mT and tunicamycin for 24 h, and with staurosporine for 4 h. Then, cells were harvested and prepared for Flow Cytometer LSR Fortessa. Data are shown as a percentage of A) calreticulin-positive (Calreticulin$^+$) or B) calreticulin$^+$/PI$^-$ cells and represent the mean ± SD of two independent replicates. Statistical significance was determined by one-way ANOVA using GraphPad PRISM software, where the values obtained from the treated cells were compared to the control values; * $p < 0.05$, ** $p < 0.01$, *** $p < 0.001$, **** $p < 0.0001$.

5. Discussion

NDRG1 is a tumour suppressor that regulates multiple processes leading to inhibition of cancer cell proliferation by modulation of a plethora of oncogenes *via* different signalling pathways [31, 32, 127, 143, 153]. Expression of NDRG1 has been shown to be up-regulated by standard iron chelators as well as by very potent thiosemicarbazones-based iron chelators Dp44mT and DpC in multiple cancers [30, 81]. One of the mechanisms by which these iron chelators elicit their effect involves stabilisation of HIF-1α and expression of a number of hypoxia-related genes, one of them being *NDRG1*. Laboratory of tumour resistance and Service technology laboratory, both from Institute of Biotechnology, Czech Academy of Sciences, located in BIOCEV, have recently synthesized several mitochondrially targeted iron chelators by linking the standard FDA approved iron chelators DFO and DFX to a TPP^+ moiety. Those mitochondrially targeted iron chelators, mitoDFO and mitoDFX, has shown potent anti-proliferative effect on cancer cells *in vitro* and *in vivo*. mitoDFO disrupts mitochondrial respiratory complexes, Fe-S cluster assembly and haem biogenesis, induce mitochondrial ROS and cause cell cycle arrest at G1 phase [37]. mitoDFX is even more potent compound that is currently under pending European patent application and its effects have not yet been published, thus we are not releasing all experimental data and its structure.

Due to the role of iron chelators on effective upregulation of NDRG1 in several types of cancer cells [31, 32, 143], we assessed the ability of our mitochondrially targeted DFO and DFX to upregulate NDRG1 in ESR-positive MCF7 breast cancer cells and MRC5 fibroblasts as MCF7 cells respond well to our chelators, while MRC5 cells are much more resistant [37]. In both cell lines, mitoDFO did not affect the expression of *NDRG1* gene after 24 h of incubation (Figure 1C, D). However, NDRG1 protein was increased in response to mitoDFO in the highest concentration in MCF7 cells, which may indicate post-translation stabilisation of NDRG1 (Figure 2C, D). Regarding mitoDFX, it significantly increased *NDRG1* in MCF7 cells compared to MRC5, where the relative mRNA induction seemed to be much lower (Figure 1E, F). Similar effect was observed at protein level (Figure 2E, F). This suggests that mitoDFO treatment results in much lower response while mitoDFX, similarly to the positive control Dp44mT induces NDRG1 to a much higher level (Figure 1A, Figure 2A). A similar, although the less pronounced effect is also elicited in the normal, non-malignant MRC5 cells (Figure 1B, Figure 2B).

It has been reported that NDRG1 can be phosphorylated at multiple sites by SGK1 and GSK3 kinases. Phosphorylation at Ser^{330} and Thr^{346} were described to be important for the ability of NDRG1 to suppress the NF-κB signalling pathway and expression of CXC chemokines in pancreatic cancer cells [83]. Another study focusing on the phosphorylation state of NDRG1 after exposition to iron chelators demonstrated that Dp44mT, DpC and DFO induce phosphorylation of NDRG1 at Ser^{330} and Thr^{346} in prostate and pancreatic cancer and HCC cells and it may be important for the anticancer function of NDRG1 [30, 72, 163]. Further studies also demonstrated that Dp44mT and DpC greatly increased the phosphorylated level of NDRG1 at Ser^{330} or Thr^{346} in the nucleus suggesting that these phosphorylations may be required for its nuclear translocation [72]. Our observations have shown that mitoDFO increased phosphorylation at Thr^{346} in MCF7 cells, however, it did not affect the level of NDRG1 phosphorylated at Ser^{330} (Figure 2C), while in non-malignant MRC5 the level of NDRG1 Ser^{330} or Thr^{346} protein remained unchanged (Figure 2D). In MCF7 as well as in MRC5 cells treated with mitoDFX for 24 h, there was the increased level of NDRG1 phosphorylated at Thr^{346} and Ser^{330} (Figure 2E, F), which is similar to results obtained from cells exposed to Dp44mT (Figure 2A, B). The differences seen for individual cell lines and iron chelators may be explained by the fact that mitoDFO is redox-inactive [17], while both Dp44mT and mitoDFX are redox-active [21, 25] and, thus, NDRG1 phosphorylation at Ser^{330} may be dependent on redox stress. Further studies using NAC or overexpressed antioxidant enzymes might help clarify the role of ROS on NDRG1 phosphorylation.

Of course, the effect of cellular origin, context and ability to metabolise drugs and elicit hypoxic response should also be taken into account. Overall, we could say that the effect of tested iron chelators is individual and for example mitochondrially targeted DFO is much less potent at inducing NDRG1 than parental non-targeted DFO. On the other hand, mitoDFX seems to be a better inducer of NDRG1 compared to parental DFX (Figure 3). Yet, it seems that the effect seen with mitochondrially targeted chelators seems to be more pronounced in the malignant cells, MCF7, compared to non-malignant fibroblasts, MRC5, being in contrast to the non-targeted chelators DFO, DFX that induced NDRG1 similarly in both cell lines. Furthermore, we have to say that the extent of NDRG1 induction does not seem to correlate with the cytotoxic and cytostatic potency of the compounds, thus indirectly suggesting that NDRG1 induction is not the key event in their mechanism of action and could be more related to their ability to induce

"pseudohypoxia" by chelating iron. Additional experiments will thus be needed to address the issue in more detail.

In the next part of our study, we focused on several known downstream effectors of NDRG1. First, the proto-oncogene c-MET and its direct effector GAB1 were assessed (Figure 8). It was found that Dp44mT at 5 μM concentration markedly increased total level of c-MET, while did not affect the level of its phosphorylated forms. Also, Dp44mT increased total GAB1 and p-GAB1 Tyr^{307}. These results do not correspond to what has already been described in DU145 prostate cancer, Huh7 hepatoma cells as well as in SCC25 oral squamous cell carcinoma, Hep3B hepatoma, PANC-1 pancreatic carcinoma, and MDA-MB-231 breast cancer cells, where Dp44mT downregulates c-MET [31]. However, we saw the expected decrease in c-MET in MRC5 cells, suggesting that the response could be specific for certain types of cells, while it could be different in others. At this point, we can only speculate why MCF7 cells respond differently compared to other cell lines. One of the possibilities is the dependence of MCF7 on oestrogen signalling [160], which might modify the cellular response. In order to tackle this issue, we might utilize the model of tamoxifen-resistant MCF7 cells, which is routinely used in the laboratory and functionally lacks the ESR signalling. Further experiments that would define, whether c-MET in these cells responds to iron chelation differently could help to answer this question. With regards to mitochondrially targeted iron chelators, mitoDFO increased total c-MET in MCF7 at 3 μM concentration, while mitoDFX did not. Conversely, in MRC5, where we observed the downregulation of c-MET by Dp44mT, we have shown that mitoDFX decreased total c-MET, while mitoDFO did not. Thus, in terms of regulating c-MET, mitoDFX seems to behave more like the Dp44mT thiosemicarbazone while mitoDFO does not seem to downregulate this oncogenic pathway.

Another very important signalling pathway that affects cell death and survival is NF-κB pathway, which has been shown to respond to NDRG1 [143]. We hypothesized that similarly to pancreatic cancer cells, NDRG1 would affect components of the NF-κB pathway in MCF7 cells. Our data suggest that 5 μM Dp44mT, 3 μM mitoDFO and 3 μM mitoDFX decrease the nuclear level of phosphorylated NF-κB at Ser^{536} in MCF7, while it is difficult to assess this for MRC5 cells, due to the very weak bands (Figure 9, Figure 10). In MRC5 cells, there seem to be slightly higher levels of IKKα and IKKβ together with higher IKKα/β phosphorylated at $Ser^{176/180}$. This should be the indication of the

activation of the NF-κB pathway, but we do not see the accumulation of nuclear NF-κB and it is thus possible that under these circumstances non-canonical signalling by other NF-κB like protein could be elicited. It is noteworthy to note that the activation of IKKα/β does not correlate with the expression of NDRG1 and rather reflects the effect of iron chelation. In order to make a final conclusion about the effect of tested chelators on the NF-κB pathway, we would need to measure the transcriptional activity elicited by the nuclear NF-κB, possibly by the luciferase assay, which is planned for the future.

Dp44mT and DpC-induced NDRG1 were found to inhibit oncogenic tyrosine kinase receptor EGFR in pancreatic PANC-1 and MIAPaCa-2 as well as the colon HT-29 and HCT-116 cells [32]. In our study, we focused on the evaluation of EGFR after 24 h incubation with our mitochondrially targeted iron chelators (Figure 11). We can say that MRC5 cells decreased expression of EGFR in 5 μM concentration of Dp44mT as well as decreased expression of EGFR after exposition to mitoDFO and mitoDFX in a dose-dependent manner, similarly to already published results. However, according to our results the MCF7 cells have very limited amounts of EGFR and thus we do not see any downregulation. It is thus possible that the EGFR pathway is not targeted in this breast cancer cell line, probably because its primary pro-proliferative signal remains the ESR signalling, which is not the case in MRC5 cells.

Based on our findings that NDRG1 induction does not seem to correlate with the cytostatic and cytotoxic potency of the compounds and the fact that downstream signalling pathways were more affected in non-malignant cells, we decided to evaluate the functional role of NDRG1 in tumour cells and constructed stable *NDRG1* knockout in MCF7 breast cancer cell line using CRISPR/AsCpf1/Cas12 system. We designed three sgRNAs that target one site within exon 4 of *NDRG1* and two sites in the closed proximity of exon 4 to increase cleavage efficiency of the system, enabling easier detection of KO clones by colony PCR from genomic DNA (Figure 12). We have obtained *NDRG1* knockout cells with decreased length of PCR products at least in one allele and no protein level after treating with 1 μM Dp44mT, which was added in attempt to induce NDRG1 (Figure 13, Figure 14). Based on these results we have selected 5 *NDRG1* knockout clones, clones 1F9, 2C11, 2F4, 3C3, and 3F5 that lack NDRG1 protein for further metabolic characterisation.

NDRG1 is a tumour suppressor gene that inhibits proliferation of many cancers, although in some cancer types it has been suggested as a tumour promoting gene [164]. Cancer cells usually exhibit uncontrolled growth, which also means high metabolic rate,

leading to an increase in the level of ROS. ROS are chemically reactive molecules containing oxygen, which can irreversibly oxidize and modify macromolecules and prevent them from realising their original functions. This can be very harmful to the cells and in order to survive, they have to develop mechanisms to protect themselves from this damage. For example, cancer cells have enhanced mechanisms that reduce the level of ROS in order to survive, but usually their ROS level is higher compared to normal cells. One of the many NDRG1 functions is to protect the cell from stress stimuli, such as DNA damage or ER stress. Both types of damage can be caused due to the increased level of ROS and their insufficient degradation. Thus, we decided to examine the basal level of ROS to see whether NDRG1 is able to affect ROS production, its degradation in breast cancer cells, or affect other cytoprotective mechanisms. To address this question, we measured cellular and mitochondrial ROS. While cellular ROS was not significantly changed in any of the *NDRG1* knockout clones (Figure 15), the level of mitochondrial ROS was mostly decreased with the pronounced significance for the clone 3F5 (Figure 16). In view of these results, NDRG1 may affect the production of mitochondrial ROS by some mechanism, although its association with mitochondria has not been well studied.

Since major ROS producing organelles are mitochondria, based on their OXPHOS system for producing ATP/GTP and reducing equivalents, we further evaluated mitochondrial inner membrane potential (Figure 17). The mitochondrial membrane potential is the main driving force for the generation of ATP by the mitochondria and consists of a proton gradient generated by the mitochondrial respiratory chain complexes. The mitochondrial membrane potential is often higher in many cancer cells compared to healthy non-malignant cell types. All our *NDRG1* knockout clones showed decreased mitochondrial membrane potential with statistical significance for the clone 3C3. Because NDRG1 contains HRE elements in its promoter and responds to HIF-1 level, its expression is dependent on the oxygen level. The observed decrease in mitochondrial membrane potential may indicate that *NDRG1* knockout clones have some feedback mechanism to suppress oxidative respiration, possibly connecting low oxygen and HIF1 activation, which would also explain a decrease in mitochondrial ROS.

Next, we tested the cell cycle in our *NDRG1* knockout clones (Figure 18). Ideally, upon knocking out a tumour suppressor gene, cells should divide faster. However, our results suggested that lack of *NDRG1* leads to slowing down of the cell cycle progression, which we saw in three of the five clones that had G1 phase cycle arrest. Further

examination of the rate of cellular proliferation showed a slight decrease in all clones compare to parental MCF7 cells (Figure 19). These results may be explained the role of NDRG1 in mitotic spindle assembly, and deletion of NDRG1 may indeed lead to a slowing of cell cycle progression. Subsequent responsiveness to chelator therapy by 30 nM mitoDFX did not show any significant differences between NDRG1 clones compared to WT (Figure 21, Figure 22), however, the experiment must be repeated to obtain significant data for statistical analysis. Regarding analysis of the number of dead cells, it seemed that all clones died a bit faster compare to WT cells exception for clone 3F5 (Figure 22). However, the different scales and numbers of dead cells, which are mostly lower for clones, are dependent on the particular place, where the picture is taken and rather than an absolute number it is about the pattern when cells start to die. In the future would be helpful to quantify these results by Annexin V/PI staining.

The use of chemotherapeutics in the fight against cancer is not the only and sufficient weapon. Currently, chemotherapy is used together with surgery, radiotherapy, or immunotherapy to maximize the anti-tumour response. A quite important role in the fight against cancers is played by the host's immune system itself, which is often much weakened in individuals with cancers, and as the disease progresses, the individual's organism becomes weaker. For the anti-tumour immune system to be activated, tumour cells need to die in response to chemotherapy by specific type of cell death, entitled “immunogenic cell death”. Danger molecules, DAMPs, then appear on the surface of such a dying cell, which the immune system perceives as signals of danger and responds to them by activating. One of these molecules is calreticulin, which is cells hidden within ER in healthy, however, upon triggering of non-apoptotic cell death is translocated on the outer leaflet of the plasma membrane. Similarly, to the phosphatidyl serine exposure which serves as the “eat me” signal, the calreticulin exposure serves as a signal that helps the immune system to recognize the dead cancer cells as the “non-self” and enables the efficient presentation of cancer-derived epitopes by phagocytic antigen presenting cells, eliciting robust anti-tumour immunity. Several anti-tumour drugs are able to activate ICD by exposing calreticulin to its surface, thereby inducing a massive host immune response [159]. Iron is also able to induce a specific type of cell death called ferroptosis, however, iron chelators have been shown to inhibit this type of cell death. Mitochondrially targeted chelators studied in our laboratory also activate cell death in cancer cells, however, the exact type of death they induce has not been determined and we only know that mitoDFO does not induce classical apoptosis. We thus measured calreticulin externalization by flow

cytometry and included known inducers of immunogenic cell death, namely staurosporine and tunicamycin, as positive controls [159]. The mitochondrially targeted chelators did induce the amount of calreticulin-positive cells, yet, the extent was significantly lower compared to the response elicited by staurosporine (Figure 23). In order to be sure that the measured calreticulin-positive cells have calreticulin on its surface we measured calreticulin^{+}/PI^{-} populations on viable non fixed cells and found out that although there is some increase in calreticulin^{+}/PI^{-} cells for staurosporine and 5 μM mitoDFO, the extent is very low. It is thus possible that the calreticulin-positive cells have exposed calreticulin on its surface, but they are already permeable to PI. Thus, the real effect of mitoDFO and mitoDFX as inducers of the immunogenic cell death requires further experiments that will address, whether calreticulin is exposed on the outer plasma membrane or not. One possibility could be confocal microscopy to see the localization of calreticulin or double staining with a control antibody that might help elucidate where exactly the calreticulin in cells exposed to mitoDFO or mitoDFX is. Nevertheless, the notion that these mitochondrially targeted chelators could enhance immunogenic cell death might be in line with the fact that mitoDFO treated mice with competent immune system seem to respond to mitoDFO more profoundly compared to the immunocompromised mice [37]. On the same line, recent reports report mitophagy and mitochondria-derived epitopes as the factors that enable robust anti-tumour immunity in the model of STAT3 induced carcinogenesis [165], being in line with mitophagy induction by mitochondrially targeted chelators.

6. Conclusions

The aims we have set have been fulfilled and can be summarized into the following points:

- We assessed *NDRG1* mRNA and protein level in malignant MCF7 and non-malignant MRC5 cell lines after exposition to targeted and non-targeted iron chelators. We found that mitoDFO does not change the *NDRG1* mRNA and only slightly increases its protein expression, while mitoDFX does increase both in a dose-dependent manner. Also, mitochondrially targeted DFO was found to be less potent in NDRG1 induction, than its non-targeted counterpart, while mitochondrially targeted DFX was more potent than non-targeted DFX.

- We evaluated the effect of the chelators on the selected NDRG1-related signalling pathways (EGFR, c-MET, NF-κB) in MCF7 and MRC5. We have observed that the chelation by Dp44mT increased c-MET expression in MCF7 cells, while in MRC5 it was downregulated. Also, the chelation changed the phosphorylation of p-NF-κB Ser^{536} in both cell lines, increased phosphorylation of IKKα/β $Ser^{176/180}$ in MRC5 and changed phosphorylation of p-IkBα Ser^{32} in MRC5. EGFR was absent in MCF7, but downregulated in MCR5 upon chelation.

- We have successfully generated *NDRG1* knockout MCF7 breast cancer cell line using CRISPR/AsCpf1/Cas12 system.

- We characterised the obtained *NDRG1* KO clones and found that deletion of *NDRG1* seems to slow down basal cellular proliferation and leads to the slight accumulation of cells in the G1 phase of the cell cycle. However, it does not affect the responsiveness to mitoDFX.

- We observed slight induction of calreticulin positive cells after exposition to mitoDFX in MCF7 cancer cells, possibly indicating induction of immunogenic cell death.

In the future, we would like to further characterize *NDRG1* KO clones with a focus on their ability to invade and metastasise. Furthermore, we would like to create and characterize MCF7 clones overexpressing various isoforms of NDRG1 and compare the

effect of stable NDRG1 overexpression with the *NDRG1* deletion. Another option is to generate *NDRG1* KO in MDA-MB-231 cells that are oestrogen independent and could therefore have a more visible effect of the *NDRG1* deletion.

7. References

[1] Alberts, B. (2015). Molecular biology of the cell. Garland Science.

[2] L. Chen, S. Liu, and Y. Tao, "Regulating tumor suppressor genes: post-translational modifications," *Signal Transduct Target Ther,* vol. 5, p. 90, Jun 10 2020.

[3] L. G. Morris and T. A. Chan, "Therapeutic targeting of tumor suppressor genes," *Cancer,* vol. 121, pp. 1357-68, May 1 2015.

[4] Y. Liu, X. Hu, C. Han, L. Wang, X. Zhang, X. He*, et al.*, "Targeting tumor suppressor genes for cancer therapy," *Bioessays,* vol. 37, pp. 1277-86, Dec 2015.

[5] L. Zhou, B. Zhao, L. Zhang, S. Wang, D. Dong, H. Lv*, et al.*, "Alterations in Cellular Iron Metabolism Provide More Therapeutic Opportunities for Cancer," *Int J Mol Sci,* vol. 19, May 22 2018.

[6] C. Renassia and C. Peyssonnaux, "New insights into the links between hypoxia and iron homeostasis," *Curr Opin Hematol,* vol. 26, pp. 125-130, May 2019.

[7] S. V. Torti and F. M. Torti, "Iron and cancer: more ore to be mined," *Nat Rev Cancer,* vol. 13, pp. 342-55, May 2013.

[8] Z. Estrov, A. Tawa, X. H. Wang, I. D. Dube, H. Sulh, A. Cohen*, et al.*, "In vitro and in vivo effects of deferoxamine in neonatal acute leukemia," *Blood,* vol. 69, pp. 757-61, Mar 1987.

[9] A. Kuban-Jankowska, K. K. Sahu, M. Gorska-Ponikowska, J. A. Tuszynski, and M. Wozniak, "Inhibitory Activity of Iron Chelators ATA and DFO on MCF-7 Breast Cancer Cells and Phosphatases PTP1B and SHP2," *Anticancer Res,* vol. 37, pp. 4799-4806, Sep 2017.

[10] L. Lan, W. Wei, Y. Zheng, L. Niu, X. Chen, D. Huang*, et al.*, "Deferoxamine suppresses esophageal squamous cell carcinoma cell growth via ERK1/2 mediated mitochondrial dysfunction," *Cancer Lett,* vol. 432, pp. 132-143, Sep 28 2018.

[11] J. L. Kim, D. H. Lee, Y. J. Na, B. R. Kim, Y. A. Jeong, S. I. Lee*, et al.*, "Iron chelator-induced apoptosis via the ER stress pathway in gastric cancer cells," *Tumour Biol,* vol. 37, pp. 9709-19, Jul 2016.

[12] H. Harima, S. Kaino, T. Takami, S. Shinoda, T. Matsumoto, K. Fujisawa*, et al.*, "Deferasirox, a novel oral iron chelator, shows antiproliferative activity against pancreatic cancer in vitro and in vivo," *BMC Cancer,* vol. 16, p. 702, Aug 31 2016.

[13] P. Li, X. Zheng, K. Shou, Y. Niu, C. Jian, Y. Zhao*, et al.*, "The iron chelator Dp44mT suppresses osteosarcoma's proliferation, invasion and migration: in vitro and in vivo," *Am J Transl Res,* vol. 8, pp. 5370-5385, 2016.

[14] D. R. Richardson, P. C. Sharpe, D. B. Lovejoy, D. Senaratne, D. S. Kalinowski, M. Islam*, et al.*, "Dipyridyl thiosemicarbazone chelators with potent and selective antitumor activity form iron complexes with redox activity," *J Med Chem,* vol. 49, pp. 6510-21, Nov 2 2006.

[15] A. R. Bogdan, M. Miyazawa, K. Hashimoto, and Y. Tsuji, "Regulators of Iron Homeostasis: New Players in Metabolism, Cell Death, and Disease," *Trends Biochem Sci,* vol. 41, pp. 274-286, Mar 2016.

[16] A. Donfrancesco, G. Deb, L. De Sio, R. Cozza, and A. Castellano, "Role of deferoxamine in tumor therapy," *Acta Haematol,* vol. 95, pp. 66-9, 1996.

[17] N. F. Olivieri and G. M. Brittenham, "Iron-chelating therapy and the treatment of thalassemia," *Blood,* vol. 89, pp. 739-61, Feb 1 1997.

[18] C. Hershko, G. Link, A. M. Konijn, and Z. I. Cabantchik, "Objectives and mechanism of iron chelation therapy," *Ann N Y Acad Sci,* vol. 1054, pp. 124-35, 2005.

[19] G. M. Brittenham, "Development of iron-chelating agents for clinical use," *Blood,* vol. 80, pp. 569-74, Aug 1 1992.

[20] C. Vermylen, "What is new in iron overload?," *Eur J Pediatr,* vol. 167, pp. 377-81, Apr 2008.

[21] Z. D. Liu, D. Y. Liu, and R. C. Hider, "Iron chelator chemistry," *Adv Exp Med Biol,* vol. 509, pp. 141-66, 2002.

[22] M. R. Bedford, S. J. Ford, R. D. Horniblow, T. H. Iqbal, and C. Tselepis, "Iron chelation in the treatment of cancer: a new role for deferasirox?," *J Clin Pharmacol,* vol. 53, pp. 885-91, Sep 2013.

[23] J. Yuan, D. B. Lovejoy, and D. R. Richardson, "Novel di-2-pyridyl-derived iron chelators with marked and selective antitumor activity: in vitro and in vivo assessment," *Blood,* vol. 104, pp. 1450-8, Sep 1 2004.

[24] D. B. Lovejoy, D. M. Sharp, N. Seebacher, P. Obeidy, T. Prichard, C. Stefani*, et al.*, "Novel second-generation di-2-pyridylketone thiosemicarbazones show synergism with standard chemotherapeutics and demonstrate potent activity against lung cancer xenografts after oral and intravenous administration in vivo," *J Med Chem,* vol. 55, pp. 7230-44, Aug 23 2012.

[25] D. B. Lovejoy, P. J. Jansson, U. T. Brunk, J. Wong, P. Ponka, and D. R. Richardson, "Antitumor activity of metal-chelating compound Dp44mT is mediated by formation of a redox-active copper complex that accumulates in lysosomes," *Cancer Res,* vol. 71, pp. 5871-80, Sep 1 2011.

[26] P. J. Jansson, P. C. Sharpe, P. V. Bernhardt, and D. R. Richardson, "Novel thiosemicarbazones of the ApT and DpT series and their copper complexes: identification of pronounced redox activity and characterization of their antitumor activity," *J Med Chem,* vol. 53, pp. 5759-69, Aug 12 2010.

[27] E. Noulsri, D. R. Richardson, S. Lerdwana, S. Fucharoen, T. Yamagishi, D. S. Kalinowski*, et al.*, "Antitumor activity and mechanism of action of the iron chelator, Dp44mT, against leukemic cells," *Am J Hematol,* vol. 84, pp. 170-6, Mar 2009.

[28] V. A. Rao, S. R. Klein, K. K. Agama, E. Toyoda, N. Adachi, Y. Pommier*, et al.*, "The iron chelator Dp44mT causes DNA damage and selective inhibition of topoisomerase IIalpha in breast cancer cells," *Cancer Res,* vol. 69, pp. 948-57, Feb 1 2009.

[29] M. Whitnall, J. Howard, P. Ponka, and D. R. Richardson, "A class of iron chelators with a wide spectrum of potent antitumor activity that overcomes resistance to chemotherapeutics," *Proc Natl Acad Sci U S A,* vol. 103, pp. 14901-6, Oct 3 2006.

[30] Z. Kovacevic, S. Chikhani, D. B. Lovejoy, and D. R. Richardson, "Novel thiosemicarbazone iron chelators induce up-regulation and phosphorylation of the metastasis suppressor N-myc down-stream regulated gene 1: a new strategy for the treatment of pancreatic cancer," *Mol Pharmacol,* vol. 80, pp. 598-609, Oct 2011.

[31] K. C. Park, B. Geleta, L. Y. W. Leck, J. Paluncic, S. Chiang, P. J. Jansson*, et al.*, "Thiosemicarbazones suppress expression of the c-Met oncogene by mechanisms involving lysosomal degradation and intracellular shedding," *J Biol Chem,* vol. 295, pp. 481-503, Jan 10 2020.

[32] Z. Kovacevic, S. V. Menezes, S. Sahni, D. S. Kalinowski, D. H. Bae, D. J. Lane*, et al.*, "The Metastasis Suppressor, N-MYC Downstream-regulated Gene-1 (NDRG1), Down-regulates the ErbB Family of Receptors to Inhibit Downstream Oncogenic Signaling Pathways," *J Biol Chem,* vol. 291, pp. 1029-52, Jan 15 2016.

[33] G. Kroemer, "Mitochondria in cancer," *Oncogene,* vol. 25, pp. 4630-2, Aug 7 2006.

[34] S. J. Parker and C. M. Metallo, "Metabolic consequences of oncogenic IDH mutations," *Pharmacol Ther,* vol. 152, pp. 54-62, Aug 2015.

[35] M. P. Murphy, "Targeting lipophilic cations to mitochondria," *Biochim Biophys Acta,* vol. 1777, pp. 1028-31, Jul-Aug 2008.

[36] L. Biasutto, L. F. Dong, M. Zoratti, and J. Neuzil, "Mitochondrially targeted anti-cancer agents," *Mitochondrion,* vol. 10, pp. 670-81, Nov 2010.

[37] C. Sandoval-Acuna, N. Torrealba, V. Tomkova, S. B. Jadhav, K. Blazkova, L. Merta*, et al.*, "Targeting Mitochondrial Iron Metabolism Suppresses Tumor Growth and Metastasis by Inducing Mitochondrial Dysfunction and Mitophagy," *Cancer Res,* vol. 81, pp. 2289-2303, May 1 2021.

[38] Y. Xia, Y. Li, X. Wu, Q. Zhang, S. Chen, X. Ma*, et al.*, "Ironing Out the Details: How Iron Orchestrates Macrophage Polarization," *Front Immunol,* vol. 12, p. 669566, 2021.

[39] N. C. Andrews, "Forging a field: the golden age of iron biology," *Blood,* vol. 112, pp. 219-30, Jul 15 2008.

[40] T. Ganz, "Macrophages and systemic iron homeostasis," *J Innate Immun,* vol. 4, pp. 446-53, 2012.

[41] R. Agoro, M. Taleb, V. F. J. Quesniaux, and C. Mura, "Cell iron status influences macrophage polarization," *PLoS One,* vol. 13, p. e0196921, 2018.

[42] G. Cairo, S. Recalcati, A. Mantovani, and M. Locati, "Iron trafficking and metabolism in macrophages: contribution to the polarized phenotype," *Trends Immunol,* vol. 32, pp. 241-7, Jun 2011.

[43] A. DeRosa and A. Leftin, "The Iron Curtain: Macrophages at the Interface of Systemic and Microenvironmental Iron Metabolism and Immune Response in Cancer," *Front Immunol,* vol. 12, p. 614294, 2021.

[44] L. Vanoaica, L. Richman, M. Jaworski, D. Darshan, S. A. Luther, and L. C. Kuhn, "Conditional deletion of ferritin h in mice reduces B and T lymphocyte populations," *PLoS One,* vol. 9, p. e89270, 2014.

[45] Z. Wang, W. Yin, L. Zhu, J. Li, Y. Yao, F. Chen*, et al.*, "Iron Drives T Helper Cell Pathogenicity by Promoting RNA-Binding Protein PCBP1-Mediated Proinflammatory Cytokine Production," *Immunity,* vol. 49, pp. 80-92 e7, Jul 17 2018.

[46] Y. Jiang, C. Li, Q. Wu, P. An, L. Huang, J. Wang*, et al.*, "Iron-dependent histone 3 lysine 9 demethylation controls B cell proliferation and humoral immune responses," *Nat Commun,* vol. 10, p. 2935, Jul 3 2019.

[47] J. N. Frost, T. K. Tan, M. Abbas, S. K. Wideman, M. Bonadonna, N. U. Stoffel*, et al.*, "Hepcidin-Mediated Hypoferremia Disrupts Immune Responses to Vaccination and Infection," *Med (N Y),* vol. 2, pp. 164-179 e12, Feb 12 2021.

[48] O. Kepp, L. Senovilla, I. Vitale, E. Vacchelli, S. Adjemian, P. Agostinis*, et al.*, "Consensus guidelines for the detection of immunogenic cell death," *Oncoimmunology,* vol. 3, p. e955691, Oct 2014.

[49] J. Li, F. Cao, H. L. Yin, Z. J. Huang, Z. T. Lin, N. Mao*, et al.*, "Ferroptosis: past, present and future," *Cell Death Dis,* vol. 11, p. 88, Feb 3 2020.

[50] B. Yu, B. Choi, W. Li, and D. H. Kim, "Magnetic field boosted ferroptosis-like cell death and responsive MRI using hybrid vesicles for cancer immunotherapy," *Nat Commun,* vol. 11, p. 3637, Jul 20 2020.

[51] D. Tang, O. Kepp, and G. Kroemer, "Ferroptosis becomes immunogenic: implications for anticancer treatments," *Oncoimmunology,* vol. 10, p. 1862949, Dec 29 2020.

[52] X. Chen, C. Yu, R. Kang, and D. Tang, "Iron Metabolism in Ferroptosis," *Front Cell Dev Biol,* vol. 8, p. 590226, 2020.

[53] Y. K. Han, G. Y. Park, M. J. Bae, J. S. Kim, W. S. Jo, and C. G. Lee, "Hypoxia induces immunogenic cell death of cancer cells by enhancing the exposure of cell surface calreticulin in an endoplasmic reticulum stress-dependent manner," *Oncol Lett,* vol. 18, pp. 6269-6274, Dec 2019.

[54] R. H. Zhou, K. Kokame, Y. Tsukamoto, C. Yutani, H. Kato, and T. Miyata, "Characterization of the human NDRG gene family: a newly identified member, NDRG4, is specifically expressed in brain and heart," *Genomics,* vol. 73, pp. 86-97, Apr 1 2001.

[55] X. Qu, Y. Zhai, H. Wei, C. Zhang, G. Xing, Y. Yu*, et al.*, "Characterization and expression of three novel differentiation-related genes belong to the human NDRG gene family," *Mol Cell Biochem,* vol. 229, pp. 35-44, Jan 2002.

[56] E. Shaw, L. A. McCue, C. E. Lawrence, and J. S. Dordick, "Identification of a novel class in the alpha/beta hydrolase fold superfamily: the N-myc differentiation-related proteins," *Proteins,* vol. 47, pp. 163-8, May 1 2002.

[57] L. Li, J. Wang, X. Shen, L. Wang, X. Li, Y. Liu*, et al.*, "Expression and prognostic value of NDRG2 in human astrocytomas," *J Neurol Sci,* vol. 308, pp. 77-82, Sep 15 2011.

[58] S. C. Choi, K. D. Kim, J. T. Kim, J. W. Kim, D. Y. Yoon, Y. K. Choe, *et al.*, "Expression and regulation of NDRG2 (N-myc downstream regulated gene 2) during the differentiation of dendritic cells," *FEBS Lett,* vol. 553, pp. 413-8, Oct 23 2003.

[59] W. Wang, Y. Li, Y. Li, A. Hong, J. Wang, B. Lin, *et al.*, "NDRG3 is an androgen regulated and prostate enriched gene that promotes in vitro and in vivo prostate cancer cell growth," *Int J Cancer,* vol. 124, pp. 521-30, Feb 1 2009.

[60] T. Li, R. Sun, M. Lu, J. Chang, X. Meng, and H. Wu, "NDRG3 facilitates colorectal cancer metastasis through activating Src phosphorylation," *Onco Targets Ther,* vol. 11, pp. 2843-2852, 2018.

[61] X. Luo, N. Hou, X. Chen, Z. Xu, J. Xu, L. Wang, *et al.*, "High expression of NDRG3 associates with unfavorable overall survival in non-small cell lung cancer," *Cancer Biomark,* vol. 21, pp. 461-469, Feb 6 2018.

[62] J. Shi, H. Zheng, and L. Yuan, "High NDRG3 expression facilitates HCC metastasis by promoting nuclear translocation of beta-catenin," *BMB Rep,* vol. 52, pp. 451-456, Jul 2019.

[63] M. A. Estiar, A. A. Zare, R. Esmaeili, L. Farahmand, H. Fazilaty, D. Jafari, *et al.*, "Clinical significance of NDRG3 in patients with breast cancer," *Future Oncol,* vol. 13, pp. 961-969, May 2017.

[64] S. H. Schilling, A. B. Hjelmeland, D. R. Radiloff, I. M. Liu, T. P. Wakeman, J. R. Fielhauer, *et al.*, "NDRG4 is required for cell cycle progression and survival in glioblastoma cells," *J Biol Chem,* vol. 284, pp. 25160-9, Sep 11 2009.

[65] R. P. Kotipatruni, D. J. Ferraro, X. Ren, R. P. Vanderwaal, D. K. Thotala, D. E. Hallahan, *et al.*, "NDRG4, the N-Myc downstream regulated gene, is important for cell survival, tumor invasion and angiogenesis in meningiomas," *Integr Biol (Camb),* vol. 4, pp. 1185-97, Oct 2012.

[66] V. Melotte, M. H. Lentjes, S. M. van den Bosch, D. M. Hellebrekers, J. P. de Hoon, K. A. Wouters, *et al.*, "N-Myc downstream-regulated gene 4 (NDRG4): a candidate tumor suppressor gene and potential biomarker for colorectal cancer," *J Natl Cancer Inst,* vol. 101, pp. 916-27, Jul 1 2009.

[67] E. H. F. Jandrey, R. P. Moura, L. N. S. Andrade, C. L. Machado, L. F. Campesato, K. R. M. Leite, *et al.*, "NDRG4 promoter hypermethylation is a mechanistic biomarker associated with metastatic progression in breast cancer patients," *NPJ Breast Cancer,* vol. 5, p. 11, 2019.

[68] J. Li and L. Kretzner, "The growth-inhibitory Ndrg1 gene is a Myc negative target in human neuroblastomas and other cell types with overexpressed N- or c-myc," *Mol Cell Biochem,* vol. 250, pp. 91-105, Aug 2003.

[69] N. van Belzen, W. N. Dinjens, M. P. Diesveld, N. A. Groen, A. C. van der Made, Y. Nozawa, *et al.*, "A novel gene which is up-regulated during colon epithelial cell differentiation and down-regulated in colorectal neoplasms," *Lab Invest,* vol. 77, pp. 85-92, Jul 1997.

[70] D. Zhou, K. Salnikow, and M. Costa, "Cap43, a novel gene specifically induced by Ni2+ compounds," *Cancer Res,* vol. 58, pp. 2182-9, May 15 1998.

[71] X. H. Shi, J. C. Larkin, B. Chen, and Y. Sadovsky, "The expression and localization of N-myc downstream-regulated gene 1 in human trophoblasts," *PLoS One,* vol. 8, p. e75473, 2013.

[72] K. C. Park, S. V. Menezes, D. S. Kalinowski, S. Sahni, P. J. Jansson, Z. Kovacevic, *et al.*, "Identification of differential phosphorylation and sub-cellular localization of the metastasis suppressor, NDRG1," *Biochim Biophys Acta Mol Basis Dis,* vol. 1864, pp. 2644-2663, Aug 2018.

[73] J. E. Lee and J. H. Kim, "SUMO modification regulates the protein stability of NDRG1," *Biochem Biophys Res Commun,* vol. 459, pp. 161-5, Mar 27 2015.

[74] J. T. Murray, D. G. Campbell, N. Morrice, G. C. Auld, N. Shpiro, R. Marquez, *et al.*, "Exploitation of KESTREL to identify NDRG family members as physiological substrates for SGK1 and GSK3," *Biochem J,* vol. 384, pp. 477-88, Dec 15 2004.

[75] A. Najafov, E. M. Sommer, J. M. Axten, M. P. Deyoung, and D. R. Alessi, "Characterization of GSK2334470, a novel and highly specific inhibitor of PDK1," *Biochem J,* vol. 433, pp. 357-69, Jan 15 2011.

[76] J. A. Gasser, H. Inuzuka, A. W. Lau, W. Wei, R. Beroukhim, and A. Toker, "SGK3 mediates INPP4B-dependent PI3K signaling in breast cancer," *Mol Cell,* vol. 56, pp. 595-607, Nov 20 2014.

[77] K. L. Agarwala, K. Kokame, H. Kato, and T. Miyata, "Phosphorylation of RTP, an ER stress-responsive cytoplasmic protein," *Biochem Biophys Res Commun,* vol. 272, pp. 641-7, Jun 16 2000.

[78] L. C. Tu, X. Yan, L. Hood, and B. Lin, "Proteomics analysis of the interactome of N-myc downstream regulated gene 1 and its interactions with the androgen response program in prostate cancer cells," *Mol Cell Proteomics,* vol. 6, pp. 575-88, Apr 2007.

[79] F. Hosoi, H. Izumi, A. Kawahara, Y. Murakami, H. Kinoshita, M. Kage*, et al.*, "N-myc downstream regulated gene 1/Cap43 suppresses tumor growth and angiogenesis of pancreatic cancer through attenuation of inhibitor of kappaB kinase beta expression," *Cancer Res,* vol. 69, pp. 4983-91, Jun 15 2009.

[80] M. K. Ghalayini, Q. Dong, D. R. Richardson, and S. J. Assinder, "Proteolytic cleavage and truncation of NDRG1 in human prostate cancer cells, but not normal prostate epithelial cells," *Biosci Rep,* vol. 33, Jun 11 2013.

[81] Z. Chen, D. Zhang, F. Yue, M. Zheng, Z. Kovacevic, and D. R. Richardson, "The iron chelators Dp44mT and DFO inhibit TGF-beta-induced epithelial-mesenchymal transition via up-regulation of N-Myc downstream-regulated gene 1 (NDRG1)," *J Biol Chem,* vol. 287, pp. 17016-28, May 18 2012.

[82] Y. Maruyama, M. Ono, A. Kawahara, T. Yokoyama, Y. Basaki, M. Kage*, et al.*, "Tumor growth suppression in pancreatic cancer by a putative metastasis suppressor gene Cap43/NDRG1/Drg-1 through modulation of angiogenesis," *Cancer Res,* vol. 66, pp. 6233-42, Jun 15 2006.

[83] Y. Murakami, F. Hosoi, H. Izumi, Y. Maruyama, H. Ureshino, K. Watari*, et al.*, "Identification of sites subjected to serine/threonine phosphorylation by SGK1 affecting N-myc downstream-regulated gene 1 (NDRG1)/Cap43-dependent suppression of angiogenic CXC chemokine expression in human pancreatic cancer cells," *Biochem Biophys Res Commun,* vol. 396, pp. 376-81, May 28 2010.

[84] C. McCaig, L. Potter, O. Abramczyk, and J. T. Murray, "Phosphorylation of NDRG1 is temporally and spatially controlled during the cell cycle," *Biochem Biophys Res Commun,* vol. 411, pp. 227-34, Jul 29 2011.

[85] K. Masuda, M. Ono, M. Okamoto, W. Morikawa, M. Otsubo, T. Migita*, et al.*, "Downregulation of Cap43 gene by von Hippel-Lindau tumor suppressor protein in human renal cancer cells," *Int J Cancer,* vol. 105, pp. 803-10, Jul 20 2003.

[86] S. Sahni, K. C. Park, Z. Kovacevic, and D. R. Richardson, "Two mechanisms involving the autophagic and proteasomal pathways process the metastasis suppressor protein, N-myc downstream regulated gene 1," *Biochim Biophys Acta Mol Basis Dis,* vol. 1865, pp. 1361-1378, Jun 1 2019.

[87] P. Lachat, P. Shaw, S. Gebhard, N. van Belzen, P. Chaubert, and F. T. Bosman, "Expression of NDRG1, a differentiation-related gene, in human tissues," *Histochem Cell Biol,* vol. 118, pp. 399-408, Nov 2002.

[88] https://psort.hgc.jp/

[89] https://wolfpsort.hgc.jp/

[90] S. K. Kurdistani, P. Arizti, C. L. Reimer, M. M. Sugrue, S. A. Aaronson, and S. W. Lee, "Inhibition of tumor cell growth by RTP/rit42 and its responsiveness to p53 and DNA damage," *Cancer Res,* vol. 58, pp. 4439-44, Oct 1 1998.

[91] T. Sugiki, Y. Taketomi, R. Kikuchi-Yanoshita, M. Murakami, and I. Kudo, "Association of N-myc downregulated gene 1 with heat-shock cognate protein 70 in mast cells," *Biol Pharm Bull,* vol. 27, pp. 628-33, May 2004.

[92] R. J. Guan, H. L. Ford, Y. Fu, Y. Li, L. M. Shaw, and A. B. Pardee, "Drg-1 as a differentiation-related, putative metastatic suppressor gene in human colon cancer," *Cancer Res,* vol. 60, pp. 749-55, Feb 1 2000.

[93] S. K. Kachhap, D. Faith, D. Z. Qian, S. Shabbeer, N. L. Galloway, R. Pili, *et al.*, "The N-Myc down regulated Gene1 (NDRG1) Is a Rab4a effector involved in vesicular recycling of E-cadherin," *PLoS One,* vol. 2, p. e844, Sep 5 2007.

[94] B. Xu, L. Lin, and N. S. Rote, "Identification of a stress-induced protein during human trophoblast differentiation by differential display analysis," *Biol Reprod,* vol. 61, pp. 681-6, Sep 1999.

[95] J. Larkin, B. Chen, X. H. Shi, T. Mishima, K. Kokame, Y. Barak, *et al.*, "NDRG1 deficiency attenuates fetal growth and the intrauterine response to hypoxic injury," *Endocrinology,* vol. 155, pp. 1099-106, Mar 2014.

[96] Y. Taketomi, K. Sunaga, S. Tanaka, M. Nakamura, S. Arata, T. Okuda, *et al.*, "Impaired mast cell maturation and degranulation and attenuated allergic responses in Ndrg1-deficient mice," *J Immunol,* vol. 178, pp. 7042-53, Jun 1 2007.

[97] E. Schmid, N. T. Xuan, N. Zahir, A. Russo, W. Yang, D. Kuhl, *et al.*, "Serum- and glucocorticoid-inducible kinase 1 sensitive NF-kappaB signaling in dendritic cells," *Cell Physiol Biochem,* vol. 34, pp. 943-54, 2014.

[98] A. Nishie, K. Masuda, M. Otsubo, T. Migita, M. Tsuneyoshi, K. Kohno, *et al.*, "High expression of the Cap43 gene in infiltrating macrophages of human renal cell carcinomas," *Clin Cancer Res,* vol. 7, pp. 2145-51, Jul 2001.

[99] K. Hirata, K. Masuda, W. Morikawa, J. W. He, A. Kuraoka, M. Kuwano, *et al.*, "N-myc downstream-regulated gene 1 expression in injured sciatic nerves," *Glia,* vol. 47, pp. 325-34, Sep 2004.

[100] L. Kalaydjieva, D. Gresham, R. Gooding, L. Heather, F. Baas, R. de Jonge, *et al.*, "N-myc downstream-regulated gene 1 is mutated in hereditary motor and sensory neuropathy-Lom," *Am J Hum Genet,* vol. 67, pp. 47-58, Jul 2000.

[101] V. Pietiainen, B. Vassilev, T. Blom, W. Wang, J. Nelson, R. Bittman, *et al.*, "NDRG1 functions in LDL receptor trafficking by regulating endosomal recycling and degradation," *J Cell Sci,* vol. 126, pp. 3961-71, Sep 1 2013.

[102] M. Hunter, D. Angelicheva, I. Tournev, E. Ingley, D. C. Chan, G. F. Watts, *et al.*, "NDRG1 interacts with APO A-I and A-II and is a functional candidate for the HDL-C QTL on 8q24," *Biochem Biophys Res Commun,* vol. 332, pp. 982-92, Jul 15 2005.

[103] H. A. Askautrud, E. Gjernes, G. Gunnes, M. Sletten, D. T. Ross, A. L. Borresen-Dale, *et al.*, "Global gene expression analysis reveals a link between NDRG1 and vesicle transport," *PLoS One,* vol. 9, p. e87268, 2014.

[104] Y. Taketomi, T. Sugiki, T. Saito, S. Ishii, M. Hisada, T. Suzuki-Nishimura, *et al.*, "Identification of NDRG1 as an early inducible gene during in vitro maturation of cultured mast cells," *Biochem Biophys Res Commun,* vol. 306, pp. 339-46, Jun 27 2003.

[105] H. Cangul, "Hypoxia upregulates the expression of the NDRG1 gene leading to its overexpression in various human cancers," *BMC Genet,* vol. 5, p. 27, Sep 2 2004.

[106] D. Piquemal, D. Joulia, P. Balaguer, A. Basset, J. Marti, and T. Commes, "Differential expression of the RTP/Drg1/Ndr1 gene product in proliferating and growth arrested cells," *Biochim Biophys Acta,* vol. 1450, pp. 364-73, Jul 8 1999.

[107] K. Salnikow, T. Kluz, and M. Costa, "Role of Ca(2+) in the regulation of nickel-inducible Cap43 gene expression," *Toxicol Appl Pharmacol,* vol. 160, pp. 127-32, Oct 15 1999.

[108] S. Stein, E. K. Thomas, B. Herzog, M. D. Westfall, J. V. Rocheleau, R. S. Jackson, 2nd, *et al.*, "NDRG1 is necessary for p53-dependent apoptosis," *J Biol Chem,* vol. 279, pp. 48930-40, Nov 19 2004.

[109] K. T. Kim, P. P. Ongusaha, Y. K. Hong, S. K. Kurdistani, M. Nakamura, K. P. Lu, *et al.*, "Function of Drg1/Rit42 in p53-dependent mitotic spindle checkpoint," *J Biol Chem,* vol. 279, pp. 38597-602, Sep 10 2004.

[110] A. M. Merlot, G. M. Porter, S. Sahni, E. G. Lim, P. Peres, and D. R. Richardson, "The metastasis suppressor, NDRG1, differentially modulates the endoplasmic reticulum stress response," *Biochim Biophys Acta Mol Basis Dis,* vol. 1865, pp. 2094-2110, Sep 1 2019.

[111] S. Bandyopadhyay, S. K. Pai, S. C. Gross, S. Hirota, S. Hosobe, K. Miura, *et al.*, "The Drg-1 gene suppresses tumor metastasis in prostate cancer," *Cancer Res,* vol. 63, pp. 1731-6, Apr 15 2003.

[112] N. Meyer and L. Z. Penn, "Reflecting on 25 years with MYC," *Nat Rev Cancer,* vol. 8, pp. 976-90, Dec 2008.

[113] S. Adhikary and M. Eilers, "Transcriptional regulation and transformation by Myc proteins," *Nat Rev Mol Cell Biol,* vol. 6, pp. 635-45, Aug 2005.

[114] J. Zhang, S. Chen, W. Zhang, J. Zhang, X. Liu, H. Shi, *et al.*, "Human differentiation-related gene NDRG1 is a Myc downstream-regulated gene that is repressed by Myc on the core promoter region," *Gene,* vol. 417, pp. 5-12, Jul 1 2008.

[115] Y. Li, P. Pan, P. Qiao, and R. Liu, "Downregulation of N-myc downstream regulated gene 1 caused by the methylation of CpG islands of NDRG1 promoter promotes proliferation and invasion of prostate cancer cells," *Int J Oncol,* vol. 47, pp. 1001-8, Sep 2015.

[116] L. L. Han, L. Hou, M. J. Zhou, Z. L. Ma, D. L. Lin, L. Wu, *et al.*, "Aberrant NDRG1 methylation associated with its decreased expression and clinicopathological significance in breast cancer," *J Biomed Sci,* vol. 20, p. 52, Jul 30 2013.

[117] P. Jaakkola, D. R. Mole, Y. M. Tian, M. I. Wilson, J. Gielbert, S. J. Gaskell, *et al.*, "Targeting of HIF-alpha to the von Hippel-Lindau ubiquitylation complex by O2-regulated prolyl hydroxylation," *Science,* vol. 292, pp. 468-72, Apr 20 2001.

[118] M. Ivan, K. Kondo, H. Yang, W. Kim, J. Valiando, M. Ohh, *et al.*, "HIFalpha targeted for VHL-mediated destruction by proline hydroxylation: implications for O2 sensing," *Science,* vol. 292, pp. 464-8, Apr 20 2001.

[119] L. E. Huang and H. F. Bunn, "Hypoxia-inducible factor and its biomedical relevance," *J Biol Chem,* vol. 278, pp. 19575-8, May 30 2003.

[120] H. Cangul, K. Salnikow, H. Yee, D. Zagzag, T. Commes, and M. Costa, "Enhanced overexpression of an HIF-1/hypoxia-related protein in cancer cells," *Environ Health Perspect,* vol. 110 Suppl 5, pp. 783-8, Oct 2002.

[121] N. T. Le and D. R. Richardson, "Iron chelators with high antiproliferative activity up-regulate the expression of a growth inhibitory and metastasis suppressor gene: a link between iron metabolism and proliferation," *Blood,* vol. 104, pp. 2967-75, Nov 1 2004.

[122] D. Hanahan and R. A. Weinberg, "Hallmarks of cancer: the next generation," *Cell,* vol. 144, pp. 646-74, Mar 4 2011.

[123] D. Hanahan and R. A. Weinberg, "The hallmarks of cancer," *Cell,* vol. 100, pp. 57-70, Jan 7 2000.

[124] S. Zhang, C. Yu, X. Yang, H. Hong, J. Lu, W. Hu, *et al.*, "N-myc downstream-regulated gene 1 inhibits the proliferation of colorectal cancer through emulative antagonizing NEDD4-mediated ubiquitylation of p21," *J Exp Clin Cancer Res,* vol. 38, p. 490, Dec 12 2019.

[125] B. Lakaye, B. Wirtzfeld, P. Wins, T. Grisar, and L. Bettendorff, "Thiamine triphosphate, a new signal required for optimal growth of Escherichia coli during amino acid starvation," *J Biol Chem,* vol. 279, pp. 17142-7, Apr 23 2004.

[126] Z. Kovacevic, D. Fu, and D. R. Richardson, "The iron-regulated metastasis suppressor, Ndrg-1: identification of novel molecular targets," *Biochim Biophys Acta,* vol. 1783, pp. 1981-92, Oct 2008.

[127] J. Sun, D. Zhang, Y. Zheng, Q. Zhao, M. Zheng, Z. Kovacevic, *et al.*, "Targeting the metastasis suppressor, NDRG1, using novel iron chelators: regulation of stress fiber-mediated tumor cell migration via modulation of the ROCK1/pMLC2 signaling pathway," *Mol Pharmacol,* vol. 83, pp. 454-69, Feb 2013.

[128] X. Wangpu, J. Lu, R. Xi, F. Yue, S. Sahni, K. C. Park, *et al.*, "Targeting the Metastasis Suppressor, N-Myc Downstream Regulated Gene-1, with Novel Di-2-Pyridylketone Thiosemicarbazones: Suppression of Tumor Cell Migration and Cell-Collagen Adhesion by Inhibiting Focal Adhesion Kinase/Paxillin Signaling," *Mol Pharmacol,* vol. 89, pp. 521-40, May 2016.

[129] J. C. Lee, L. C. Chung, Y. J. Chen, T. H. Feng, and H. H. Juang, "N-myc downstream-regulated gene 1 downregulates cell proliferation, invasiveness, and tumorigenesis in human oral squamous cell carcinoma," *Cancer Lett,* vol. 355, pp. 242-52, Dec 28 2014.

[130] P. Carmeliet and R. K. Jain, "Angiogenesis in cancer and other diseases," *Nature,* vol. 407, pp. 249-57, Sep 14 2000.

[131] J. Wang, J. Cai, Z. Li, S. Hu, L. Yu, L. Xiao*, et al.*, "Expression and biological function of N-myc down-regulated gene 1 in human cervical cancer," *J Huazhong Univ Sci Technolog Med Sci,* vol. 30, pp. 771-6, Dec 2010.

[132] H. Urra, E. Dufey, T. Avril, E. Chevet, and C. Hetz, "Endoplasmic Reticulum Stress and the Hallmarks of Cancer," *Trends Cancer,* vol. 2, pp. 252-262, May 2016.

[133] J. M. Mulcahy Levy and A. Thorburn, "Autophagy in cancer: moving from understanding mechanism to improving therapy responses in patients," *Cell Death Differ,* vol. 27, pp. 843-857, Mar 2020.

[134] S. Sahni, D. H. Bae, D. J. Lane, Z. Kovacevic, D. S. Kalinowski, P. J. Jansson*, et al.*, "The metastasis suppressor, N-myc downstream-regulated gene 1 (NDRG1), inhibits stress-induced autophagy in cancer cells," *J Biol Chem,* vol. 289, pp. 9692-709, Apr 4 2014.

[135] K. C. Park, J. Paluncic, Z. Kovacevic, and D. R. Richardson, "Pharmacological targeting and the diverse functions of the metastasis suppressor, NDRG1, in cancer," *Free Radic Biol Med,* vol. 157, pp. 154-175, Sep 2020.

[136] K. Taniguchi and M. Karin, "NF-kappaB, inflammation, immunity and cancer: coming of age," *Nat Rev Immunol,* vol. 18, pp. 309-324, May 2018.

[137] S. C. Sun, J. H. Chang, and J. Jin, "Regulation of nuclear factor-kappaB in autoimmunity," *Trends Immunol,* vol. 34, pp. 282-9, Jun 2013.

[138] S. Beinke and S. C. Ley, "Functions of NF-kappaB1 and NF-kappaB2 in immune cell biology," *Biochem J,* vol. 382, pp. 393-409, Sep 1 2004.

[139] H. Yu, L. Lin, Z. Zhang, H. Zhang, and H. Hu, "Targeting NF-kappaB pathway for the therapy of diseases: mechanism and clinical study," *Signal Transduct Target Ther,* vol. 5, p. 209, Sep 21 2020.

[140] A. R. Brasier, "The NF-kappaB regulatory network," *Cardiovasc Toxicol,* vol. 6, pp. 111-30, 2006.

[141] M. S. Hayden and S. Ghosh, "Shared principles in NF-kappaB signaling," *Cell,* vol. 132, pp. 344-62, Feb 8 2008.

[142] M. Karin and F. R. Greten, "NF-kappaB: linking inflammation and immunity to cancer development and progression," *Nat Rev Immunol,* vol. 5, pp. 749-59, Oct 2005.

[143] S. V. Menezes, L. Fouani, M. L. H. Huang, B. Geleta, S. Maleki, A. Richardson*, et al.*, "The metastasis suppressor, NDRG1, attenuates oncogenic TGF-beta and NF-kappaB signaling to enhance membrane E-cadherin expression in pancreatic cancer cells," *Carcinogenesis,* vol. 40, pp. 805-818, Jul 6 2019.

[144] K. Pardali and A. Moustakas, "Actions of TGF-beta as tumor suppressor and pro-metastatic factor in human cancer," *Biochim Biophys Acta,* vol. 1775, pp. 21-62, Jan 2007.

[145] M. Sibilia, R. Kroismayr, B. M. Lichtenberger, A. Natarajan, M. Hecking, and M. Holcmann, "The epidermal growth factor receptor: from development to tumorigenesis," *Differentiation,* vol. 75, pp. 770-87, Nov 2007.

[146] A. Okines, D. Cunningham, and I. Chau, "Targeting the human EGFR family in esophagogastric cancer," *Nat Rev Clin Oncol,* vol. 8, pp. 492-503, Apr 5 2011.

[147] S. V. Menezes, Z. Kovacevic, and D. R. Richardson, "The metastasis suppressor NDRG1 down-regulates the epidermal growth factor receptor via a lysosomal mechanism by up-regulating mitogen-inducible gene 6," *J Biol Chem,* vol. 294, pp. 4045-4064, Mar 15 2019.

[148] H. Wang, B. Rao, J. Lou, J. Li, Z. Liu, A. Li*, et al.*, "The Function of the HGF/c-Met Axis in Hepatocellular Carcinoma," *Front Cell Dev Biol,* vol. 8, p. 55, 2020.

[149] B. Geleta, K. C. Park, P. J. Jansson, S. Sahni, S. Maleki, Z. Xu, *et al.*, "Breaking the cycle: Targeting of NDRG1 to inhibit bi-directional oncogenic cross-talk between pancreatic cancer and stroma," *FASEB J,* vol. 35, p. e21347, Feb 2021.

[150] E. Gherardi, W. Birchmeier, C. Birchmeier, and G. Vande Woude, "Targeting MET in cancer: rationale and progress," *Nat Rev Cancer,* vol. 12, pp. 89-103, Jan 24 2012.

[151] R. Ishizawar and S. J. Parsons, "c-Src and cooperating partners in human cancer," *Cancer Cell,* vol. 6, pp. 209-14, Sep 2004.

[152] M. Guarino, "Src signaling in cancer invasion," *J Cell Physiol,* vol. 223, pp. 14-26, Apr 2010.

[153] W. Liu, F. Yue, M. Zheng, A. Merlot, D. H. Bae, M. Huang, *et al.*, "The proto-oncogene c-Src and its downstream signaling pathways are inhibited by the metastasis suppressor, NDRG1," *Oncotarget,* vol. 6, pp. 8851-74, Apr 20 2015.

[154] L. S. Chaturvedi, H. M. Marsh, and M. D. Basson, "Role of RhoA and its effectors ROCK and mDia1 in the modulation of deformation-induced FAK, ERK, p38, and MLC motogenic signals in human Caco-2 intestinal epithelial cells," *Am J Physiol Cell Physiol,* vol. 301, pp. C1224-38, Nov 2011.

[155] P. K. Smith, R. I. Krohn, G. T. Hermanson, A. K. Mallia, F. H. Gartner, M. D. Provenzano, *et al.*, "Measurement of protein using bicinchoninic acid," *Anal Biochem,* vol. 150, pp. 76-85, Oct 1985.

[156] E. Eruslanov and S. Kusmartsev, "Identification of ROS using oxidized DCFDA and flow-cytometry," *Methods Mol Biol,* vol. 594, pp. 57-72, 2010.

[157] M. E. Kauffman, M. K. Kauffman, K. Traore, H. Zhu, M. A. Trush, Z. Jia, *et al.*, "MitoSOX-Based Flow Cytometry for Detecting Mitochondrial ROS," *React Oxyg Species (Apex),* vol. 2, pp. 361-370, 2016.

[158] T. Panaretakis, O. Kepp, U. Brockmeier, A. Tesniere, A. C. Bjorklund, D. C. Chapman, *et al.*, "Mechanisms of pre-apoptotic calreticulin exposure in immunogenic cell death," *EMBO J,* vol. 28, pp. 578-90, Mar 4 2009.

[159] M. Obeid, A. Tesniere, F. Ghiringhelli, G. M. Fimia, L. Apetoh, J. L. Perfettini, *et al.*, "Calreticulin exposure dictates the immunogenicity of cancer cell death," *Nat Med,* vol. 13, pp. 54-61, Jan 2007.

[160] S. Comsa, A. M. Cimpean, and M. Raica, "The Story of MCF-7 Breast Cancer Cell Line: 40 years of Experience in Research," *Anticancer Res,* vol. 35, pp. 3147-54, Jun 2015.

[161] D. J. Lane, F. Saletta, Y. Suryo Rahmanto, Z. Kovacevic, and D. R. Richardson, "N-myc downstream regulated 1 (NDRG1) is regulated by eukaryotic initiation factor 3a (eIF3a) during cellular stress caused by iron depletion," *PLoS One,* vol. 8, p. e57273, 2013.

[162] https://www.atcc.org/products/ccl-171

[163] K. M. Dixon, G. Y. Lui, Z. Kovacevic, D. Zhang, M. Yao, Z. Chen, *et al.*, "Dp44mT targets the AKT, TGF-beta and ERK pathways via the metastasis suppressor NDRG1 in normal prostate epithelial cells and prostate cancer cells," *Br J Cancer,* vol. 108, pp. 409-19, Feb 5 2013.

[164] R. Ai, Y. Sun, Z. Guo, W. Wei, L. Zhou, F. Liu, *et al.*, "NDRG1 overexpression promotes the progression of esophageal squamous cell carcinoma through modulating Wnt signaling pathway," *Cancer Biol Ther,* vol. 17, pp. 943-54, Sep 2016.

[165] P. K. Ziegler, J. Bollrath, C. K. Pallangyo, T. Matsutani, O. Canli, T. De Oliveira, *et al.*, "Mitophagy in Intestinal Epithelial Cells Triggers Adaptive Immunity during Tumorigenesis," *Cell,* vol. 174, pp. 88-101 e16, Jun 28 2018.